TÉCNICO LISBOA

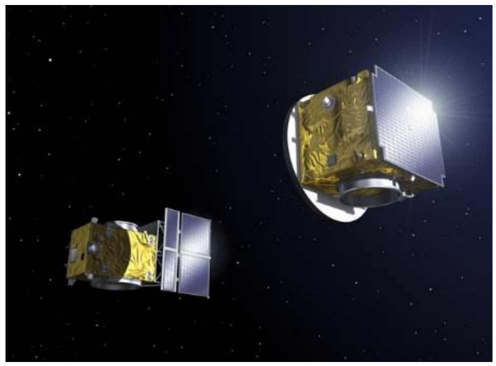

Attitude Control for a Group of Space Vehicles

António César Roque Gameiro Neto Santos

Dissertação para a obtenção do Grau de Mestre em

Engenharia Aerospacial

Júri

Presidente: Prof. João Manuel Lage de Miranda Lemos
Orientador: Prof. Paulo Jorge Coelho Ramalho Oliveira
Arguente: Prof. Pedro Manuel Urbano de Almeida Lima

Outubro 2013

Resumo

É desenvolvida uma estratégia de control de atitude para um grupo de três veículos espaciais.

O equipamento a bordo é apresentado. Cada veículo dispõe de medições de Earth vector, de Sun vector, de attitude quaternion e de leituras de velocidade angular. Rodas de inércia e propulsores de atitude constituem os actuadores.

É implementado o algoritmo de determinação de atitude por Wahbas e, apresentado um Filtro de Kalman Extendido para estimação de atitude e estimação de desvio do giroscópio.

A estratégia de controlo para um veículo isolado utiliza uma variante de LQR de forma a extender o seu uso para manobras de grande amplitude angular.

Uma estratégia de grupo consiste numa abordagem de seguimento de líder onde cada veículo dispõe de estimativas da sua atitude inercial. Num cenário em que dois veículos não têm acesso às suas atitudes inerciais, um algoritmo de determinacao de atitude relativa é utilizado. Uma terceira estratégia consiste em comandar os veículos para uma atitude central ao grupo.

São apresentados e analisados resultados de estimação, controlo de um veículo isolado e de grupo.

Abstract

Attitude control for a group of three space vehicles is developed.

The on-board attitude apparatus is presented. Each vehicle measures the Sun vector, the Earth vector, the attitude quaternion and angular velocity. Attitude control is provided by reaction wheels or attitude thrusters.

The Wahba's attitude determination algorithm is implemented and an Extended Kalman Filter is derived for attitude estimation and for gyroscope bias estimation.

A control strategy for stand-alone vehicle attitude reorientation is implemented using a modified LQR design to cope with large reorientation manoeuvres.

One group strategy consists in a leader following approach where inertial attitude estimates are available to the entire group. A relative attitude determination algorithm is used in a scenario where two vehicles do not possess the inertial attitude instrumentation. A third strategy forces the vehicles to target a common mid-attitude point.

Results for estimation, single vehicle control and group control are presented and analysed.

Acknowledgments

Special acknowledgement goes to Professor Paulo Oliveira for the wise and patient guidance during the entire course of my thesis.

I would like to thank my family for the immeasurable support ever since, especially my parents João and Dalila who have always been present when I most needed.

I want to thank my most special friends who I will always remember for the great moments spent during academic life. Without them my task would have been less connected and less vibrant.

Index

List of Symbols

The following lists the most relevant symbols that appear in the context of each chapter.

The Space Vehicle and the Space Environment

θ:	General Angle
α:	Elevation angle
φ:	Azimuth angle
$\boldsymbol{e}$:	General vector
I:	Space vehicle inertia matrix
I^w:	Wheels inertia
$I_{n\times n}$:	Identity matrix n×n
$\boldsymbol{\omega}$:	Angular velocity vector
ψ, θ, φ:	Euler angles (yaw, pitch, roll)
$\boldsymbol{M}$:	External Momentum
$\boldsymbol{M}^W$:	Wheels Applied Momentum
$\boldsymbol{T}$:	Thrusters Torque
$\boldsymbol{b}$:	Lever-arm
$\boldsymbol{r}$:	Space vehicle position vector
$\boldsymbol{v}$:	Space vehicle velocity vector
V:	Vehicle speed (norm of velocity vector)
$\boldsymbol{p}$:	Space vehicle determined position
r_c:	Mean distance from Earth to the Sun
r:	Distance from space vehicle to centre of the Earth
$\rho_{\oplus}$:	Angular radius of the Earth
T:	Orbit period
M:	Mass of large body
σ:	Standard deviation
N:	Normal Distribution
$\boldsymbol{m}$:	Two angle measurement set
$\bar{q}$:	Attitude quaternion
$\boldsymbol{q}$:	Quaternion vector component
q:	Quaternion scalar component
$\boldsymbol{\omega}$:	Angular velocity vector
W^a:	Wheels axes matrix
Δt:	Time increment

$\boldsymbol{\mu}$: Gyro-drift vector

$\boldsymbol{a}$: Three-component attitude error

Attitude Estimation

$\boldsymbol{z}$: Measurement vector

$\boldsymbol{n}$: Noise vector

$\delta\bar{q}$: Error quaternion

L: Wahba's loss Function

K: Matrix gain

P: Covariance matrix

H: Measurement sensitivity matrix

R: Measurement noise covariance matrix

Q: Model error covariance matrix

x: State vector

x^*: Auxiliary state vector

Attitude Control of Single Vehicle

P: Solution matrix of the *Riccati* equation

R: State weighting matrix

J: Cost function

$\bar{q}_{rot}$: Rotation quaternion

$\boldsymbol{e}$: Axis of rotaion

K_w: Gain for wheels resetting operation

Δq: Quaternion additive error

$\Delta\omega$: Angular velocity error

Group Attitude

$\boldsymbol{m}$: Measurement image vector

σ: RMS error

$\boldsymbol{b}^{x}_{x/y}$: LOS vector from frame x to frame y written in frame x

$\bar{q}_{xy}$: Relative attitude quaternion of x relatively to y

$\bar{q}_{conv_x}$: Converse attitude quaternion of x

1. Introduction

Guidance Navigation and Control

Guidance Navigations and Control (abbreviated GNC) is a research area of engineering that addresses the problem of controlling the movement of vehicles in a given space (linear and rotational movement). An increasing number of applications must deal with high complex dynamics or too fast dynamics which make them impractical for human control. Further, fine control for high precision or energy optimization are generally increased with automatic control systems.

Guidance refers to the problem of determining the path (trajectory) from the current state to the target which might include the specification of velocities, accelerations and rotations to attain it. Navigation is the component responsible for determining the position, velocity, attitude and other variables that make up the system's state. Control refers to the strategies and algorithms that calculate the actuation upon the system in order to track guidance commands.

GNC systems or some of its elements are found in all-autonomous or semi-autonomous systems as for example: airplane and boat autopilots, driverless cars such as the Stanford's Stanley vehicle, Unmanned Air vehicles (UAV's) and space vehicle attitude control systems as addressed in this thesis.

Space Vehicle Systems Overview

The space Vehicle (SV) system can be divided into several subsystems. Depending on the mission profile these comprise: life support, command and data handling, power management, thermal monitoring and control, structures, propulsion, payload, launch vehicle, communication system, and of our main concern here, the GNC system. The attitude determination and control system (ADCS) is regarded as a subsystem of the GNC system.

The GNC system, and more concretely the ADCS is one of the most influential subsystems. Its decisions are based on a wide number of parameters and variables provided by other subsystems. For instance the thermal control subsystem might trigger a temperature overload warning in a given component due to Sun excessive light exposure; in such case the GNC must reorient the SV in order to place this component at the shadow region to cool down. Another example is the dependence on the power management subsystem if the latter relies on solar panels to feed batteries; proper orientation of the panels towards the Sun is crucial to extract maximum power. Similarly, the communication subsystem requires antenna specific orientations that might vary over the course of operation. Orbit control in general is also dependent on attitude, because orbit thrusters propulsive force is imposed by SV inertial orientation.

It is now clear that the attitude of the SV is extremely impactful on the operational conditions, and reciprocally the latter impose restrictions on the attitude, therefore most of the subsystems are directly or indirectly linked to the ADCS.

Attitude Determination and Control System (ADCS)

Attitude is represented as the rotation a given reference frame must undergo in order to align its axes with the fixed body axes of the object concerned. Attitude determination is the process of acquiring an estimate of the true attitude normally resorting to algorithms which relate observations with attitude representations. Attitude control refers to the computation of the necessary actuation to point the spacecraft to a desired orientation, whether it is a constant orientation (pointing) or a variable one (tracking).

Attitude Determination and Control is a problem touching several subfields including: control systems design, dynamics and modelling of systems, software design, user interface design and spacecraft operations. The scope of this text only covers the first three. The algorithms developed are implemented in the *Simulink/Matlab* simulation environment.

ADCS terms

Pointing accuracy: also referred to as the attitude control accuracy, generally refers to how close to a desired commanded attitude the space vehicle can be controlled.

Estimation accuracy: it is a measure of how well the orientation of the SV is known.

Sensor accuracy is the sum of the ultimate accuracy of the measurement provided by the sensors and includes mounting errors and other bias effects.

Jitter: refers to the error in controlled attitude of a frequency too high to be controlled by the ADCS.

Spacecraft Formation Flying and Consensus

Although formation of vehicles in many areas has been on the spotlight for several years, formation flying of spacecraft is a relatively recent concept. A growing number of space applications have lately been identified that will utilize distributed systems of satellites. There is a great level of interest in both the scientific and defence communities to develop mature systems and software for autonomous rendezvous and formation flying.

A cooperative control system consists generally of a group of autonomous agents with sensing, actuation and communication. The goal of the group is to achieve prescribed agent and group behaviours using relative sensing and flow of information between agents. The most relevant subset of cooperative control in the context of this dissertation is the consensus problem where the group objective is convergence to a common attitude.

Formation Flying refers to maintenance of relative positions between vehicles and position reconfiguration which is not in the scope of the present work. Although relative position between vehicles do affect attitude related issues.

Examples of applications that greatly benefit from multi spacecraft techniques include: better tracking of moving targets, reconfigurable instantaneous synthetic aperture radar, satellite relay systems, stereo-imaging, theatre-wide surveillance, all-weather operation and performance, in general component substitution is cheaper (replacement of one small satellite versus a single large and costly one), inspection and maintenance services, etc. The advantages of space formation and consensus however come with the added cost of group control.

In this text

The order of presentation of the various issues discussed follows the natural order in which they were developed over the course of this dissertation.

First the space environment is briefly described along with orbital dynamics of Earth satellites. The space vehicle configuration is established by selecting adequate sensors and actuators. Actuators models capture only major real actuator behaviours and sensors noise figures are prescribed.

The second chapter addresses state estimation algorithms employed for one vehicle standalone. Several estimation processes are discussed and compared. The Wahbas' problem solution is used as a deterministic attitude method. An Extended Kalman Filter (EKF) for angular velocity estimation is developed. Attitude estimation is performed by a modified version of the EKF algorithm (the Multiplicative Extended Kalman Filter) which might also include gyro drift bias estimation.

A feedback control law based on LQR design with additional supervising logic is developed. A resetting operation for the reaction wheels set is conceived such that fine pointing accuracy can be maintained throughout the event. Simulation results of the controlled SV applying the two actuator types and for different initial conditions are presented and compared. Steady-state pointing accuracies are investigated.

A deterministic relative attitude method that uses line of sight measurements between three vehicles is presented. Relative attitude information is used in a scenario where two vehicles do not possess inertial measurement unit (IMU) package and so group consensus is attainable by nulling relative attitude.

In another scenario all vehicles possess IMU and can reorient independently. A group coordinator (GC) is introduce for monitoring and triggering operations in the group. Additionally the GC enables the group to converge to a mid-attitude point. Group transient responses are investigated.

2. The Space Vehicle and the Space Environment

We elaborate on a particular three-axis stabilized SV with a gyrostat configuration. We establish its hardware features in regard of attitude control, such as sensors and actuators. Afterwards the space environment is addressed, which include orbit, planetary position and influence of viewing and lighting conditions. Lastly in this chapter, the attitude dynamics are derived. The majority of the information presented here is based on [1].

This section discusses the basic hardware systems that must be on board the SV in order to perform its proposed functions. A controlled satellite must be equipped with proper actuators, sensors, process unit, and as customary a communication system. The attitude hardware embodies the physical components of the ADCS. The more critical components of the ADCS are briefly explained and reason about in order to make an adequate and realistic choice.

2.1. Attitude Hardware

A. Sun Sensor

Sun sensors are widely used in a vast majority of space applications regarding attitude determination and have flown on nearly every satellite. Unlike the Earth, the angular radius of the Sun is nearly orbit independent and sufficiently small (0.267° at 1 UA) and so for most applications a point source approximation is valid. The Sun is sufficiently bright to allow the use of simple, reliable equipment without need to discriminate among sources and has minimal power requirements.

Knowledge of the relative position of the Sun allows protection of sensitive equipment such as Star Trackers, provides a reference for on-board attitude control and for position solar power arrays.

The measurement of the Sun sensor is the set of azimuth φ and elevation α angles of the Sun line direction in the sensor frame coordinates. These angles relate to the Sun vector according to:

$$azim \equiv \varphi = \arctan(e_y/e_x) \tag{2.1}$$

$$elev \equiv \alpha = \arctan\left(e_z/\sqrt{e_x^2 + e_y^2}\right) \tag{2.2}$$

where $\boldsymbol{e}_s = \left(\left[e_x\ e_y\ e_z\right]^T\right)$ is the true Sun unit vector written in sensor coordinates. We define also the angle observation set $m = [\varphi \quad \alpha]^T$.

There are essentially three basic types of Sun sensors: analogue sensors, which have an output signal that is a continuous function of the Sun angles and is usually monotonic; Sun presence sensors, providing constant output whenever the Sun is present in the field of view (FOV); and digital sensors, which provide an encoded, discrete output.

The digital Sun sensor operation

The digital Sun sensor generates an output which is a digital representation of the angle between the Sun vector and the normal of the sensor face when the Sun is in the FOV. The Sun image passes the entrance slit while is refracted by a material of index of refraction n (might be unity) and illuminates a pattern of slits. Each slit has a corresponding row of photocell beneath it. There are 4 types of rows: (1) automatic threshold adjust (ATA), (2) a sign bit, (3) encoded bits and, (4) fine bits.

The sign bit indicates which side of the sensor the Sun is on. The encoded bits provide a discrete measure of the displacement of the Sun image, allowing the Sun angle to be obtained by decoding the given bits in a logic unit. The ATA slit is half the width of the other slits. Its photocell output power is half of the others and independent of the Sun angle, therefore working as a threshold for the corresponding turn on or off of the sensor where it is mounted. Figure 2.1 illustrates the digital sun sensor.

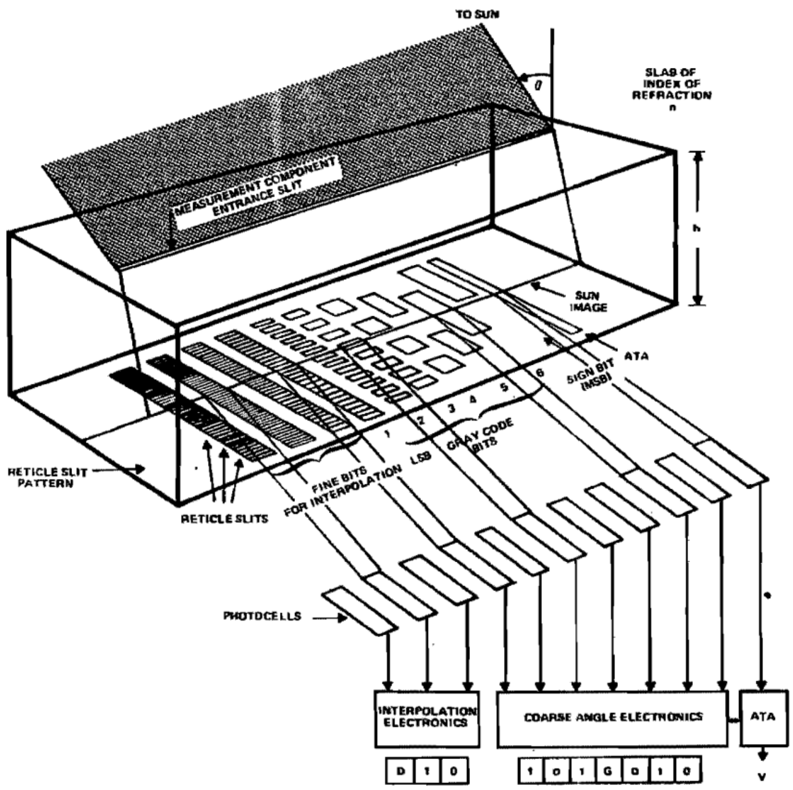

Figure 2.1 – Digital Sun Sensor

In particular it is interesting to use a two axis Sun sensor, utilizing two measurement components at 90° angles, yielding a 64°-by-64° or 128°-by-128° FOV. Full 4π *sr* coverage is accomplished by use of five or more 128°-by-128° sensors, disposed appropriately along the satellite's surface panels. This was the configuration admitted for the SV. Together they are able to provide two axis Sun measurement angles in all possible orientations as long as there is direct Sun light illuminating it.

Sun sensor measurement model

In order to reflect Sun sensor measurement inaccuracies zero mean additive Gaussian noise is added to the true angles. Hence the Sun sensor measurement model is:

$$\widehat{m} = m + n_{SS}$$

where $\widehat{m} = [\widehat{\varphi} \quad \widehat{\alpha}]^T$ is the measured quantity and $n_{SS} \sim N(0, \sigma_{SS}^2 I_{2\times2})$.

The digital sensor provides angular readings with standard deviation (σ_{SS}) typically ranging from 0.5° to 0,01°. An intermediate value of $\sigma_{SS} = 0{,}1°$ is adopted.

As it will be clear later, the necessary quantity for attitude computation is the Sun vector itself. Thus, the measured Sun vector is obtained as a function of the measured angles in the sensor frame:

$$\hat{e}_S = [\cos\widehat{\alpha} \,.\, \cos\widehat{\varphi} \quad \cos\widehat{\alpha} \,.\, \sin\widehat{\varphi} \quad \sin\widehat{\alpha}]^T \tag{2.3}$$

Shadow problems

Because Sun sensors need direct Sun light, one must take into consideration situations when direct Sun light is blocked. In this context, there are three potential sources of shadow: the Earth, another artificial satellite in the vicinity, and the moon. The first one is rather frequent and as so it is included in the simulation model as discussed later. The second and third are infrequent and so they are ignored in the model.

B. Horizon Sensor

Scanner

Horizon sensors are the principal means for directly determining the orientation of the spacecraft with respect to the Earth. Contrary to the Sun sensor, the horizon sensor has a small FOV to scan across the celestial sphere in a conical pattern and detect the presence of the large and dim Earth disc in order to measure it. In some cases the aperture of the conical angle can be controlled as well as the centreline of the cone (Figure 2.2).

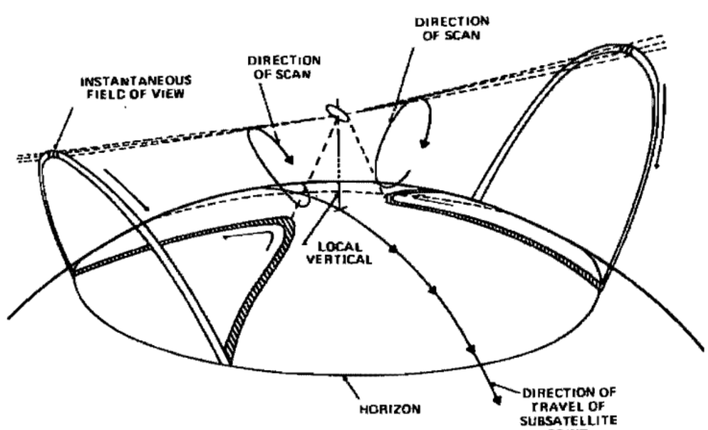

Figure 2.2 – Horizon scanning principle

The horizon sensor has four basic components: a scanning mechanism, an optical system, a radiance detector, and signal processing electronics.

The scanning system has several variations. For a spinning satellite the simplest way is to rigidly mount the sensor on its surface. Wheel-mounted sensors use the same principle but are attached to the momentum wheel which provides the scanning motion. A slightly different approach is the scanning-wheel when other spacecraft rotating parts are not available or heavy wheels are too costly to maintain in rotation. Other methods exist which employ a rotating turret or a mirror to deflect the Sun light to the optical system. The optical system consists of a filter to limit the observed spectral band and a lens to focus the target image on the radiance detector. The radiance detector is a temperature sensitive element such as a photodiode or a pyro-electric generating a current or a voltage respectively dependent on the captured radiation. A bolometer used to detect an infrared radiation can sense temperature changes in the order of 0.001 K due to radiation despite normal ambient temperature variations up to orders of magnitude four times higher. The great sensitivity to infrared radiation allows the sensor to operate even in umbra conditions, when the visible light from the Earth is minimum. It is important to notice that due to this device sensitivity to radiation protection measures against direct Sunlight must be taken during operation. A common solution is to use Sun detectors to sense the intrusion of the Sun in the FOV while baffling the radiance detector.

The raw output of the sensor is the time interval between a reference pulse triggered by the electronics system and the instant when the radiance detector reaches or falls below a certain threshold. If the detector output is increasing across the threshold, the pulse corresponds to a dark-to-light transition or acquisition of signal (AOS). If the detector output is decreasing across the threshold, the pulse corresponds to a light-to-dark transition or loss of signal (LOS).

The AOS and LOS pulses are also referred to as in-crossings and out-crossings, or in-triggering and out-triggering, respectively. The Earth-width time ($t_w = t_{LOS} - t_{AOS}$) gives a measure of the Earth disk scanned by the sensor in one rotation. This along with the mid-scan time ($t_M = (T_{LOS} + t_{AOS})/2 - t_{REF}$) and knowledge of the scan rate, or duty cycle – percentage of scan period the radiance is above threshold – permits conversion from time to angle of the Earth relatively to the sensor frame. The angle this way determined corresponds to the elevation angle α. The azimute φ is directly retrieved from the centreline of the conical section relatively to some reference axis of the sensor.

Like the Sun sensor, the horizon sensor system outputs the angles of elevation $\hat{\alpha}$ and azimuth $\hat{\varphi}$ to the centre of the Earth in sensor coordinates $\hat{m} = [\hat{\varphi} \quad \hat{\alpha}]^T$.

In simulation the true angles are obtained in the same manner as for the sun Sensor:

$\varphi = \arctan(e_y/e_x)$ and $\alpha = \arctan\left(e_z/\sqrt{e_x^2 + e_y^2}\right)$, with $\boldsymbol{e}_h = \left[e_x \; e_y \; e_z\right]^T$ being the true Earth unit vector (or nadir) pointing to the Earth centre in sensor coordinates.

In order to obtain $\boldsymbol{e}_h$ we utilize the right hand side expression of Eq. (2.3).

During attitude manoeuvres, the centreline of the conical scanning becomes variable especially if the angular velocity has normal components to the scanning axis.

Other technologies such as the static horizon sensor are more suitable for low or non-spinning spacecraft like geosynchronous and observatory satellites, and so their interest in this context is limited.

The Earth sensor technology installed on board the SV is summarized:

- Horizon scanners with a mirror or prism scanner mechanism, providing full 4π sr angle coverage
- infrared sensitive radiance detectors to reduce the optical error due to light dispersion around the Earth's limb
- The standard deviation (σ) in nominal conditions varies with altitude, being lower for high altitudes than for low altitudes. Here we considered it to be within the 0,2° interval during all operations.
- Continuous operation altitude: from 200 Km to 140000 km

The DATA provided by this sensor shall be carefully used because during high angular speed manoeuvres and significant nutation angles the measurements might be affected by modulation comprised by the vehicle's rotational motion. The scanner ultimate accuracy should coincide with a three axis stabilized state. Therefore a noise component dependent on the SV's velocity is added in order to account appropriately for this modulation phenomenon.

Accordingly to what has been mentioned the measurement yields:

$$\widehat{m} = m + n_{HS}$$

with the total noise (n_{HS}) added modelled as follows:

$$n_{HS} = n_{HS,1} + n_{HS,2}$$

with $n_{HS} = \left[n_{\varphi}\ n_{\alpha}\right]^T$, $n_h \sim N(0, \sigma_{HS,1}^2 I_3)$ with $\sigma_{HS,1} = 0{,}2°$, and $n_{HS,2} \sim N(0, \sigma_{HS,2}^2 I_3)$, where $\sigma_{HS,2} = f.\|\boldsymbol{\omega}\|$

The value of f is such that at an angular velocity of $5°/s$ the horizon sensor experiences an additional RMS error of $0{,}5°/s$, i.e. $f = 0{,}1\ s$. The units of f are coherent with the hypothesis that this parameter behaves as an integration time of a modulation error given by $\|\boldsymbol{\omega}\|$.

C. Star Tracker

Star sensors measure star coordinates in the spacecraft frame and provide attitude information when these observed coordinates are compared with known star directions obtained from a star catalogue. Star Trackers are the most accurate of attitude sensors. The main disadvantages are their cost, weight, complexity of electronics and software for processing data, and they are typically inoperable within 30° of the Sun due to stray light.

The SV is equipped with a gimballed Star Tracker providing full determination of attitude quaternion, with the very relaxed total RMS error of 174 arc-sec compared to current technology (see Table 1). An important issue with gimballed cameras is aging of mechanical parts which degrade precision and build up biased errors with time.

The Star Tracker error is modelled by the multiplicative quaternion error according to:

$$\boldsymbol{q}_m = \delta\boldsymbol{q} \otimes \boldsymbol{q}_{true} \tag{2.4}$$

With $\boldsymbol{q}_m$ being the measured quaternion, $\boldsymbol{q}_{true}$ the true quaternion and $\delta\boldsymbol{q}$ the error quaternion. For small errors this can be approximately related to the three incremental Euler error angles: yaw ($\delta\psi$), pitch ($\delta\theta$) and roll ($\delta\varphi$) as:

$$\delta\boldsymbol{q} \approx \left[\frac{\delta\psi}{2}\ \frac{\delta\theta}{2}\frac{\delta\varphi}{2}\ 1\right]^{\mathrm{T}} = \left[\frac{\boldsymbol{a}^T}{2}\quad 1\right]^T \tag{2.5}$$

After normalization $\delta\boldsymbol{q}_{norm} = \delta\boldsymbol{q}/\|\boldsymbol{q}\|$, it becomes an error with the formal properties of a quaternion and can be inserted directly in Eq. (2.4) to obtain a realistic measurement $\boldsymbol{q}_m$. Table 2.1 resumes typical values of current Star tracker technology.

Table 2.1 – Typical performance characteristics of current Star Tracker technology

Relative Accuracy [arc-sec**]**	$\delta\varphi / \delta\theta < 2 - 5$ (1 σ) $\delta\psi < 15 - 40$ (1 σ)
Bias [arc-sec]	$\Delta\varphi$ / $\Delta\theta < 3 - 10$ (1 σ) $\Delta\psi < 1 - 10$ (1 σ)
Update Rate [Hz]	1 to 20
Field of View	8°×8° to 30°×30°

D. Frame Transformation

It is convenient to transform vectors in sensor frame coordinates to vectors in SV body coordinates. Knowledge of the mounting orientation of the particular sensor on the SV body, R_b^s allows the computation of the respective vector in body coordinates:

$$e_b = (R_b^s)^T e_s \tag{2.6}$$

The star-tracker measured quaternion is converted to the corresponding SV body quaternion by applying the following quaternion product

$$\bar{q}_b = \bar{q}_{bs} \otimes \bar{q}_s \tag{2.7}$$

For simulation purposes rotations (2.6) and (2.7) are only worth being implemented if one is to model constant sensor mounting errors, otherwise they do not have much impact on results. In fact for simplicity we assume $\bar{q}_{bs} = [0\ 0\ 0\ 1]^T$ and $R_s^b = I_{3\times3}$, which means sensor frame coincides with the body frame.

E. Gyroscope

There are two main types of gyroscope in terms of their output measurement: rate gyros (RGs) and rate-integrating gyros (RIGs). *Rate gyros* (RGs) measure spacecraft angular rates in the body coordinates:

$$\boldsymbol{\omega}^{gyr} = \left[\omega_x\ \omega_y\ \omega_z\right]^T$$

This can be integrated on-board to provide an estimate of spacecraft attitude displacement from some initial reference. *Rate integrating gyros* (RIGs) measure spacecraft angular displacements directly. Incremental displacements performed during small time intervals can be integrated resulting in the full rotation after a wider time span and also allow the computation of the instantaneous rate in each of the incremental steps. RIGs not only provide more information than the RGs as they are also more accurate. For these reasons a RIG is preferred to a RG as the angular rate sensor.

The latest gyro technology comes in the form of MEMs (Micro Electro-Mechanical Systems). These are much smaller, lighter, lower cost gyroscopes but in general outperformed by larger physical platforms.

As far as we are concerned, the technology itself is not important but rather its performance. It comprises the accuracy, measurement range, bandwidth, temperature dependence, nonlinear effects, amongst others. The first four are the most relevant for simulation purposes.

The main source of error in a RIG is drift rate instability. The systematic errors of drift, input axis misalignment, and scale error factor can be modelled and corrected. Most of the residual drift instability results from random null shifts in the torque rebalanced control loop which can also be modelled and predicted. A third type of error comes from fluctuations due to changes in the magnetic environment which are almost impossible to predict.

The typical noise affecting the RIG in the rate mode is described here by two additive terms:

- Electromechanical noise, formulated as white Gaussian noise (σ_v) on the gyro rate readings with
- Float torque derivative noise corresponding to derivative White Gaussian noise (σ_u)

The RIG output is considered to be the true angular velocity of the spacecraft plus the additive types of noise originated by the two last sources of noise mentioned:

$$n_{RIG}(t) = n_v(t) + \int_{t_0}^{t} n_u(\tau)d\tau \qquad (2.8)$$

Both $n_v(t)$ and $n_u(\tau)$ are considered Gaussian noise with zero mean, more rigorously:

$$n_v \sim N(0, \Sigma_v^2), \quad n_u \sim N(0, \Sigma_u^2), \text{ with}$$

$$\Sigma_v^2 = I_{3\times3}\sigma_v^2 \text{ and } \Sigma_u^2 = I_{3\times3}\sigma_u^2$$

Gyro measurements are a discrete event occurring at $t = nT_s$, where n is the corresponding index in discrete time. Hence Eq. (2.8) can be translated into the following discrete noise version:

$$n_{RIG}(n) = n_v(nTs) + \sum_{k=0}^{n} n_u(kTs)$$

Most gyroscope manufacturers instead of specifying the noise variance (in σ values) they much often provide ARW (Angle Random Walk) and RRW (Rate Random Walk) values, which relate to their corresponding σ values as follows:

$$\sigma_v = \frac{ARW}{\sqrt{T_s}}$$

$$\sigma_u = RRW\sqrt{\frac{3}{T_s}}$$

These values are dependent on the gyro technology. For instance for the ARW, it can range from a thousand of $1°/h^{1/2}$ (high precision) to almost $1°/h^{1/2}$ (coarse). Typical values for high accuracy gyro according to [2] are:

$$ARW = 0.22\, arcsecs/s^{1/2} = 0{,}0037°/h^{1/2}$$

$$\mathrm{RRW} = 4.7 \times 10^{-5}\, arcsecs/s^{3/2} = 0{,}0028°/h^{1/2}$$

Their corresponding standard noise deviation values with $T_s = 0{,}1\ s$ are:

$$\sigma_v = 0{,}6957\ arcsec/s$$
$$\sigma_u = 2{,}5743 \times 10^{-4}\ arcsec/s^2$$

Due to the RRW term, rate drift will build up in the gyroscope. After some time (hours, days) this will be the main cause of error in the angular rate measurement. However certain gyroscope technologies applying feedback mechanisms guarantee a limit in drift influence. In such cases RRW can be neglected after some time.

Additionally unknown bounded bias always exist which can be regarded as a constant drift. The bias effect should be known prior to launch or estimated in orbit, as its influence on added error to the measurement might often be larger than the noise itself. In Chapter 3 an estimation process for bias (or constant drift) is included alongside with attitude estimation, enabling correction of the gyro zero reference.

F. Actuators

Various classes of actuators for reorientation or stabilization of a spacecraft are available: control moment gyros, momentum or reaction wheels, gas thrusters, ion thrusters or extension booms.

Reaction wheels were selected for fine control during most of the operations. Gas thrusters provide redundancy and for situations where it is necessary to damp high angular velocities, or to provide compensating actuation during reaction wheels resetting operation.

G. Reaction Wheels

The storage momentum capacity of a wheel ranges from 0.4 to 40 kg.m^2/s typically and can be achieved either with a small fast spinning wheel or with a large low spinning one. For reasons of weight minimization designers tend to favour the former type, though this has the disadvantage of greater wear on the bearings. Table 2.2 shows manufacturers reaction wheel parameters.

Table 2.2 – Examples of reaction wheel characteristics

Manufacturer	Spacecraft	Mass (Kg)	Moment of Inertia $kg.m^2$)	Speed Range (RPM)	Angular Momentum ($kg.m^2/s$)
APL	Geos-3, 5AS-1	3,18	0,0115	2000	2,41 @ 2000 RPM
Bendix	AYE	8,84	0,0880	1450	11,52 @ 1250 RPM
	NIMBUS	7,78	0,0034	1400	0,04451 @ 1250 RPM
	OAO SERIES	5,13	0,0297	900	2,8 @ 900 RPM
RCA	AE SERIES, ITOS SERIES	16,66	3,4804 14,43	95-382 120-160	128,03 @ 353,32 RPM

Because reaction wheels are operated with nominally zero momentum, they are used primarily for fine pointing in a closed loop control fashion, absorbing cyclic torques, to temporarily store momentum from the body during slew or reorientation manoeuvres.

As the satellite faces nonzero mean disturbance torques the reaction wheels have to maintain constant actuation to compensate for. This will eventually saturate the momentum storage capacity; hence provision is made for periodic momentum damping through external torques produced by gas jets or magnetic coils. These are both considered external torques because contrary to internal ones they do change the vehicle total angular momentum.

Although three orthogonal wheels are sufficient to provide full attitude control, normally a fourth wheel is employed giving one degree of redundancy allowing for momentum management and provision against failure of one of the other three.

The reaction wheel model comprise modelling of the electromagnetic torque and friction characteristics A reaction wheel uses an electric motor to transform voltage into torque. Each type of motor has its own relation between generated torque, command voltage and rotor speed which is equal to the wheel speed.

A two-phase induction motor is assumed for the SV, which is driven by square pulses. More precisely the torque level is controlled by varying the duty cycle within the interval [-1, 1] which in turn is set by the control voltage. A linear relation between duty cycle and control voltage is typically desirable. However in reality this is not the case as the electronics face a 'dead zone' near the origin, like the one depicted in Figure 2.3 for the positive side – the dead zone width is exaggerated for purposes of illustration. When large enough the dead zone will impact significantly on the pointing accuracy. We consider a dead zone of $X_{dc} = 0{,}001$.

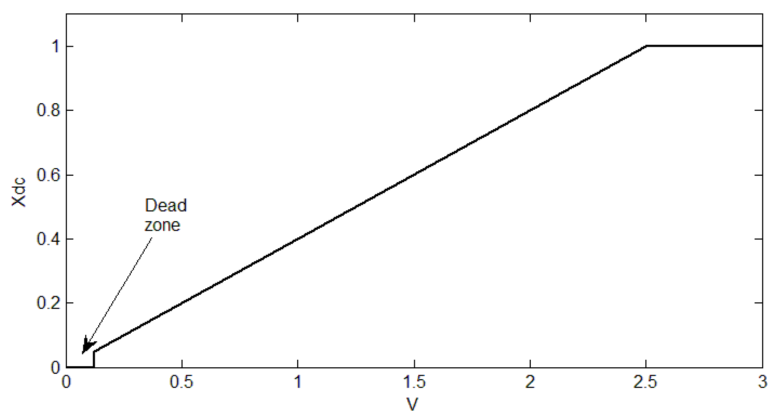

Figure 2.3 - Duty cycle as a function of control voltage

The net torque on the wheel is given by:

$$M = X_{dc} M_{em} - M_{friction} \tag{2.9}$$

Where M_{em} is the electromagnetic torque when the duty cycle is unity, $M_{friction}$ is the bearing friction torque dependent on the wheel speed (s). The electric motor technology – DC or AC, synchronous or asynchronous – defines the dependence of M_{em} with the wheel speed. The model chosen follows the approximation given in [1].

$$M_{em} = 2M_0\alpha r(\alpha^2 + r^2)^{-1} \tag{2.10}$$

Where $r = 1 - s/s_{max}$ for $X_{dc} > 0$, $r = 1 + s/s_{max}$ for $X_{dc} < 0$. s_{max} is the synch speed, α is the value of r for which M_{em} has the maximum magnitude, M_0. Admitting this simplified but approximate model, a maximum wheel speed is established in 1500 rpm, and the speed for maximum torque is fixed in 500 rpm. The resulting torque curve as a function of wheel speed is depicted in Figure 2.4. We see that the electromagnetic torque has values superior to $0{,}6M_0$ for speeds ranging from -1500 rpm up to more than 1000 rpm, meaning that for most of the operational situation there will be torque available in the wheels system.

The friction torque is simply modelled as the sum of Coulomb and viscous terms:

$$M_{friction} = M_c.sgn(s) + f.s \tag{2.11}$$

The constants M_c and f are different for each reaction wheel in use, but they are normally dependent on their size, weight and area of contact of its beam. The torque friction always opposes the rotation motion, therefore dissipating energy in form of heat. This can become a problem especially for high operational speeds because the dissipative rate is proportional to the square of the speed (factor $f.s^2$), depleting the batteries much faster. Moreover if these cannot be recharged for any reason during long periods, it is of utmost importance to keep the wheels working near the zero speed point.

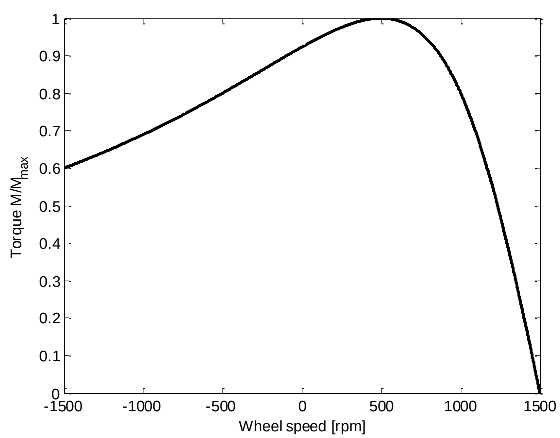

Figure 2.4 - Torque-speed curve of the reaction wheel

More accurate and realistic models do exist though in practice the simple Coulomb term is normally sufficient to emulate the nonlinearity near zero speed. The wheel parameters chosen are listed in Table 2.3.

Table 2.3 – Reaction Wheels nominal parameters

I^w [kg. m^2]	M_0 [N. m]	M_c [N. m]	f [$N.m.s/rad$]	s_{max} [RPM]	s_0 [RPM]
0,038	7,1628	$7{,}06 \times 10^{-3}$	$1{,}21 \times 10^{-3}$	1500	500

We consider the reaction wheels to have the shape of a perfect disc which means that the inertia about its rotation axis is given by $I^w = \frac{1}{2}m_w {r_w}^2$ and that a value of $r_d = 0{,}2\ m$ is realistic we retrieve that the mass of the disc is $m_d = 1{,}9$ kg. Therefore a four wheels set has a total mass of 7,6 kg. This is important in order to set an appropriate and realistic SV inertia matrix, which is done in the end of this chapter.

H. Gas Thrusters

Thrusters or jets produced thrust by expelling propellant in the opposite direction. Torque is generated as the thrust is decentred and applied at a certain distance from the spacecraft centre of mass as given by the following equation:

$$\boldsymbol{M} = \boldsymbol{T} \times \boldsymbol{b} \tag{2.12}$$

where $\boldsymbol{M}$ is the applied torque vector due to one thruster, $\boldsymbol{T}$ is the thrust force vector and $\boldsymbol{b}$ is the lever arm vector from the SV centre of mass to the gas jet exit.

Thrust torques aim for five principal functions: attitude control, spin rate control, nutation control, resetting of wheels or control gyros. Orbits readjustments in general are carried out by the main propulsion system which is made typically independent of the attitude thrusters.

There are two main types of gas jets employed in satellite orientation, namely cold gas and hot gas. The former is superior in performance whereas the latter is more consistent and reliable. Technology already available permits combination of the high thrust level of the hot jets with the trustworthiness of the cold ones. Hot jets rely on a chemical reaction typically generating thrust levels over 5 N. Thrust impulses can be made very small for precise control by firing in a spaced pulse mode.

Two thruster modes will be considered: the continuous thruster and the pulse thruster. The former functions as a linear actuator providing the requested torque from the controller, whereas the latter triggers in a pulse mode providing increments of angular impulse.

In simulations there is freedom to change thruster's parameters in order to put to the test the robustness of the control strategy. The SV inertia and the required manoeuvrability will ultimately dictate the amount of available control needed, implying that the thrust and lever arm must be dimensioned accordingly and realistically. The parameters selected for the SV thrusters are presented in 2.4.

Table 2.4 – Thruster parameters

b	T_{max}	M_{max}	Period	Quantization step
$0{,}5\ m$	$1\ N$	$0{,}5\ N.m$	$0{,}1\ s$	$0{,}01\ N.m$

In order to emulate the impulse characteristic of the thrusters, a coarse quantization is performed to the requested control momentum. Therefore the constant magnitude pulse with varying width is replaced by an equivalent constant width pulse with varying magnitude. The main objective is to convey the impact of a non-ideal coarse actuator on accuracy and transient response near the target attitude where small incremental impulses are required. The quantization considered divides the thruster's control input in $n = 201$ values, from -1 to 1 in 0,01 steps. For instance a value of $0{,}014\ N.m$ is clipped to $0{,}01\ N.m$, whereas a value of $0{,}018\ N.m$ is rounded up to $0{,}02\ N.m$.

Attitude thrusters are actually paired in order to minimize increments of linear momentum that cause undesired orbit changes. Therefore the actual maximum momentum about each axis is $2M_{max}$.

The limited propellant supply is a major limitation on the use of such systems. Dimensioning the fuel budget is an important part of the mission planning but it will not be done in this work.

I. Determining Position

The need to determine the Sun and Earth vector in Earth Centred Inertial (ECI) coordinates poses the problem of updating the satellite's position regularly. There are mainly two solutions to it:

- Use of tracking stations on Earth to monitor the satellite's orbit. The information is then sent via uplink to the satellite
- Use of GPS receiver on board

The first one is obviously more expensive as it requires the service of a network of dedicated or shared grounding stations which provide a tracking and uplink service, and it might be mandatory to install dedicated antennas to receive the signal.

On the other hand [7] proves usefulness of GPS signals for determining position of the satellite in its orbit from Low Earth Orbit (LEO) to geosynchronous altitudes. A GPS receiver for LEO is sufficient to ensure signal strength and reliability, but still there is room to explore High Earth Orbit (HEO) adapted receivers. In recent years most satellites operated with conventional LEO receivers and its reliability has been both experimentally and operationally consistent. Therefore the SV is considered to rely on the GPS system to obtain its position in ECI with an error modelled as additive Gaussian noise:

$$\widehat{\boldsymbol{p}}_{GPS} = \boldsymbol{p}_{ECI} + \boldsymbol{n}_{GPS} \tag{2.13}$$

where $\boldsymbol{n}_{GPS} \sim N(0, \sigma_{GPS}^2)$ having $\sigma_{GPS} = 10\ m$

In reality this value is a little conservative given current GPS technology, which guarantees that the simulation results are not masked by an over-performance of this sensor.

2.2. Orbit Conditions

A. Keplerian Orbits

Newton's laws are used to model the dynamics of translational motion of the satellite about the Earth centre. Regarding artificial satellites orbiting the Earth the contribution of the mass of the satellite (m) to the gravitational force can be neglected because of its much smaller order of magnitude compared to the Earth mass. The orbital dynamics is accordingly given by:

$$\ddot{\boldsymbol{r}} = -\frac{\mu}{r^3}\boldsymbol{r} \tag{2.14}$$

with $\mu = GM$ being the constant gravitation of the Earth, $\boldsymbol{r}$ being the SV position relatively to the Earth centre in ECI coordinates, and r its norm or equivalently the distance to the Earth centre.

It is assumed that the satellite is a point mass and the Earth is a perfectly spherical object. Typical perturbations to this idealistic model, such as the Earth's oblateness, third body interactions, drag due to solar wind and aerodynamic forces due to atmosphere interference are not introduced in the framework as the main concern is attitude control.

Solutions to Newton's law for the two body problem constitute the orbit which is well-known to be a conic section. The solutions depends only on launching conditions, namely initial position and velocity vectors. Once these two quantities are established one can determine the ideal Keplerian orbit for all time instants using the classical orbital parameter description as in [4].

For simulation purposes it is important to note that finite numerical precision on the integration of Eq. (2.14) constitutes a source of error which tends to increase with simulation time.

B. Viewing and Lighting Conditions

An important factor regarding attitude acquisition sensors such as the Sun sensor and Horizon sensor is viewing conditions to the Sun and Earth respectively.

There is the possibility that the Earth get in front of the Sun, blocking the Sunlight necessary to measure the Sun angle. Two particular situations can occur: transit and occultation. Transit is the passage of the satellite in front of the disk of a planet as seen by the observer. Occultation is the passage of the satellite behind the disk. The geometry that leads to the aforesaid configurations is illustrated on Figure 2.6.

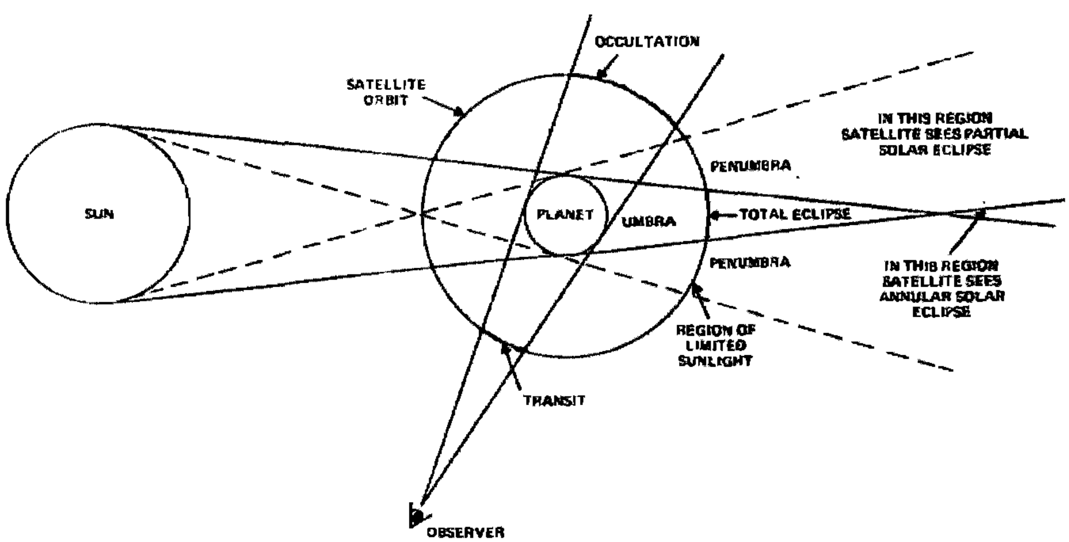

Figure 2.6 - Planar geometry for viewing and lighting conditions for the Sun, planet, satellite and observer

The umbra is the region behind the planet where the satellite is completely shadowed from the Sun. In the vicinity of the umbra lies the penumbra, the region where the satellite partially sees the Sun disk, causing its illumination to be reduced.

In practice because the Sun angular width is small compared to the Earth width for Earth orbiting spacecraft, for simulation purposes considering the Sun as a point largely simplifies the lighting conditions evaluation and still keeps the necessary realism. Therefore the conditions for transit and occultation, which are now derived constitute a fairly good description. Let $\boldsymbol{X}$ be a vector from the Sun to the SV, $\boldsymbol{P}$ be a vector from the Sun to the centre of the Earth, and $R_{\oplus}$ be the radius of the Earth.

The satellite is in transit relatively to the Sun whenever:

$$\rho_{\oplus} > arccos\left(\frac{\boldsymbol{P}.\boldsymbol{X}}{\|\boldsymbol{P}\|.\|\boldsymbol{X}\|}\right) \quad \text{and} \quad X < P$$

On the other hand 0ccultation occurs when:

$$\rho_{\oplus} > arc\cos\left(\frac{\boldsymbol{P}.\boldsymbol{X}}{\|\boldsymbol{P}\|.\|\boldsymbol{X}\|}\right) \quad \text{and} \quad X > P$$

For simulation purposes the quantity $\frac{\boldsymbol{P}.\boldsymbol{X}}{\|\boldsymbol{P}\|.\|\boldsymbol{X}\|}$ is badly conditioned so in alternative we use the infinite light source distance approximation which renders evaluation of a different quantity. Let $\boldsymbol{s}_p$ be the position of the Sun (observer) relatively to the Earth and $\boldsymbol{d}$ the normal component of the SV position relatively to the Earth:

$$\boldsymbol{d} = \boldsymbol{r} - \left(\frac{\boldsymbol{s_p}}{\|\boldsymbol{s_p}\|}\cdot\frac{\boldsymbol{r}}{\|\boldsymbol{r}\|}\right)\boldsymbol{r}$$

This way condition $\rho_p > arc\cos\left(\frac{\boldsymbol{P}.\boldsymbol{X}}{\|\boldsymbol{P}\|.\|\boldsymbol{X}\|}\right)$ is replaced by $R_{\oplus} > \|\boldsymbol{d}\|$. Whenever this inequality is true the Sun sensor is disabled and so no Sun vector measurement is available.

C. Model of the Sun Position in ECI

The Earth revolves around the Sun in an ellipse of eccentricity $e = 0{,}016751$. Because of this relatively low value a circular orbit is sufficient to capture the essence of its trajectory. Also there is no point in adding a more accurate Earth orbit description once its role in the following development is unimportant. The orbit radius is considered equal to the mean distance from the Earth to the Sun:

$$r_c = 1\,UA = 149597870700\,m$$

Therefore the Earth trajectory in the ecliptic frame is modelled by

$$\boldsymbol{r}_E^{ec} = r_c\begin{bmatrix}\cos\nu\\ \sin\nu\\ 0\end{bmatrix} \qquad (2.15)$$

where $\nu = \frac{2\pi}{T}t$, with T the orbital period (365,25636 days) and t the time elapsed since vernal equinox. With this choice the transformation from the ecliptic frame to the ECI frame is a rotation $R_z(\pi)$ followed by a rotation $R_x(i_e)$, where $i_e = 23.4°$ is the inclination of the ecliptic relatively to the Earth equator.

$$\boldsymbol{r}_E^{ECI} = r_c R_x(i_e) R_z(\pi)\boldsymbol{r}_E^{ec} \qquad (2.16)$$

$$\boldsymbol{r}_E^{ec} = r_c \begin{bmatrix} \cos\nu \\ \cos i_e \sin\nu \\ \sin i_e \sin\nu \end{bmatrix} \boldsymbol{r}_E^{ec} \tag{2.17}$$

2.3. Attitude Kinematic and Dynamics

In this work, the quaternion parameterization is used to represent the attitude of the single SV. This has been extensively used in the literature because it yields no singularities as opposed to other parameterizations such as Euler angles or rotation matrixes (see [10] for details). The quaternion properties and kinematics are presented in Appendix A.

Let the quaternion $\bar{q}$ represent the orientation of the rigid body with respect to a reference frame. The kinematics of the quaternion is governed by the following differential equation:

$$\dot{\bar{q}} = \frac{1}{2}\Omega(\boldsymbol{\omega})\bar{q} \tag{2.18}$$

dependent on the instantaneous angular velocity through $\Omega(\boldsymbol{\omega})$ defined as:

$$\Omega(\boldsymbol{\omega}) = \begin{bmatrix} -[\boldsymbol{\omega}\times] & \boldsymbol{\omega} \\ -\boldsymbol{\omega}^T & 0 \end{bmatrix} \tag{2.19}$$

Once established the kinematic equations of motion the focus turns now to the dynamics which relates the motion to the moments applied to the satellite. The satellite is assumed to behave approximately like a rigid body in free space housing three or four reaction wheels allowed to rotate in a fixed axis with respect to the satellite. Such system obeys the well-known rigid body mechanics with additional terms due to the reaction wheels inclusion. Hence the total angular momentum of the entire satellite is given by:

$$\boldsymbol{H} = I\boldsymbol{\omega} + \boldsymbol{h_r} \tag{2.20}$$

with $\boldsymbol{H}$ being the total angular momentum, I the inertia matrix of the satellite including the wheels, and $\boldsymbol{h_r}$ the additional momentum provided by the rotation of the reaction wheels:

$$\boldsymbol{h_r} = \sum_{\boldsymbol{i}}^{\boldsymbol{n}} I_i^w \boldsymbol{e}_i.\omega_i^w = [I_1^w \boldsymbol{e}_1 \quad \dots \quad I_n^w \boldsymbol{e}_n].\boldsymbol{\omega}^w = W^I \boldsymbol{\omega}^w \tag{2.21}$$

where I_i^w is the moment of inertia of the i^{th} wheel with respect to its axis of rotation given by versor $\boldsymbol{e}_i$, $\boldsymbol{\omega}^w$ is a vector whose elements are the rotational speeds of each of the n wheels ω_i^w, and $W^I = [I_1^w \boldsymbol{e}_1 \quad \dots \quad I_n^w \boldsymbol{e}_n]$ is the inertia matrix of the wheels set. The time derivative of $\boldsymbol{H}$ relatively to an inertial referential equals the external applied torque, resulting in the dynamic equations of motion, which can be written in the body frame coordinates as:

$$\boldsymbol{M} = \left(\frac{d\boldsymbol{H}}{dt}\right)^i = \left(\frac{d\boldsymbol{H}}{dt}\right)^b + \boldsymbol{\omega} \times \boldsymbol{H} \tag{2.22}$$

The term $\left(\frac{d\boldsymbol{H}}{dt}\right)^b$ is the derivative relatively to the body frame. The term $\boldsymbol{\omega} \times \boldsymbol{H}$ comprises the gyroscopic effect which accounts for the fact that the satellite is in rotation relatively to the inertial frame. Vectors in Eq.

(2.22) are conveniently written in the body frame as it will be seen ahead. Substitution of the expression of $\boldsymbol{H}$ in the above equation yields:

$$\left(\frac{d\boldsymbol{H}}{dt}\right)^{i} = \left(\frac{d}{dt}(I\boldsymbol{\omega} + \boldsymbol{h_r})\right)^{b} + \boldsymbol{\omega} \times (I\boldsymbol{\omega} + \boldsymbol{h_r}) \tag{2.23}$$

Resolving terms:

$$\left(\frac{d\boldsymbol{H}}{dt}\right)^{i} = I\dot{\boldsymbol{\omega}} + \boldsymbol{\omega} \times I\boldsymbol{\omega} + \left(\frac{d}{dt}\boldsymbol{h_r}\right)^{b} + \boldsymbol{\omega} \times \boldsymbol{h_r} \tag{2.24}$$

The first two terms in Eq. 190 correspond to the contribution of the entire body of the satellite as a rigid body including reaction wheels (at zero rotational speed), whereas the third and fourth terms account for the effect of the rotation of the wheels. The term $\left(\frac{d}{dt}\boldsymbol{h_r}\right)^{b}$ can be rewritten as the following:

$$\left(\frac{d}{dt}\boldsymbol{h_r}\right)^{b} = \frac{d}{dt}(W^{I}\boldsymbol{\omega}^{w}) = W^{I}\dot{\boldsymbol{\omega}}^{w} + \boldsymbol{\omega}^{w}\frac{d}{dt}W^{I} \tag{2.25}$$

The moments of Inertia I_i^w and their respective wheels' axes are constant relatively to the satellite's body as this was the frame of reference chosen, hence $\frac{d}{dt}W^{I} = 0$. Thus the last term in Eq. (2.25) is eliminated

$$\left(\frac{d}{dt}\boldsymbol{h_r}\right)^{b} = W^{I}\dot{\boldsymbol{\omega}}^{w} \tag{2.26}$$

Eq. (2.22) can be rewritten by replacing $\left(\frac{d\boldsymbol{H}}{dt}\right)^{i} = \boldsymbol{M}$, using Eq. (2.26) and isolating the term $\dot{\boldsymbol{\omega}}$:

$$\dot{\boldsymbol{\omega}} = I^{-1}(\boldsymbol{M} - \boldsymbol{\omega} \times I\boldsymbol{\omega} - W^{I}\dot{\boldsymbol{\omega}}^{w} - \boldsymbol{\omega} \times W^{I}\boldsymbol{\omega}^{w}) \tag{2.27}$$

Eq. (2.27) is a nonlinear differential equation that can be directly implemented in simulation. The reaction wheels respond to the control system via $\dot{\boldsymbol{\omega}}^{w}$. Wheels acceleration is provided by the wheels net applied torque, $\boldsymbol{M}^{w} = [M_1^w \quad M_2^w \quad M_3^w \quad M_4^w]^T$, which ultimately constitutes the control input variable:

$$I_i^w \dot{\omega}_i^w = M_i^w \tag{2.28}$$

Making the common assumption that all wheels are identical then:

$$I^{w}\dot{\boldsymbol{\omega}}^{w} = \boldsymbol{M}^{w} \tag{2.29}$$

Thus the input term can be rewritten as $W^{I}\dot{\boldsymbol{\omega}}^{w}$ as

$$W^{I}\dot{\boldsymbol{\omega}}^{w} = W^{a}\boldsymbol{M}^{w} \tag{2.30}$$

where W^{a} is defined as the wheels axes matrix: $W^{a} = \frac{W^{I}}{I^{w}}$

The inertia matrix value for the SV is dimensioned as if the SV inertia corresponded to the one of an equivalent cylinder with radius r_S, height h_S and mass m_s. Considering the z-axis coincident with the symmetry-rotation axis it renders the following expression for the SV inertia matrix:

$$I = \begin{bmatrix} \frac{1}{12}m_s\left(3{r_s}^2 + {h_s}^2\right) & 0 & 0 \\ 0 & \frac{1}{12}m_s\left(3{r_s}^2 + {h_s}^2\right) & 0 \\ 0 & 0 & \frac{1}{2}m_s{r_s}^2 \end{bmatrix}$$

The selection of these values shall be realistic and according to the previously dimensioned wheels and thruster lever arm. Thus we establish $m_s = 150\ kg$, $r_s = 0{,}4\ m$ and $h_s = 1\ m$, resulting in the following SV inertia matrix about its centre of mass and including reaction wheels:

$$I = \begin{bmatrix} 18{,}5 & 0 & 0 \\ 0 & 18{,}5 & 0 \\ 0 & 0 & 12 \end{bmatrix} kg.m^2$$

We conclude this section by reflecting on the nature of the external moment $\boldsymbol{M}$. This includes all external moments applied to the satellite which include the control moment by the aforesaid gas thrusters and disturbance torques due to uncontrolled causes. Among these the most common are: gravity gradient torque, asymmetric solar radiation pressure on the satellite's surfaces, aerodynamic torques at low altitudes, and magnetic torques due to the Earth magnetic field.

3. Attitude Estimation

3.1. Initial Considerations

Like any other navigation problem, satellite navigation poses the need of acquiring position and orientation relatively to a certain frame of reference. For the case of a single SV it is also generally necessary to obtain its angular velocity.

A state space representation is a mathematical model that describes the behaviour of a given system by differential equations. State space refers to the algebraic space whose coordinated axes are the state variables. State estimation is the process of retrieving an estimate of the true state.

Regarding attitude one is particularly interested in estimating the quaternion attitude ($\bar{q}$) and the angular velocity ($\boldsymbol{\omega}$) provided the Sun vector, the nadir or the Star Tracker quaternion. The angular velocity readings from the gyro as well as the Star Tracker quaternion constitute themselves direct estimates. However knowledge of the dynamics can provide estimates in periods where new sensor readings are not yet available and most important it allows for reduction of sensor errors. Furthermore, and contrary to deterministic methods, state estimation does not require full information to output an estimate. This capability allows for integration of multiple readings at different rates and from independent sensors; no synchrony is required between them. Thus data fusion becomes rather simple and in the event of sensor failure, though accuracy might be reduced, the estimation flow is not compromised.

Deterministic methods are an alternative solution to estimation. They are simple to interpret physically and geometrically. However they are algebraically cumbersome and difficult to model for biases and time-varying parameters. Large sets of data are difficult to combine with the proper statistical balance.

In contrast state estimation can provide statistically optimal solutions. It is relatively easy to expand the state vector to represent a wide range of related attitude parameters, such as biases, model perturbations, orbit parameters and time-varying coefficients. The major disadvantage of state estimation processes are the possibility of divergence and occasionally they require initial guesses that are more accurate than for deterministic methods.

In practice both solution methods are frequently used in a complementary fashion. The deterministic method is often used to obtain a priori estimate which is used as the initial guess in the estimator. Moreover, supervision of the filter can be performed by comparison of values with deterministic results.

One of the most successful estimation techniques in a wide range of fields is the **Kalman Filter (KF)**. It is a relatively simple algorithm to implement yet devoted to linear systems. The **Extended Kalman Filter (EKF)** constitutes an adaptation to nonlinear systems estimation. It is particularly well suited algorithm for attitude estimation of the nonlinear SV system once its dynamics present soft nonlinearities as the angular velocities found in practice are generally low. The quaternion representation however reserves a few subtleties as we shall see in the sequel.

In this work two strategies for obtaining attitude data are utilized: the first is a deterministic method consisting in the q-method solution of the Wahba's problem. The second is a **Multiplicative Extended Kalman Filter** (**MEKF**) for quaternion and gyro drift estimation

3.2. An Attitude Deterministic Method – The Wahba's problem

Regarding attitude the Wahba's problem is a well-known classical solution [11]. It computes an optimal estimate given at least two measurement pairs of vectors. Specifically two line of sight (LOS) vectors available to the SV are the Sun vector and the nadir. –

Generally speaking, suppose that we have access to two unit vector $\boldsymbol{b}_1$ and $\boldsymbol{b}_2$ measured in the spacecraft body frame. Each of these unit vectors contains two independent scalar pieces of information. It is also necessary to know the components of the two measured vectors $\boldsymbol{r}_1$ and $\boldsymbol{r}_2$ in some reference frame. The reference frame is obviously chosen to be ECI frame, though this is not mandatory. One can use a rotating frame such as the orbit normal referenced frame or the local vertical. The attitude parameterization of this method is the attitude matrix (A) defined as the matrix that rotates vectors from the reference frame to the spacecraft body frame. According to [11], we seek an attitude matrix such that:

$$A\boldsymbol{r}_1 = \boldsymbol{b}_1 \tag{3.2.1}$$

$$A\boldsymbol{r}_2 = \boldsymbol{b}_2 \tag{3.2.2}$$

Combining both expressions yields

$$\boldsymbol{b}_1.\boldsymbol{b}_2 = A\boldsymbol{r}_1.A\boldsymbol{r}_2 = \boldsymbol{r}_1.\boldsymbol{r}_2 \tag{3.2.3}$$

This equality is true for error free measurements; however in the presence of errors this is not generally true. The equivalent happens for (3.2.1) and (3.2.2), where matrix A might not be equal in both relations if errors exist.

The earliest algorithm for determining SV attitude from two vector measurements was the TRIAD algorithm; a very simple method but that does not treat the information in the two observations optimally. Wahba introduced a loss function such that its minimization renders the proper and orthonormal matrix A.

$$L(A) \equiv \frac{1}{2}\sum_i a_i |b_i - Ar_i|^2 \tag{3.2.4}$$

Where $\{\boldsymbol{b}_i\}$ is the set of unit vectors measurements in the SV body frame and $\{\boldsymbol{r}_i\}$ is the corresponding unit vectors in the reference frame, $\{a_i\}$ are non-negative weights which should be selected beforehand. An adequate choice is to assign the inverse of the standard deviation of the corresponding sensor, i.e. $a_i = 1/\sigma_i$.

Notice that the number of vector measurements is not limited to two measurements as mentioned before. Indeed it might comprise any larger set, so additional observations can be inserted and contribute with information for attitude determination.

The loss function in (3.2.4) can be rewritten as:

$$L(A) = \sum_i a_i - tr(AB^T) \tag{3.2.5}$$

where

$$B = \sum_i a_i \, \boldsymbol{b}_i \boldsymbol{r}_i^T \tag{3.2.6}$$

Therefore minimization of (3.2.5) comes down to maximization of $tr(AB^T)$. The original solutions solve for the attitude matrix A directly, but most practical applications have been solving for the attitude quaternion through Davenport's q-method [12] which is of greater interest. We present it here.

Making the quaternion attitude appear in expression $tr(AB^T)$, through $A = A(\bar{q}) = (q_4^2 - |\boldsymbol{q}|^2)I_{3\times3} + 2\boldsymbol{q}\boldsymbol{q}^T - 2q_4[\boldsymbol{q}\times]$ and evolving it renders:

$$tr(AB^T) = \bar{q}^T K \bar{\bar{q}} \tag{3.2.7}$$

where K is the symmetric traceless matrix:

$$K = \begin{bmatrix} B + B^T - Itr(B) & \sum_i a_i b_i \times r_i \\ \sum_i a_i (b_i \times r_i)^T & tr(B) \end{bmatrix} \tag{3.2.8}$$

Clearly minimization of $L(A)$ is equivalent to maximization of the modified function $L'(\bar{q})$

$$L'(\bar{q}) = \bar{q}^T K \bar{q} \tag{3.2.9}$$

The extrema of L' subject to the normalization constrain $\bar{q}^T\bar{q} = 1$ is found by the method of Lagrange multipliers. We define the corresponding Lagrange auxiliary function

$$G(\bar{q}) = \bar{q}^T K \bar{q} - \lambda(1 - \bar{q}^T \bar{q}) \tag{3.2.10}$$

where λ is the Lagrange multiplier. Now $G(\bar{q})$ is maximized without constrain, and λ is satisfied to normalization constrain. Differentiating Eq. (3.2.10) and equalling to zero, one obtains the eigenvector equation

$$K\bar{q} = \lambda\bar{q} \tag{3.2.11}$$

The solution is a quaternion that is an eigenvector of K. Substituting (3.2.11) into (3.2.9) results $L'(\bar{q}) = \bar{q}^T \lambda \bar{q} = \lambda$. T Thus the q-method finds the optimal quaternion estimate as the normalized eigenvector with the largest eigenvalue:

$$K\bar{q}_{opt} = \lambda_{max}\bar{q}_{opt} \tag{3.2.12}$$

There is no solution when the two eigenvalues of K are equal. This is not a failure of the q-method, rather it means the data are not sufficiently rich to determine the attitude uniquely. It can be shown that when at least two of the vectors b_i are not collinear, the eigenvalues of K are distinct and therefore this procedure yields an unambiguous quaternion.

The application of this algorithm carries a subsequent operation because the optimal attitude has two possible quaternion representations. Therefore if one leaves the q-method to compute $\bar{q}_{opt}$ without any supervision it is most certain that discontinuities will occur via change of sign. Such changes in the point of view of an external observer appear as sudden jumps which might generate discontinuities downstream the overall control system.

In order to counteract this undesired behaviour every time new observations are available the q-method based estimator must compare the new estimate value with the previous one. It is expected that this estimates do not differ largely from one another if the sampling period is small enough. Thus if the difference is larger than a fixed amount the optimal quaternion is changed to its dual representation:

$$if\ \left\|\bar{q}_{opt_k} - \bar{q}_{opt_{k-1}}\right\| > \text{Threshold: do } \bar{q}_{opt_k} = -\bar{q}_{opt_k}$$

A different solution is to use one-half of the quaternion set, say for instance the quaternions which have a positive scalar component, i.e.

$$\bar{q}_{opt} \in \bar{q}: q_4 \geq 0$$

Nevertheless with this quaternion subset there is still ambiguity for quaternions with scalar part $q_4 = 0$, reason being the first solution was adopted.

To finish this determination algorithm the measurement weights must be dimensioned. One typical approach is to use the inverse of the standard deviation of the corresponding measurement:

$$a_i = {}^{1}\!/_{\sigma_i} \tag{3.2.13}$$

Despite the attitude covariance estimates were not derived, one can argue that they are dependent on the particular orientation between the two sensors. Similarly to what happens with the TRIAD algorithm, the Wahba problem solution gives better estimates when the quantities $\|\boldsymbol{b}_1 \times \boldsymbol{b}_2\|$ and $\|\boldsymbol{r}_1 \times \boldsymbol{r}_2\|$ are maximized (i.e. close to 1) then when they drop to lower values. So in a hypothetical but realistic situation where the SV finds the nadir near alignment with the Sun line, small errors in the LOS vector quantities translate into large errors in the attitude quaternion. Hence the system must be aware of the degree of uncertainty present in the estimate by assessing the current line of sight configuration.

3.3. Kalman Filtering

The Kalman Filter equations are presented in Appendix B. They are only repeated for the attitude estimator because it constitutes a particular variant of the EKF common frame operations as we will see. For angular velocity estimation, the necessary quantities to use in the Extended Kalman filter are computed, namely the propagation matrix and the observations sensitivity matrix.

A. Extended Kalman Filter for Angular Velocity Estimation

Dynamics Model

Eq. (2.27) governs the dynamics of $\boldsymbol{\omega}$. The discrete version of this equation is relatively straightforward to obtain considering the following approximation:

$$\dot{\boldsymbol{\omega}} \approx \frac{\boldsymbol{\omega}(t+\Delta t) - \boldsymbol{\omega}(t)}{\Delta t} \tag{3.3.1}$$

Resorting to the following notation: $\boldsymbol{\omega}_k = \boldsymbol{\omega}(t)$ and $\boldsymbol{\omega}_{k+1} = \boldsymbol{\omega}(t+\Delta t)$ and after little algebra, we get the discrete version of the dynamics $\omega_{k+1} = f\left(\boldsymbol{\omega}_k, \boldsymbol{h}_r, \left(\frac{d}{dt}\boldsymbol{h}_r\right)^{\boldsymbol{b}}\right)$ as:

$$\omega_{k+1} = -I^{-1}\Delta t(\boldsymbol{\omega}_k \times I\boldsymbol{\omega}_k + \boldsymbol{\omega}_k \times \boldsymbol{h}_r) + I^{-1}\Delta t\left(M - \left(\frac{d}{dt}\boldsymbol{h}_r\right)^b\right) + \boldsymbol{\omega}_k \tag{3.3.2}$$

The propagation matrix $\Phi_k = \frac{\partial f}{\partial \omega_k}$ needs to be computed for the propagation of the covariance matrix.

$$\Phi_k = -I^{-1}\Delta t\left(\frac{\partial}{\partial \omega}(\boldsymbol{\omega}_k \times I\boldsymbol{\omega}_k) + \frac{\partial}{\partial \omega}(\boldsymbol{\omega}_k \times \boldsymbol{h}_r)\right) + \frac{\partial}{\partial \omega}\boldsymbol{\omega}_k$$

The first term in brackets decomposes into two terms:

$$\frac{\partial}{\partial \omega}(\boldsymbol{\omega} \times I\boldsymbol{\omega}) = \frac{\partial}{\partial \omega}\boldsymbol{\omega} \times I\boldsymbol{\omega} + \boldsymbol{\omega} \times \frac{\partial}{\partial \omega}(I\boldsymbol{\omega}) = I_{3\times 3} \times I\boldsymbol{\omega} + \boldsymbol{\omega} \times (II_{3\times 3})$$

Where the cross product between vectors and matrices is generalized by performing the cross product with each row of the corresponding matrix and placing the result in the corresponding columns:

$$I_{3\times 3} \times I\boldsymbol{\omega} = \left[\begin{bmatrix}1\\0\\0\end{bmatrix} \times I\boldsymbol{\omega} \quad \begin{bmatrix}0\\1\\0\end{bmatrix} \times I\boldsymbol{\omega} \quad \begin{bmatrix}0\\0\\1\end{bmatrix} \times I\boldsymbol{\omega}\right]$$

$$\boldsymbol{\omega} \times (II_{3\times 3}) = \left[\boldsymbol{\omega} \times I\begin{bmatrix}1\\0\\0\end{bmatrix} \quad \boldsymbol{\omega} \times I\begin{bmatrix}0\\1\\0\end{bmatrix} \quad \boldsymbol{\omega} \times I\begin{bmatrix}0\\0\\1\end{bmatrix}\right]$$

Similarly the second term in brackets leads to

$$\frac{\partial}{\partial \omega}(\boldsymbol{\omega} \times \boldsymbol{h}_r) = I_{3\times 3} \times \boldsymbol{h}_r = \left[\begin{bmatrix}1\\0\\0\end{bmatrix} \times \boldsymbol{h}_r \quad \begin{bmatrix}0\\1\\0\end{bmatrix} \times \boldsymbol{h}_r \quad \begin{bmatrix}0\\0\\1\end{bmatrix} \times \boldsymbol{h}_r\right]$$

where we used the cross product generalization again. The last term of Φ_k is simply $\frac{\partial}{\partial \omega}\boldsymbol{\omega}_k = I_{3\times 3}$, rendering the propagation matrix in the following compact form:

$$\Phi_k = -I^{-1}dt(I_{3\times 3} \times I\boldsymbol{\omega} + \boldsymbol{\omega} \times (II_{3\times 3}) + I_{3\times 3} \times \boldsymbol{h}_r) + I_{3\times 3} \tag{3.3.3}$$

The model covariance Q_ω translates the model errors as Additive White Gaussian Noise (AWGN). It is defined in the parameter tuning section along with the initial covariance P_0 that must be defined prior to estimation.

Observation Model

The observation is simply given by gyro readings which are assumed to be affected only by AWGN

$$\boldsymbol{z}_k = \boldsymbol{\omega}_{gyr,k} = \boldsymbol{\omega}_k + \boldsymbol{n}_{gyr,k} \tag{3.3.4}$$

This is a linear model, with a constant sensitivity matrix given by

$$H_\omega = I_{3\times3} \tag{3.3.5}$$

The gyro covariance was given earlier in section 2.1 when the gyroscope technology was described. The derivative noise torque is not taken in account to establish the observations covariance, therefore we set $R_{gyr} = E\{\boldsymbol{n}_{gyr,k}^T \boldsymbol{n}_{gyr,k}\} = \sigma_v^2 I_{3\times3}$

B. The Multiplicative Extended Kalman Filter for Attitude Estimation

The formulation here derived follows references [8] and [9]. We derive the equations for two filters: a pure attitude estimator, and an augmented state estimator. The second estimator adds the gyro drift to the state representation so that gyro biases can be compensated for.

Hence the former outputs an estimate $\boldsymbol{x} = [\bar{q}]$ whereas the latter outputs an augmented state $\boldsymbol{x} = \begin{bmatrix} \bar{q} \\ \boldsymbol{\mu} \end{bmatrix}$.

Dynamics Model

For the gyro drift defined as the difference from the true angular velocity and the reference angular velocity, $\boldsymbol{\mu} = \boldsymbol{\omega} - \boldsymbol{\omega}_{ref}$, the discrete model is assumed to be simply:

$$\boldsymbol{\mu}_{k+1} = \boldsymbol{\mu}_k + \boldsymbol{n}_{\omega,k} \tag{3.3.6}$$

where $\boldsymbol{n}_{\omega,k}$ is an additive white noise vector with noise power (n_ω^2).

Quaternion dynamics are quite more complicated. Generally there are two Kalman filter strategies for quaternion estimation: the Additive EKF (AEKF) and the Multiplicative EKF (MEKF). The first one regards the four quaternion components as independent parameters, therefore having an inherent redundant nature, whereas the second one makes use of a three-component representation of the deviations from the reference quaternion. The latter strategy was adopted as it uses a non-singular representation for the attitude through a reference quaternion $\bar{q}_{ref}$, and simultaneously a non-redundant parameterization of the deviations.

The MEKF represents the attitude as the quaternion product (see [8] or [9]):

$$\bar{q} = \delta\bar{q}(\boldsymbol{a}) \otimes \bar{q}_{ref} \tag{3.3.7}$$

where $\bar{q}$ is the true quaternion, $\bar{q}_{ref}$ is the aforesaid reference quaternion and $\delta\bar{q}(a)$ is the rotation of $\bar{q}_{ref}$ relatively to $\bar{q}$ parameterized by vector $\boldsymbol{a}$. Several parameterizations of $\delta\bar{q}(\boldsymbol{a})$ exist. We adopt a unit parameterization here:

$$\delta\bar{q}(\boldsymbol{a}) = \frac{1}{\sqrt{4 + |\boldsymbol{a}|^2}} \begin{bmatrix} a \\ 2 \end{bmatrix} \tag{3.3.8}$$

For a null rotation notice that $\delta\bar{q}(\boldsymbol{a}) = [0\ 0\ 0\ 1]^T \Rightarrow \boldsymbol{a} = 0$. For small rotations the following approximation is valid,

$$\delta\bar{q}(\boldsymbol{a}) \approx \begin{bmatrix} \frac{\boldsymbol{a}^T}{\boldsymbol{2}} & 1 \end{bmatrix}^T \tag{3.3.9}$$

The basic idea of the MEKF is to compute an unconstrained estimate of the three-component $\boldsymbol{a}$ yet using the correct normalized $\bar{q}_{ref}$ to provide a globally nonsingular attitude representation.

The MEKF computes an estimate $\widehat{\boldsymbol{a}} = E\{\boldsymbol{a}\}$ of $\boldsymbol{a}$. We remove the redundancy of the attitude representation by choosing the reference quaternion $\bar{q}_{ref}$ such that $\widehat{\boldsymbol{a}}$ is identically zero, meaning that $\delta\bar{q}(\boldsymbol{0})$ is the identity quaternion. Identifying $\bar{q}_{ref}$ as the attitude estimate means that $\boldsymbol{a}$ is a three-component representation of the attitude error. This provides a consistent treatment of the attitude error statistics, with the covariance of the attitude error in the body frame represented by the covariance of $\boldsymbol{a}$.

The true quaternion kinematics equation is:

$$\dot{\bar{q}} = \frac{1}{2}\bar{\boldsymbol{\omega}}\otimes\bar{q} \tag{3.3.10}$$

Since $\bar{q}_{ref}$ is also a unit quaternion, it must obey:

$$\dot{\bar{q}}_{ref} = \frac{1}{2}\bar{\boldsymbol{\omega}}_{ref}\otimes\bar{q}_{ref} \tag{3.3.11}$$

Computing the time derivative of (3.3.10) and using (3.3.7) and (3.3.11) yields:

$$\frac{1}{2}\bar{\boldsymbol{\omega}}\otimes\bar{q} = \delta\dot{\bar{q}}\otimes\bar{q}_{ref} + \frac{1}{2}\delta\bar{q}\otimes\bar{\boldsymbol{\omega}}_{ref}\otimes\bar{q}_{ref} \tag{3.3.12}$$

Substituting $\bar{q}$ using (3.3.7) on the left side term of (3.3.12), then right multiplying this entire equation by $\bar{q}_{ref}^{-1}$ and rearranging renders the propagation equation for the quaternion error

$$\delta\dot{\bar{q}} = \frac{1}{2}\left(\bar{\boldsymbol{\omega}}\otimes\delta\bar{q} - \delta\bar{q}\otimes\bar{\boldsymbol{\omega}}_{ref}\right) \tag{3.3.13}$$

Evolving this equation

$$\delta\dot{\bar{q}} = \begin{bmatrix} \dot{\boldsymbol{q}} \\ \dot{q}_4 \end{bmatrix} = \frac{1}{2}\left\{\begin{bmatrix} \delta q_4\boldsymbol{\omega} - \boldsymbol{\omega}\times\delta\boldsymbol{q} \\ -\boldsymbol{\omega}.\delta\boldsymbol{q} \end{bmatrix} - \begin{bmatrix} \delta q_4\boldsymbol{\omega}_{ref} - \delta\boldsymbol{q}\times\boldsymbol{\omega}_{ref} \\ -\delta\boldsymbol{q}.\boldsymbol{\omega}_{ref} \end{bmatrix}\right\} \tag{3.3.14}$$

And simplifying:

$$\delta\dot{\bar{q}} = \frac{1}{2}\begin{bmatrix} \delta q_4\left(\boldsymbol{\omega} - \boldsymbol{\omega}_{ref}\right) - \left(\boldsymbol{\omega} + \boldsymbol{\omega}_{ref}\right)\times\delta\boldsymbol{q} \\ \delta\boldsymbol{q}.\left(\boldsymbol{\omega}_{ref} - \boldsymbol{\omega}\right) \end{bmatrix} \tag{3.3.15}$$

Recalling the fact that under the small incremental rotation condition $\boldsymbol{a} \approx 2\boldsymbol{\delta q}/\delta q_4$, the dynamics of the three-component vector are redrawn by computing the time derivative of $\boldsymbol{a}$:

$$\dot{a} = 2\left(\frac{\delta\dot{\boldsymbol{q}}.\delta q_4 - \delta\dot{q}_4.\delta\boldsymbol{q}}{\delta q_4^2}\right) \tag{3.3.16}$$

Substituting the time derivatives terms of (3.3.16) by the respective expression components of (3.3.15) yields:

$$\dot{\bar{a}} = 2\,\frac{\left(\frac{1}{2}\delta q_4\left(\boldsymbol{\omega} - \boldsymbol{\omega}_{ref}\right) - \frac{1}{2}\left(\boldsymbol{\omega} + \boldsymbol{\omega}_{ref}\right)\times\delta\boldsymbol{q}\right)\delta q_4 - \frac{1}{2}\delta\boldsymbol{q}.\left(\boldsymbol{\omega}_{ref} - \boldsymbol{\omega}\right)\delta\boldsymbol{q}}{\delta q_4^2} \tag{3.3.17}$$

Evolving and simplifying Eq. (3.3.17) renders the kinematics dynamics for $\boldsymbol{a}$:

$$\dot{\bar{\boldsymbol{a}}} = I_{3\times3}\left(\boldsymbol{\omega} - \boldsymbol{\omega}_{ref}\right) + \frac{1}{4}\boldsymbol{a}^T\left(\boldsymbol{\omega} - \boldsymbol{\omega}_{ref}\right)\boldsymbol{a} - \frac{1}{2}\left(\boldsymbol{\omega} + \boldsymbol{\omega}_{ref}\right)\times\boldsymbol{a} \tag{3.3.18}$$

The second term can be rewritten in the more useful form:

$$\frac{1}{4}\boldsymbol{a}^T(\boldsymbol{\omega}-\boldsymbol{\omega}_{ref})\boldsymbol{a}=\frac{1}{4}diag(\boldsymbol{a}\boldsymbol{a}^T)(\boldsymbol{\omega}-\boldsymbol{\omega}_{ref})$$

where $diag(A)$ stands for the matrix whose diagonal elements equal the diagonal of A and all off-diagonal elements being zero. We make $\boldsymbol{\mu}$ appear in (18) in both terms through the substitutions $\boldsymbol{\omega}-\boldsymbol{\omega}_{ref}=\boldsymbol{\mu}$ and $\boldsymbol{\omega}+\boldsymbol{\omega}_{ref}=\boldsymbol{\mu}+\mathbf{2}\boldsymbol{\omega}_{ref}$:

$$\dot{\boldsymbol{a}}=\left(I_{3\times3}+\frac{1}{4}diag(\boldsymbol{a}\boldsymbol{a}^T)\right)\boldsymbol{\mu}-\frac{1}{2}(\boldsymbol{\mu}+2\boldsymbol{\omega}_{ref})\times\boldsymbol{a} \tag{3.3.19}$$

Eq. (3.3.19) is a nonlinear and coupled differential equation in $\boldsymbol{a}$ and $\boldsymbol{u}$, so we define an auxiliary state $\boldsymbol{x}^*=[\boldsymbol{a}^T\ \boldsymbol{\mu}^T]^T$ for the purpose of obtaining the dynamics written in terms of $\boldsymbol{x}^*$. This auxiliary state allows the computation of the rotation quaternion $\delta\bar{q}(\boldsymbol{a})$ which is applied to the propagated quaternion. Because $\boldsymbol{x}^*$ is assumed to represent small deviations from reference values, then $|\boldsymbol{a}|\ll\mathbf{1}$ and $|\boldsymbol{u}|\ll 1$. By definition $\boldsymbol{a}$ is seen as an error through the $\delta\bar{q}(\boldsymbol{a})$ rotation in the end of the update step that results in the new quaternion estimate $\bar{q}_{k+1|k+1}$, with $\boldsymbol{a}$ being set to zero for the next filter cycle. Therefore its dynamics are solely needed to propagate its covariance matrix. Linearization of (3.3.19) renders:

$$\dot{\boldsymbol{a}}=I_{3\times3}\boldsymbol{\mu}-\boldsymbol{\omega}_{ref}\times\boldsymbol{a} \tag{3.3.20}$$

Discretization of (3.3.20) yields the discrete propagation equation:

$$\boldsymbol{a}_{k+1|k}=\left(I_{3\times3}-[\boldsymbol{\omega}_{ref}\Delta t\ \times]\right)\boldsymbol{a}_{k|k}+\Delta t\boldsymbol{\mu}_{k|k}+\boldsymbol{n}_{a,k} \tag{3.3.21}$$

This is the general prediction model for $\boldsymbol{a}$ taking into account the presence of gyro biases. It is readily adequate to be used in the augmented state estimator previously mentioned. The first and simpler filtering strategy does not consider $\boldsymbol{\mu}$ and so the corresponding model equals (3.3.21) with the $\Delta t\boldsymbol{\mu}_{k|k}$ term disappearing.

$$\boldsymbol{a}_{k+1|k}=\left(I_{3\times3}-[\boldsymbol{\omega}_{ref}\Delta t\ \times]\right)\boldsymbol{a}_{k|k}+\boldsymbol{n}_{a,k} \tag{3.3.22}$$

Putting together Eqs. (3.3.6) and (3.3.21) holds the linearized model dynamics in discrete time for the auxiliary state estimator in matrix form:

$$\boldsymbol{x}^*_{k+1|k}=\begin{bmatrix}F_k & I_{3\times3}\Delta t\\ 0 & I_{3\times3}\end{bmatrix}\boldsymbol{x}^*_{k|k}+\begin{bmatrix}I_{3\times3} & 0\\ 0 & I_{3\times3}\end{bmatrix}\boldsymbol{n}_k \tag{3.3.23}$$

with $F_k=I_{3\times3}-[\boldsymbol{\omega}_{ref}\Delta t\ \times]$ and $\boldsymbol{n}_k=\begin{bmatrix}\boldsymbol{n}_{a,k}\\ \boldsymbol{n}_{\omega,k}\end{bmatrix}$.

For estimation of $\boldsymbol{a}$ exclusively this becomes simply:

$$\boldsymbol{a}_{k+1|k}=F_k\boldsymbol{a}_{k|k}+I_{3\times3}\boldsymbol{n}_k \tag{3.3.24}$$

The model covariance $Q_k=E\{\boldsymbol{n}_k.\boldsymbol{n}_k^T\}$ represents the magnitudes of the errors in the model and in the absence of more information it is assumed to be a diagonal matrix whose dimensions must be consistent with each version of the filter respectively.

The covariance error of the state $\boldsymbol{x}^*_{k+1|k}$ is propagated according to the general Kalman filter rule in [Appendix B] which is repeated here:

$$P_{k+1|k}=\Phi_kP_{k|k}\Phi_k^T+GQ_kG^T \tag{3.3.25}$$

where $\Phi_k=F_k$ and $G_k=I_{3\times3}$ for the first version, or $\Phi_k=\begin{bmatrix}F_k & I_{3\times3}\Delta t\\ 0 & I_{3\times3}\end{bmatrix}$ and $G=\begin{bmatrix}I_{3\times3} & 0\\ 0 & I_{3\times3}\end{bmatrix}$ with inclusion of gyro drift estimation

To finish the predict step the quaternion discrete propagation needs to be derived through discretization of (3.3.10) which is a time varying parametric differential equation due to the varying nature of $\boldsymbol{\omega}$ during the iteration time lapse. Assuming though that $\boldsymbol{\omega}$ varies little in one time step which is reasonable for satellite operation, and that Δt is sufficiently small, for instance $O(\Delta t) \leq 0{,}1\ s$, then it becomes a linear differential equation whose solution is well known and renders the discrete quaternion propagation directly:

$$\bar{q}_{k+1|k} = e^{\frac{1}{2}\Omega(\omega_k)\Delta t}\bar{q}_{k|k} \tag{3.3.26}$$

with $\boldsymbol{\omega}_k$ taken from gyro readings and shifted $\boldsymbol{\mu}$, which yields the propagation for $\boldsymbol{\omega}$ as:

$$\boldsymbol{\omega}_k = \boldsymbol{\omega}_{gyr} + \boldsymbol{\mu}_{k-1|k-1} \tag{3.3.27}$$

Again particularizing for attitude estimation exclusively, $\boldsymbol{\mu}$ is neglected and so

$$\boldsymbol{\omega}_k = \boldsymbol{\omega}_{gyr} \tag{3.3.28}$$

Observation Model

In this derivation only the augmented state estimator is considered here. The reason being that the simpler filter is a particular situation of the latter by eliminating all terms and variables related to $\boldsymbol{\mu}$. Furthermore, as we are about to see, $\boldsymbol{\mu}$ does not affect the observation models here presented.

The observation determines the amount of feedback that should be applied to the state update. Though its final objective is to update the state $\boldsymbol{x}$, the observation model performs under the auxiliary state description. Therefore the relation between measurement $\boldsymbol{z}$ and $\boldsymbol{x}^*$ must be obtained.

- **Sun and Earth vectors**

Both Sun and Earth sensors provide a body vector measurement in the body coordinates given by:

$$\boldsymbol{z} \equiv \boldsymbol{v}_b = h_s(\boldsymbol{a}) + \boldsymbol{n}_z = A(\bar{q})\boldsymbol{v}_i + \boldsymbol{n}_z \tag{3.3.29}$$

where $\boldsymbol{v}_i$ is the same vector written in ECI coordinates. The measurement covariance $R_S = E\{\boldsymbol{n}_z\boldsymbol{n}_z^T\}$ is related to the measurement angles $\hat{m} = [\hat{\alpha} \quad \hat{\varphi}]$ in the next section. After applying some algebra and the same approximations for $\delta\bar{q}(\boldsymbol{a})$ as previously yields:

$$h_s(\boldsymbol{a}) = \hat{\boldsymbol{v}}_b + [\hat{\boldsymbol{v}}_b \times]\boldsymbol{a} \tag{3.3.30}$$

with $\hat{\boldsymbol{v}}_b$ being the measurement predicted by the reference quaternion or put differently, as if there was no rotation error, i.e. $\delta\bar{q}(0)$ or equivalently $\bar{q} = \bar{q}_{ref} = \bar{q}_{k+1|k}$:

$$\hat{\boldsymbol{v}}_b = A(\bar{q}_{ref})\boldsymbol{v}_i \tag{3.3.31}$$

The derivative of $h_s(\boldsymbol{a})$ with respect to $\boldsymbol{x}^*$ gives the measurement sensitivity matrix:

$$H_s \equiv \frac{\partial h_s(a)}{\partial \boldsymbol{x}^*} = [[\hat{\boldsymbol{v}}_b \times] \quad 0_{3\times3}] \tag{3.3.32}$$

- **Star Tracker quaternion**

The Star Tracker outputs a quaternion measurement, resulting in the simple observation model:

$$\boldsymbol{z} \equiv \bar{q}_m = \bar{q} + \boldsymbol{n}_q = \delta\bar{q}(\boldsymbol{a})\otimes\bar{q}_{ref} + \boldsymbol{n}_q \tag{3.3.33}$$

The noise covariance matrix for the Star Tracker is assumed to be isotropic

$$R_T = E\{\boldsymbol{n}_z\boldsymbol{n}_z^T\} = \sigma_q^2 I_{4\times4} \tag{3.3.34}$$

Putting the term $\delta\bar{q}(\boldsymbol{a})\otimes\bar{q}_{ref}$ into matrix form results in

$$\delta\bar{q}(\boldsymbol{a})\otimes\bar{q}_{ref} = \begin{bmatrix} \delta q\boldsymbol{q}_{ref} + q_{ref}\delta\boldsymbol{q} - [\delta q\,\times]\boldsymbol{q}_{ref} \\ \delta q.\,q_{ref} - \delta\boldsymbol{q}^T\boldsymbol{q}_{ref} \end{bmatrix}$$

Applying approximation (3.3.9) to the above expression yields:

$$\delta\bar{q}(\boldsymbol{a})\otimes\bar{q}_{ref} \approx \begin{bmatrix} \boldsymbol{q}_{ref} + q_{ref}\frac{\boldsymbol{a}}{2} - \frac{1}{2}[\boldsymbol{a}\,\times]\boldsymbol{q}_{ref} \\ q_{ref} - \frac{1}{2}\boldsymbol{a}^T.\boldsymbol{q}_{ref} \end{bmatrix} = \begin{bmatrix} \left(I_{3\times3} - \frac{1}{2}[\boldsymbol{a}\,\times]\right)\boldsymbol{q}_{ref} + q_{ref}\frac{\boldsymbol{a}}{2} \\ q_{ref} - \frac{1}{2}\boldsymbol{a}^T.\boldsymbol{q}_{ref} \end{bmatrix}$$

Hence the predicted measure model used in the filter is assumed to correspond to the approximation just presented:

$$h_T(a,\bar{q}_{ref}) = \begin{bmatrix} (I_{3\times3} - \frac{1}{2}[\boldsymbol{a}\,\times])\boldsymbol{q}_{ref} + \bar{q}_{4,ref}\frac{\boldsymbol{a}}{\boldsymbol{2}} \\ \bar{q}_{4,ref} - \frac{1}{2}\boldsymbol{a}^T\boldsymbol{q}_{ref} \end{bmatrix} \tag{3.3.35}$$

Recall that the predicted measurement however is done assuming $\boldsymbol{a} = 0$. Therefore this expression is only meant to compute the corresponding sensitivity matrix of the Star Tracker:

$$H_T \equiv \frac{\partial h_T(a)}{\partial \boldsymbol{x}^*} = \begin{bmatrix} \frac{1}{2}\Xi(\bar{q}_{ref}) & 0_{4\times3} \end{bmatrix} \tag{3.3.36}$$

with $\Xi(\bar{q})$ defined in Appendix (A). The propagated quaternion $\bar{q}_{k+1|k}$ is used as the reference quaternion ($\bar{q}_{ref} = \bar{q}_{k+1|k}$).

Notice that as mentioned earlier both observation types are independent of $\boldsymbol{\mu}$, hence the $0_{3\times3}$ and $0_{4\times3}$ present in the sensitivity matrices of H_S and H_T respectively.

The Kalman gain is given by:

$$K_k = P_{k+1|k}\,H_k\left(H_kP_{k+1|k}H_k^T + R\right)^{-1} \tag{3.3.37}$$

The covariance state update yields:

$$P_{k+1|k+1} = P_{k+1|k} - P_{k+1|k}H_k^T\left(H_kP_{k+1|k}H_k^T + R\right)^{-1}H_kP_{k+1|k} \tag{3.3.38}$$

The Kalman gain can be evidenced in the last expression to yield the more compact form:

$$P_{k+1|k+1} = (I - K_kH_k)P_{k+1|k} \tag{3.3.39}$$

The state update as mentioned before is performed under the auxiliary state $\boldsymbol{x}^*$ current estimate according to:

$$x^*_{k+1|k+1} = x^*_{k+1|k} + K_k\left(z_k - h_k\left(x^*_{k+1|k}\right)\right) \tag{3.3.40}$$

Recall that because $\boldsymbol{a}$ represents the attitude error its value before update is null, i.e. $x^*_{k+1|k} = \begin{bmatrix} \boldsymbol{a}_{k+1|k} \\ \boldsymbol{\mu}_{k+1|k} \end{bmatrix} = \begin{bmatrix} \boldsymbol{0} \\ \boldsymbol{\mu}_{k+1|k} \end{bmatrix}$. The sensitivity matrix is given according to the type of observation:

$$H_k = \begin{cases} H_S, \text{if measure } \mathrm{z_k} \text{ is a vector from Sun or Earth sensor} \\ H_T, \text{if measure is } \mathrm{z_k} \text{ is a quaternion from Star Tracker} \end{cases}$$

and likewise for the observation function:

$$h_k = \begin{cases} h_S(\boldsymbol{0},\bar{q}_{k+1|k}), \text{if measure } \mathrm{z_k} \text{ is a vector from Sun or Earth sensor} \\ h_T(\boldsymbol{0},\bar{q}_{k+1|k}), \text{if measure } \mathrm{z_k} \text{ is a quaternion from Star Tracker} \end{cases}$$

The error $\boldsymbol{a}_{k+1|k+1}$ parameterization propagates to the predicted quaternion resulting in the updated quaternion estimate and ending the MEKF iteration:

$$\bar{q}_{k+1|k+1} = \delta\bar{q}(\boldsymbol{a}_{k+1|k+1})\otimes\bar{q}_{k+1|k} \tag{3.3.41}$$

A summary of the augmented state MEKF operations is presented next:

Predict Step

1. $x_{k|k} = \begin{bmatrix} \bar{q}_{k|k} \\ \boldsymbol{\mu}_{k|k} \end{bmatrix}$
2. $\boldsymbol{\omega}_k = \boldsymbol{\omega}_{gyro} + \boldsymbol{\mu}_{k|k}$
3. $\bar{q}_{k+1|k} = e^{\frac{1}{2}\Omega(\boldsymbol{\omega}_k)\Delta t}\bar{q}_{k|k}$
4. $\boldsymbol{\mu}_{k+1|k} = \boldsymbol{\mu}_{k|k}$
5. $F = I_{3\times3} - [\boldsymbol{\omega}_k \Delta t\,\times]$
6. $\Phi_k = \begin{bmatrix} F & I_{3\times3}\Delta t \\ 0 & I_{3\times3} \end{bmatrix}$
7. $P_{k+1|k} = \Phi_k P_{k|k} \Phi_k^T + G Q_k G^T$

Update Step

1. $h_k(x^*_{k+1|k}) = \begin{cases} h_S(\boldsymbol{a}), \text{if measurement from Sun or Earth Vector} \\ h_T(\boldsymbol{a}), \text{if measurement from Star Tracker} \end{cases}$
2. $H_k = \begin{cases} H_S(\boldsymbol{a}), \text{if measurement from Sun or Earth Vector} \\ H_T(\boldsymbol{a}), \text{if measurement from Star Tracker} \end{cases}$
3. $K_k = P_{k+1|k}\, H_k\left(H_k P_{k+1|k} H_k^T + R\right)^{-1}$
4. $P_{k+1|k+1} = (I - K_k H_k) P_{k+1|k}$
5. $x^*_{k+1|k} = \begin{bmatrix} \mathbf{0} \\ \boldsymbol{\mu}_{k+1|k} \end{bmatrix}$
6. $x^*_{k+1|k+1} = x^*_{k+1|k} + K_k\left(z_k - h_k(x^*_{k+1|k})\right)$
7. $\delta\bar{q} = \delta\bar{q}(\boldsymbol{a})$
8. $\bar{q}_{k+1|k+1} = \delta\bar{q}\otimes\bar{q}_{k+1|k}$
9. $x_{k+1|k+1} = \begin{bmatrix} \bar{q}_{k+1|k+1} \\ \boldsymbol{\mu}_{k+1|k+1} \end{bmatrix}$

C. Tuning of Estimator Parameters

We now turn our attention to the no less important task of tuning the filter parameters.

When a relation between the covariance and the variables of the process, whether state, input, output or a combination of the three is not available, one can only resort to a trial and error procedure. This method was adopted for the angular velocity EKF:

$Q_{\omega} = 10^{-14} I_{3\times3}$
$P_0 = 10^{-6} I_{3\times3}$.

For the model covariance of the MEKF we distinguish between two covariance groups: the constant covariance and the variable covariance. In the case of the measurements covariance, we derive a function that relates it to the observations themselves.

Model Covariance

For the augmented state MEKF the covariance of the propagation process is defined as

$$Q_k = \begin{bmatrix} Q_{a,k} & 0 \\ 0 & Q_{\mu} \end{bmatrix} \tag{3.3.42}$$

$Q_{a,k}$ is the covariance corresponding to the generalized vector component of the quaternion error which is indexed to k to indicate that it is time-varying. On the other hand Q_{μ} is considered to be constant. An alternative fixed model covariance for the vector component of the quaternion error is:

$$Q_a = \sigma_a^2 I_{3\times3} \tag{3.3.43}$$

with $\sigma_a^2 = 1{,}85 \times 10^{-11}$.

Recalling the approximations that led to (3.3.26), it becomes evident that higher angular velocities lead to larger errors in the predicted quaternion. Moreover the larger the sampling period the more coarsely Eq. (3.3.26) represents the continuous dynamics of the SV. Based on such facts a varying covariance for the three-component of the quaternion error is assumed to be parameterized as follows:

$$Q_{a,k} = g(\|\boldsymbol{\omega}_k\| + b)^n . \left(\frac{\Delta t}{f}\right)^p I_{3\times3} \tag{3.3.44}$$

Notice that $Q_{a,k}$ is always a diagonal matrix as one admits there is no cross correlation between error components. Dimensioning $Q_{a,k}$ comes down to setting values for parameters g, b, n, p and f. Parameter g is a magnitude factor; b establishes a lower bound in $\|\boldsymbol{\omega}_k\|$ units; n establishes the polynomial dependence with angular velocity norm; f is the sampling period normalization factor; and p the polynomial dependence with sampling time. One criteria used is that gb^n should be equal to σ_a^2 at a sample period of 0,1 s. Table 3.1 presents the choice of parameters.

Table 3.1 - Parameter selection of the three-component vector covariance

$\boldsymbol{n}$	$\boldsymbol{g}$	$\boldsymbol{b}\ [\boldsymbol{rad/s}]$	$\boldsymbol{f}\ [\boldsymbol{s}]$	$\boldsymbol{p}$
2	$2{,}0556 \times 10^{-8}$	3×10^{-2}	0,1	2

Measurements Covariance

- **Sun and Earth vectors measurements**

Once the inertial position error produced by GPS is relatively small, measurement errors are assumed to be solely a consequence of Sun and Horizon sensors noises. Therefore we evaluate their impact on LOS vector errors by finding the relation between their covariance matrices.

We pose the problem in the general variables x and y such that $x = x(y)$. Here x represents the computed n values, which are function of the vector of m measurements y. Using a first-order Taylor series renders the approximate error relation:

$$\delta x_i \approx \sum_{j=1}^{m} \frac{\partial x_i}{\partial y_j} \delta y_j \tag{3.3.45}$$

or put into matrix form

$$\delta x = H \delta y \tag{3.3.46}$$

where H is the $n \times m$ matrix of partial derivatives with the elements $H_{ij} \equiv \partial x_i / \partial y_j$. The covariance of x is then given by:

$$E\{\delta x \delta x^T\} = E\{H \delta y \delta y^T H^T\} = HE\{\delta y \delta y^T\} H^T \tag{3.3.47}$$

which in terms of LOS and angle measurements translates into:

$$R_c = H_m^v R_m {H_m^v}^T \tag{3.3.48}$$

where R_v is the covariance of the computed vector, R_m the covariance of angle measurements and $H_m^v = \frac{\partial v}{\partial m}$. To obtain H_m^v we recall the relation expressed in Eq. (2.3):

$$v = [\cos\alpha . \cos\varphi \quad \cos\alpha . \sin\varphi \quad \sin\alpha]^T$$

Deriving v with respect to $m = [\alpha \;\; \varphi]^T$ renders:

$$H_m^v = \begin{bmatrix} -\sin\alpha\cos\varphi & -\cos\alpha\sin\varphi \\ -\sin\alpha\sin\varphi & \cos\alpha\cos\varphi \\ \cos\alpha & 0 \end{bmatrix} \tag{3.3.49}$$

Eq. (3.3.49) uses true angles to compute H_m^v. However, because the noise is relatively low, a fairly reasonable approximation holds with the use of the measured set $\hat{m} = [\hat{\varphi} \quad \hat{\alpha}]^T$.

- **Start Tracker Measurement**

In Section 2.1 the Star Tracker measurement is regarded as a small rotation error from the true quaternion given by (2.4). Substituting approximation (2.5) into (2.4) yields the following approximation:

$$\bar{q}_m \cong \begin{bmatrix} \boldsymbol{q} + q_4 \dfrac{\boldsymbol{a}}{2} & -\dfrac{\boldsymbol{a}}{2} \times \boldsymbol{q} \\ q_4 - \dfrac{\boldsymbol{a}}{2} . \boldsymbol{q} \end{bmatrix} \tag{3.3.50}$$

where $\bar{q} = [\boldsymbol{q} \; q_4]^T$ here is the true quaternion for matters of abbreviation. The covariance of the Star Tracker measurement relates to the covariance of the three-component vector using (3.3.47), with H substituted by:

$$H_a^q = \frac{\partial \bar{q}}{\partial \boldsymbol{a}} = \frac{1}{2} \begin{bmatrix} (q_4 I_{3\times3} + [\boldsymbol{q} \times]) \\ -\boldsymbol{q}^T \end{bmatrix}$$

and $E\{\delta y \delta y^T\}$ substituted by $E\{\boldsymbol{n}_{a,k}\boldsymbol{n}_{a,k}{}^T\} \equiv R_a$, resulting in the compact form for the Star Tracker covariance:

$$R_{ST} = H_a^q R_a \left(H_a^q\right)^T$$

The quaternion is unknown, however a very good approximation holds if one uses the measurement or the estimated quaternion for the purpose of computing H_a^q.

The Star Tracker RMS error was specified in Section 2.1 as 174 arcsec. Translation of this value in terms of vector $\boldsymbol{a}$ is necessary not only for the estimation algorithm but also for noise emulation purposes.

As explicit in Eq. (2.5) the contributions of the small Euler angles $(\delta\psi, \delta\theta, \delta\varphi)$ to the measurement error are approximately decoupled from each other when introduced via $\boldsymbol{a} = [\delta\psi \quad \delta\theta \quad \delta\varphi]^T$. This means that they can be seen as orthogonal to each other, leading to the following approximation for the total RMS angular error (σ_ε):

$$\sigma_\varepsilon \simeq \sqrt{\sigma_\psi^2 + \sigma_\theta^2 + \sigma_\varphi^2} \tag{3.3.51}$$

Assuming an equal error distribution in the three angles:

$$\sigma_\psi^2 = \sigma_\theta^2 = \sigma_\varphi^2 = \frac{1}{3}\sigma_\varepsilon^2$$

the Star Tracker covariance in terms of $\boldsymbol{a}$ becomes:

$$R_a = 0{,}2388 \times 10^{-6} I_{3\times3} \ (rad/s)^2$$

A simplified version of the Star Tracker quaternion covariance extends R_a to a 4-by-4 matrix to account for the scalar quaternion component as well:

$$R_{ST} = 0{,}2388 \times 10^{-6} I_{4\times4}$$

Although this procedure is not very elegant, this fixed value for R_{ST} leads to particularly good results as demonstrated in Chapter 6.

4. Attitude Control of Single Vehicle

4.1. Dynamics Linearization

The Linear Quadratic Regulator (LQR) is used in a wide number of applications in control. It was developed to address regulation problems in linear systems. The LQR implies a state space description of systems and finds the optimal control law in the sense that it minimizes a cost function dependent on the state deviation and control inputs. See [13] for more insight into LQR theory.

Although the LQR applied to a nonlinear system does not guarantee stability, nor optimality, approximating the SV attitude dynamics to a linear system is relatively simple. Moreover assuming moderate angular velocities the linear approximation becomes a fairly reasonable assumption for satellite operation specially when maintaining a desire fixed attitude. During large attitude manoeuvres gyroscopic effects increase due to rotation of the satellite and reaction wheels speed. Hence the system departs from a linear dynamics, making the LQR more prone to failure. This can be partially counteracted through segmentation of the manoeuvre into smaller attitude changes and applying small angular velocities to the SV. The linearization of the SV dynamics follows in order to pave the way for the LQR design

First of all we shall recall that the control objective is to force a given state of the single SV given as:

$$x_{ref} = \begin{bmatrix} \bar{q}_{ref} \\ \boldsymbol{\omega}_{ref} \end{bmatrix} \tag{4.1}$$

It turns out that such entity is incompatible with the LQR objective – bringing the state of a given system to $\mathbf{0}$ – because $\left\|\bar{q}_{ref}\right\| = 1 \neq 0$. The unit quaternion is incompatible with LQR implementation, and so a slight modification has to be made.

The Kinematics of $\bar{q}$ can be written in terms of the reference state and additional deviation terms as

$$\dot{\bar{q}} = \dot{\bar{q}}_{ref} + \Delta\dot{q} = \frac{1}{2}\Xi(\bar{q}_{ref} + \Delta q)(\omega_{ref} + \boldsymbol{\Delta\omega}) \tag{4.2}$$

where $\boldsymbol{\Delta q}$ represents an additive error and $\boldsymbol{\Delta\omega}$ represents the angular speed error. This right hand side can be split into four terms:

$$\dot{\bar{q}}_{ref} + \Delta\dot{q} = \frac{1}{2}\Xi\left(\bar{q}_{ref}\right)\omega_{ref} + \frac{1}{2}\Xi(\Delta q)\omega_{ref} + \frac{1}{2}\Xi\left(\bar{q}_{ref}\right)\Delta\boldsymbol{\omega} + \frac{1}{2}\Xi(\Delta q)\Delta\boldsymbol{\omega} \tag{4.3}$$

The first term of the right hand side equals $\dot{\bar{q}}_{ref}$ by definition:

$$\dot{\bar{q}}_{ref} = \frac{1}{2}\Xi\left(\bar{q}_{ref}\right)\boldsymbol{\omega}_{ref}$$

The incremental quaternion dynamics are retrieved by elimination of both these terms in Eq. (4.3) resulting in:

$$\Delta\dot{q} = \frac{1}{2}\Xi(\Delta q)\boldsymbol{\omega}_{ref} + \frac{1}{2}\Xi\left(\bar{q}_{ref}\right)\Delta\boldsymbol{\omega} + \frac{1}{2}\Xi(\Delta q)\Delta\boldsymbol{\omega} \tag{4.4}$$

Notice that Δq is not a quaternion, instead it is a 4x1 vector which represents the additive deviation from the reference quaternion. It does not represent a rotation and its norm is not constricted to unity.

Assuming small deviations from the reference state such that higher order deviation terms can be neglected, namely $\frac{1}{2}\Xi(\Delta q)\Delta\boldsymbol{\omega}$, then the dynamics of Δq becomes (approximated):

$$\Delta\dot{q} = \frac{1}{2}\Xi(\Delta q)\boldsymbol{\omega}_{ref} + \frac{1}{2}\Xi(\bar{q}_{ref})\Delta\boldsymbol{\omega}$$

Rewriting the first term renders:

$$\Delta\dot{\bar{q}} = \frac{1}{2}\Omega(\boldsymbol{\omega}_{ref})\Delta q + \frac{1}{2}\Xi(\bar{q}_{ref})\Delta\boldsymbol{\omega} \tag{4.5}$$

We now linearize the dynamics of $\boldsymbol{\omega}$ around a given reference $\boldsymbol{\omega}_{ref}$. Recalling Eq. (2.27), we rewrite it in terms of $\boldsymbol{\omega}_{ref}$ plus an incremental $\Delta\boldsymbol{\omega}$ such that $\boldsymbol{\omega} = \boldsymbol{\omega}_{ref} + \Delta\boldsymbol{\omega}$:

$$\dot{\boldsymbol{\omega}}_{ref} + \Delta\dot{\boldsymbol{\omega}} = I^{-1}\big(\boldsymbol{M} - (\boldsymbol{\omega}_{ref} + \Delta\boldsymbol{\omega}) \times I(\boldsymbol{\omega}_{ref} + \Delta\boldsymbol{\omega}) - W^a\boldsymbol{M}^w - (\boldsymbol{\omega}_{ref} + \Delta\boldsymbol{\omega}) \times W^I\boldsymbol{\omega}_w\big) \tag{4.6}$$

Expanding terms:

$$\begin{aligned}\dot{\boldsymbol{\omega}}_{ref} + \Delta\dot{\boldsymbol{\omega}} = I^{-1}\big(&\boldsymbol{M} - \boldsymbol{\omega}_{ref} \times I\boldsymbol{\omega}_{ref} - \boldsymbol{\omega}_{ref} \times I\Delta\boldsymbol{\omega} - \Delta\boldsymbol{\omega} \times I\boldsymbol{\omega}_{ref} - \Delta\boldsymbol{\omega} \times I\Delta\boldsymbol{\omega} - W^a\boldsymbol{M}^w \\ &- \boldsymbol{\omega}_{ref} \times W^I\boldsymbol{\omega}_w - \Delta\boldsymbol{\omega} \times W^I\boldsymbol{\omega}_w\big)\end{aligned} \tag{4.7}$$

Assuming small incremental $\Delta\boldsymbol{\omega}$ values, the quadratic term $\Delta\boldsymbol{\omega} \times I\Delta\boldsymbol{\omega}$ can be neglected which renders the linear approximation for the rotation dynamics:

$$\begin{aligned}\dot{\boldsymbol{\omega}}_{ref} + \Delta\dot{\boldsymbol{\omega}} = I^{-1}\big(&\boldsymbol{M} - \boldsymbol{\omega}_{ref} \times I\boldsymbol{\omega}_{ref} - \boldsymbol{\omega}_{ref} \times I\Delta\boldsymbol{\omega} - \Delta\boldsymbol{\omega} \times I\boldsymbol{\omega}_{ref} - W^a\boldsymbol{M}^w - \\ &\boldsymbol{\omega}_{ref} \times W^I\boldsymbol{\omega}_w - \Delta\boldsymbol{\omega} \times W^I\boldsymbol{\omega}_w\big)\end{aligned} \tag{4.8}$$

At this stage some thought on an appropriate selection for $\boldsymbol{\omega}_{ref}$ should be made. One choice is to invoke the three axes stabilized characteristic of the SV stated in chapter 2, so to assume in practice low angular velocities whether the satellite is in stationary pointing operation or even during manoeuvres; in such case $\boldsymbol{\omega}_{ref} = 0$ and $\dot{\boldsymbol{\omega}}_{ref} = 0$, hence the dynamics significantly simplifies to:

$$\Delta\dot{\boldsymbol{\omega}} = I^{-1}(\boldsymbol{M} - W^a\boldsymbol{M}^w) = I^{-1}(\boldsymbol{M} - W^a\boldsymbol{M}^w) \tag{4.9}$$

Eq. (4.9) describes the dynamics of an integrator with entrances in $\boldsymbol{M}$ or $\boldsymbol{M}^w$. Recall that $\boldsymbol{M}$ is the vector of external moments (disturbances apart, $\boldsymbol{M}$ equals the moment generated by the thrusters), and $\boldsymbol{M}^w$ the reaction wheels applied torque. Naturally that control with the two actuator types is regarded separately.

The second option implies a non-null choice for the reference $\boldsymbol{\omega}_{ref}$. This leads to a tracking control problem to be addressed by resorting to a modified LQR that is overseen by a manoeuvre supervisor, as detailed next. If $\boldsymbol{\omega}_{ref} \neq \boldsymbol{0}$ the system representation is still linear but the terms that were nulled and lead to Eq. (4.9) now appear in the dynamics. Among these we distinguish two types of terms, those dependent on the small incremental velocity $\Delta\boldsymbol{\omega}$ and those independent. In addition, we define trim values for the control inputs: $\boldsymbol{M}_{trim}$ and $(\boldsymbol{M}^w)_{trim}$ such that

$$\boldsymbol{M} = \boldsymbol{M}_{trim} + \Delta\boldsymbol{M} \qquad \boldsymbol{M}^w = (\boldsymbol{M}^w)_{trim} + \Delta\boldsymbol{M}^w$$

The quantities of $\boldsymbol{M}_{trim}$ and $(\boldsymbol{M}^w)_{trim}$ have the purpose of forcing $\dot{\boldsymbol{\omega}}_{ref}$ to a certain value – normally fixed to be 0 – counteracting gyroscopic effects. The remaining terms describe the dynamics around the reference point, resulting in an equation on the incremental variables $\Delta\boldsymbol{\omega}$, $\Delta\boldsymbol{M}$ and $\Delta\boldsymbol{M}^w$. Concretizing what has just been explained, the trimming equation has the following form:

$$\dot{\boldsymbol{\omega}}_{ref} = I^{-1}\big(\boldsymbol{M}_{trim} - \boldsymbol{\omega}_{ref} \times I\boldsymbol{\omega}_{ref} - \boldsymbol{\omega}_{ref} \times W^I\boldsymbol{\omega}_w - W^a(\boldsymbol{M}^w)_{trim}\big) \tag{4.10}$$

The incremental dynamics is ruled by:

$$\Delta\dot{\boldsymbol{\omega}} = I^{-1}\left(\Delta\boldsymbol{M} - \boldsymbol{\omega}_{ref} \times I\Delta\boldsymbol{\omega} - \Delta\boldsymbol{\omega} \times I\boldsymbol{\omega}_{ref} - \Delta\boldsymbol{\omega} \times W^{I}\boldsymbol{\omega}_{w} - W^{a}\Delta\boldsymbol{M}^{w}\right) \tag{4.11}$$

Terms in $\Delta\boldsymbol{\omega}$ can be grouped by inverting the sign and order of the cross product ($a \times b = -b \times a$) yielding:

$$\Delta\dot{\boldsymbol{\omega}} = I^{-1}\left(\Delta\boldsymbol{M} + \left(-\left[\boldsymbol{\omega}_{ref} \times\right]I + \left[I\boldsymbol{\omega}_{ref} \times\right] + \left[W^{I}\boldsymbol{\omega}_{w} \times\right]\right)\Delta\boldsymbol{\omega} - W^{a}\Delta\boldsymbol{M}^{w}\right) \tag{4.12}$$

Eq. (4.12) is free of trimming control variables. Therefore we have reached a stage where there exist two simultaneous processes in parallel contemplating the control of one single system. Both processes add up in the overall physical process of attitude control. In subsequent developments a **manoeuvre planner** is responsible for outputting the reference value $\boldsymbol{\omega}_{ref}$ in a discontinuous step-like fashion and to assume $\dot{\boldsymbol{\omega}}_{ref} = 0$. This way the trimming controls $\boldsymbol{M}_{trim}$ or $(\boldsymbol{M}^{w})_{trim}$, depending on the actuation used, are such that the reference angular acceleration is nulled ($\dot{\boldsymbol{\omega}}_{ref} = 0$):

$$0 = \boldsymbol{M}_{trim} - \boldsymbol{\omega}_{ref} \times I\boldsymbol{\omega}_{ref} - \boldsymbol{\omega}_{ref} \times W^{I}\boldsymbol{\omega}_{w} - W^{a}(\boldsymbol{M}^{w})_{trim} \tag{4.13}$$

so trimming with the thrusters leads to

$$\boldsymbol{M}_{trim} = \boldsymbol{\omega}_{ref} \times I\boldsymbol{\omega}_{ref} + \boldsymbol{\omega}_{ref} \times W^{I}\boldsymbol{\omega}_{w} \tag{4.14}$$

whereas trimming with reaction wheels leads to:

$$W^{a}(\boldsymbol{M}^{w})_{trim} = -\boldsymbol{\omega}_{ref} \times I\boldsymbol{\omega}_{ref} - \boldsymbol{\omega}_{ref} \times W^{I}\boldsymbol{\omega}_{w} \tag{4.15}$$

4.2. LQR Controller

Two descriptions of the linearized equations of the dynamics around some reference condition were derived; the first one being more simplistic, not accounting for gyroscopic and therefore suited to situations where low angular speeds are encountered; the second and more general description linearizes the SV system around any working point. The former constitutes in fact a particular situation of the latter, thus we only focus on the generalized description here.

The LQR is devoted do linear systems whose state dynamics are described by the following general linear differential equation in the state $\boldsymbol{x}$ and control input vector $\boldsymbol{u}$:

$$\dot{\boldsymbol{x}} = A\boldsymbol{x} + B\boldsymbol{u} \tag{4.16}$$

As mentioned the objective of the LQR is to force $\boldsymbol{x}$ to zero, i.e. $\boldsymbol{x}_{ref} = 0$. In the nonlinear description of the system however the reference might correspond to a nonzero value. The linearization in our previous analysis gave rise to a deviation vector state which is the stack of the deviation vectors from the references:

$$\boldsymbol{x} = \begin{bmatrix} \Delta q \\ \boldsymbol{\Delta\omega} \end{bmatrix} \tag{4.17}$$

Which means that the LQR controller computes the needed actuation to null the deviations from the reference state vector $x_{ref} = \begin{bmatrix} \bar{q}_{ref} \\ \boldsymbol{\omega}_{ref} \end{bmatrix}$.

The LQR minimizes a cost quadratic function on both the state and control input over a given time interval. Here we adopt an infinite time span:

$$J = \int_{0}^{\infty} \left(x(t)^{T}Qx(t) + u(t)^{T}Ru(t)\right)dt \tag{4.18}$$

The state and control variables are evidenced as time dependent in the above definition. Matrix Q is semi-positive definite ($Q \geq 0$), matrix R is positive definite ($R > 0$) , and they constitute weighting matrices in the sense that they weight the cost of having x and u different from zero.

Minimization of J leads to the following linear relation for the feedback:

$$u(t) = -Kx(t) \tag{4.19}$$

where K is the feedback gain given by:

$$K = R^{-1}B^T P \tag{4.20}$$

with P being the solution of the *Riccati* algebraic equation:

$$PA + A^T P - PBR^{-1}B^T P + Q = 0 \tag{4.21}$$

If A, B, Q and R are constant matrices during the time span of the control process, than P is also a constant matrix which implies a constant feedback gain K. Otherwise one has to deal with a detuned gain for possibly large periods of time. One solution to cope with variations is to repeat the gain computation with the appropriate matrices when significant changes are verified in their parameters. More concretely A and B rule the linearized dynamics of the corresponding nonlinear system around reference values. Nonlinear behaviours therefore are reflected in the linearized system through variations in A and B.

Instead of regularizing the full state x we can specifically aim to control only the output ($y = \Delta q$). So alternatively define the LQRy cost function as

$$J_y = \int_0^\infty \left(y(t)^T Q_y y(t) + u(t)^T R u(t) \right) dt \tag{4.22}$$

In order to describe the system in the desired matrix form of Eq. (4.16) we first write Eq. (4.12) as:

$$\Delta\dot{\boldsymbol{\omega}} = \boldsymbol{A}^{\omega}\Delta\boldsymbol{\omega} + B'\boldsymbol{u} \tag{4.23}$$

where $A^{\omega} = I^{-1}\left(-\left[\boldsymbol{\omega}_{ref} \times\right]I + \left[I\boldsymbol{\omega}_{ref} \times\right] + \left[I^{w}\boldsymbol{\omega}_{w} \times\right]\right)$, and B' and $\boldsymbol{u}$ are defined as:

$$\{B', \boldsymbol{u}\} = \begin{cases} \{I^{-1}, \Delta\boldsymbol{M}\} & \text{with thrusters} \\ \{-I^{-1}W^{a}, \Delta\boldsymbol{M}^{w}\} & \text{with reaction wheels} \end{cases}$$

Stacking Eqs. (4.5) and (4.23) renders the description in the desired form of (4.16) with:

$$A = \begin{bmatrix} \frac{1}{2}\Omega\left(\omega_{ref}\right) & \frac{1}{2}\Xi\left(\bar{q}_{ref}\right) \\ 0_{3\times4} & A^{\omega} \end{bmatrix} \qquad B = \begin{bmatrix} 0_{4\times3} \\ B' \end{bmatrix}$$

However as mentioned before $\bar{q}$ is a constrained quantity. This is reflected on the dynamics of Δq making the LQR unsolvable. The solution is to trim Δq to the corresponding deviation vector component of $\bar{q}$, i.e. Δq is replaced with $\Delta\boldsymbol{q} = [\Delta q(1)\ \Delta q(2)\ \Delta q(3)]^T$. Then the state considered for the LQR becomes $\boldsymbol{x} = \begin{bmatrix} \Delta\boldsymbol{q} \\ \Delta\boldsymbol{\omega} \end{bmatrix}$ and the fourths lines and columns of A and B are eliminated holding:

$$A = \begin{bmatrix} -\frac{1}{2}\left[\boldsymbol{\omega}_{ref} \times\right] & \frac{1}{2}\left(q_{ref,4}\, I_{3\times3} - \left[\boldsymbol{q}_{ref} \times\right]\right) \\ 0_{3\times3} & I^{-1}\left(-\left[\boldsymbol{\omega}_{ref} \times\right]I + \left[I\boldsymbol{\omega}_{ref} \times\right] + \left[W^{I}\boldsymbol{\omega}_{w} \times\right]\right) \end{bmatrix} \qquad B = \begin{bmatrix} 0_{3\times3} \\ B' \end{bmatrix} \tag{4.24}$$

As mentioned earlier the matrix of the dynamics is in fact dependent on the reference value $\boldsymbol{\omega}_{ref}$ as well as in the value of the wheels reference speed $\boldsymbol{\omega}_{w}$. In the event of large differences between these values and the corresponding real ones, the linearized description departs from the actual dynamics and as a consequence the computed feedback gain K will no longer be tuned.

The strategy here used includes a process that monitors the current values and compares them with the current references. In order to perform this function, an additional block named manoeuvre supervisor is included upstream the controller. The controller itself is named the Modified LQR (MLQR) because it allows for recalculation of the feedback gains whenever the supervisor detects a significant difference between the reference values and the real (estimated) values.

4.3. Manoeuvre Supervisor

The function of the manoeuvre supervisor is to establish the reference values ($\bar{q}_{ref}$, $\boldsymbol{\omega}_{ref}$, $(\boldsymbol{\omega}_w)_{ref}$) used in the linearization that renders the MLQR. In order to do this the supervisor collects the relevant data that influence the dynamics, namely $\bar{q}_{est}$, $\boldsymbol{\omega}_{est}$, $(\boldsymbol{\omega}_w)_{ref}$. The target attitude $\bar{q}_{target}$ is also input to the supervisor instead of being input to the controller directly. The supervisor monitors the estimation values and compares them with the current reference. When the differences become larger than a given threshold it triggers a flag indicating the MLQR block that it must update its gains by linearizing around new points of reference. The new reference points output by the supervisor are either their corresponding current estimated values coming from sensor readings directly or from the attitude estimator, or they are imposed by the supervisor as a required condition for the manoeuvre.

The supervisor forces $(\boldsymbol{\omega}_w)_{ref} = (\boldsymbol{\omega}_w)_{est}$ whenever $\left\|(\boldsymbol{\omega}_w)_{est} - (\boldsymbol{\omega}_w)_{ref}\right\|$ becomes larger than a threshold.

The reference attitude $\bar{q}_{ref}$ is computed from the great circle angle from $\bar{q}_{est}$ to $\bar{q}_{target}$. The supervisor provides a reference attitude to the controller that varies in a step discrete fashion. The reference attitude is updated when the estimated attitude has approached the previous reference attitude within a given threshold, otherwise it remains equal to the previous reference meaning that the SV is still manoeuvring to that point. The supervisor only assigns $\bar{q}_{ref} = \bar{q}_{target}$ when the distance between $\bar{q}_{target}$ and $\bar{q}_{est}$ becomes lower than another threshold value.

It is a well-known problem that rotations from one orientation to another suffer from ambiguity. This is directly impacted on the quaternion entity which allows two representations for the same rotation: $\bar{q}_{rot}$ and $-\bar{q}_{rot}$ for the same great circle. In general, one prefers the rotation corresponding to the smaller angular displacement with amplitude θ, whereas the other corresponds to a rotation in the opposite direction with amplitude $2\pi - \theta$. A solution exclusively based on dynamical systems does not exist. Although introduction of logic enables the supervisor to choose which rotation to attain: if $\theta_{rot} > pi$ then instead of $\bar{q}_{rot}$ the supervisor picks $-\bar{q}_{rot}$ as the required rotation and computes $\bar{q}_{ref}$ accordingly.

For the choice of $\boldsymbol{\omega}_{ref}$ in fact two reference angular velocities are used simultaneously. The first $\boldsymbol{\omega}_{ref,1}$ is the angular velocity around which the dynamics are linearized. The second $\boldsymbol{\omega}_{ref,2}$ is the reference value to be attained by the controller. $\boldsymbol{\omega}_{ref,1}$ is set by monitoring the norm $\left\|\boldsymbol{\omega}_{ref,1} - \boldsymbol{\omega}_{est}\right\|$; when it becomes larger than a given threshold the supervisor updates $\boldsymbol{\omega}_{ref,1} = \boldsymbol{\omega}_{est}$. On the other hand $\boldsymbol{\omega}_{ref,2}$ should be assigned a value that allows the necessary rotation from $\bar{q}_{est}$ to $\bar{q}_{ref}$, by other words, it is dependent on $\bar{q}_{rot}$. The axis of rotation from $\bar{q}_{est}$ to $\bar{q}_{target}$ is $\boldsymbol{e}_{rot} = \frac{\boldsymbol{q}_{rot}}{\sin\left(\frac{\theta_{rot}}{2}\right)}$. The adopted solution is $\boldsymbol{\omega}_{ref,2} = k.\boldsymbol{e}_{rot}$, where $k = \frac{1}{50}\theta_{rot}$. With this choice the angular velocity required to the controller is proportional to the total angle of rotation to complete the manoeuvre. As the estimated attitude approaches the target attitude the angular velocity diminishes. The following pseudo-code resumes the main operations performed by the supervisor.

$sets\_ref\,(\bar{q}_{target}, \bar{q}_{est}, \boldsymbol{\omega}_{est}, \boldsymbol{\omega}_{\mathrm{w}})$	$\bar{q}^{p}_{ref}, \boldsymbol{\omega}^{p}_{ref}, \boldsymbol{\omega}^{p}_{w}$ - previous reference values
$\bar{q}_{rot} = \bar{q}_{est} \otimes q^{-1}_{target}$	
$\delta\theta_1 = 2\mathrm{acos}(\bar{q}_{rot,4})$	
$if\ \delta\theta_1 \leq\ threshold_1$: {	
$\bar{q}_{ref} = \bar{q}_{target};\ \bar{q}^{p}_{ref} = \bar{q}_{target}$ }	
$else$: {	
$\bar{q}_{rot_2} = \bar{q}_{est} \otimes \left(\bar{q}^{p}_{ref}\right)^{-1}$	
$\delta\theta_2 = 2\mathrm{acos}(\bar{q}_{rot_2,4})$ }	
$if\ \delta\theta_2 \leq\ threshold_2: \bar{q}_{ref} = \overline{\delta q}_{rot} \otimes \bar{q}_{est};$	$\overline{\delta q}_{rot}$ is a 10° rotation in the direction of $\bar{q}_{target}$
$else: \bar{q}_{ref} = \bar{q}^{p}_{ref}$	
$if\ \left\Vert \boldsymbol{\omega}_{ref,1} - \boldsymbol{\omega}_{est} \right\Vert > threshold_{\omega 1}: \boldsymbol{\omega}_{ref,1} = \boldsymbol{\omega}_{est}$	
$else: \boldsymbol{\omega}_{ref,1} = \boldsymbol{\omega}^{\boldsymbol{p}}_{ref}$	
$if\ \left\Vert \boldsymbol{\omega}_{\mathrm{w}} - \boldsymbol{\omega}^{\boldsymbol{p}}_{\mathrm{w}} \right\Vert > threshold_{w}: (\boldsymbol{\omega}_{w})_{ref} = \boldsymbol{\omega}_{w}$	
$else:\ (\boldsymbol{\omega}_{w})_{ref} = \boldsymbol{\omega}^{p}_{w}$	
$if\ \delta\theta_1 < threshold_3:\ \boldsymbol{\omega}_{ref,2} = 0$	
$else: \boldsymbol{\omega}_{ref,2} = \frac{\boldsymbol{q}_{rot}}{\sin\left(\frac{\delta\theta_1}{2}\right)} \frac{\delta\theta_1}{pi}$	
$\bar{q}^{p}_{ref} = \bar{q}_{ref};\ \boldsymbol{\omega}^{\boldsymbol{p}}_{ref} = \boldsymbol{\omega}_{ref,1};\ \boldsymbol{\omega}^{\boldsymbol{p}}_{w} = (\boldsymbol{\omega}_{w})_{ref}$	Update internal references
return $[q_{ref}, \boldsymbol{\omega}_{ref,1}, \boldsymbol{\omega}_{ref,2}$ and $(\boldsymbol{\omega}_{w})_{ref}]$	Output

To sum up, the supervisor comprises two main functions:

1. manoeuvre planning by setting the target state to the controller as the vector reference $[\bar{q}_{ref} \quad \boldsymbol{\omega}_{ref,2}]^T$
2. monitoring values $\boldsymbol{\omega}_{ref,1}$ and $(\boldsymbol{\omega}_{w})_{ref}$.

The MLQR is responsible to update the gain whenever any of the reference variables $\bar{q}_{est}$, $\boldsymbol{\omega}_{ref,1}$ or $(\boldsymbol{\omega}_{w})_{ref}$ used in the linearization is updated by the supervisor.

Also the trimming control input is computed in the MLQR. For the thrusters it renders:

$$\boldsymbol{M}_{trim} = \boldsymbol{\omega}_{ref,1} \times \left(I\boldsymbol{\omega}_{ref,1} + W^{I}(\boldsymbol{\omega}_{w})_{ref}\right) \tag{4.25}$$

For control with reaction wheels:

$$\boldsymbol{M^w}_{trim} = -W^{a+}\left(\boldsymbol{\omega}_{ref,1} \times \left(I\boldsymbol{\omega}_{ref,1} + W^I(\boldsymbol{\omega}_w)_{ref}\right)\right) \tag{4.26}$$

where W^{a+} is defined as the pseudo inverse of $W^{\boldsymbol{a}}$.

Adaptation for relative attitude tracking

In Chapter 5 a group control strategy is presented where some SVs only have access to relative attitude information. Their control quest is to null relative attitude. Hence the supervisor must be adapted to cope with an input of the form $\bar{q}_{21}$ (attitude of frame 2 relatively to frame 1) for instance, instead of the pair target and estimate quaternions. The simple setting of $\bar{q}_{rot} = \bar{q}_{21}$ renders the solution. In fact this is equivalent to shifting $\bar{q}_{target} = [0 \quad 0 \quad 0 \quad 1]^T$, i.e. a null rotation, and seeing the estimate as $\bar{q}_{est} = \bar{q}_{21}$. Reference criteria selection by the supervisor remains unchanged as well as the dynamics of the MLQR.

4.4. Wheels Reset Operation

Wheel desaturation is performed normally in a steady state, when the SV has a low angular velocity. The control strategy remains the same, yet information about the applied wheel torques during resetting is necessary for counteraction by the thrusters trimming control component:

$$\boldsymbol{M}_{trim} = \boldsymbol{\omega}_{ref} \times \left(I\boldsymbol{\omega}_{ref} + W^I\boldsymbol{\omega}_w\right) + W^a\boldsymbol{M^w}$$

The $\Delta\boldsymbol{M}$ quantity does not suffer any modification and so it is computed through the LQR feedback gain as given before.

Each wheel speed is reset to zero through the commanded torque computed in the following manner:

$$M^c = -K_w\omega_w$$

Recalling that the dynamics of the wheel is a simple integrator: $\dot{\omega}_w = M^c/I^w$, it renders the following dynamics for the commanded wheel:

$$\dot{\omega}_w = -\frac{K_w}{I^w}\omega_w$$

Such a controlled mechanism is known to belong to classic linear control. It is a first order system with pole at $s_1 = -\frac{K_w}{I^w}$. The value of K_w defines the pole which is chosen to be $s_1 = -\frac{1}{40}\ rad/s$, so that the time constant has a high corresponding value of 40 s.

4.5. Control Schemas

The block diagram for one SV simulation at this stage is the result of putting together the system dynamics (orbital dynamics and attitude dynamics), the attitude estimator and the controller closing the loop.

Figure 4.1 shows the control scheme for one SV using a simple LQR, i.e. without the manoeuvre supervisor included.

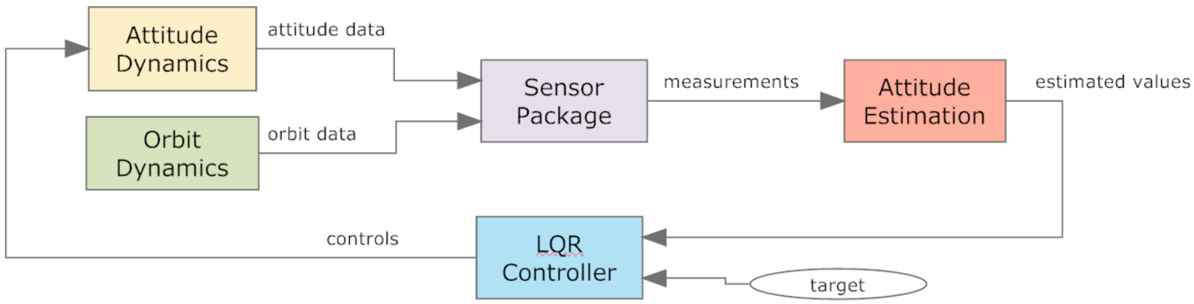

Figure 4.1 - Block diagram with simple LQR control

As we observe the target attitude is directly input in the LQR controller. The reference quaternion of the controller therefore equals the target quaternion and so it remains throughout the entire manoeuver. If a large manoeuvre is requested to this control system, convergence is dependent on the particular pair of initial and target attitude. Two possible undesired situations can occur after an unsuccessful manoeuver: the SV will end up wobbling in an uncontrolled motion with reaction wheels or thrusters acting ineffectively; or the SV converges to an attitude different than the target attitude.

In order to avoid both aforementioned situations the proposed MLQR and manoeuvre supervisor block are tied in the loop rendering the control mechanism depicted in the block diagram of Figure 4.2. As shown the target is input to the supervisor along with the attitude estimate. The controller is fed with reference values smoothen by the supervisor which informs the controller when it should update its gains through an output flag. The controller outputs the necessary control amount for trimming as well as the incremental regulation control.

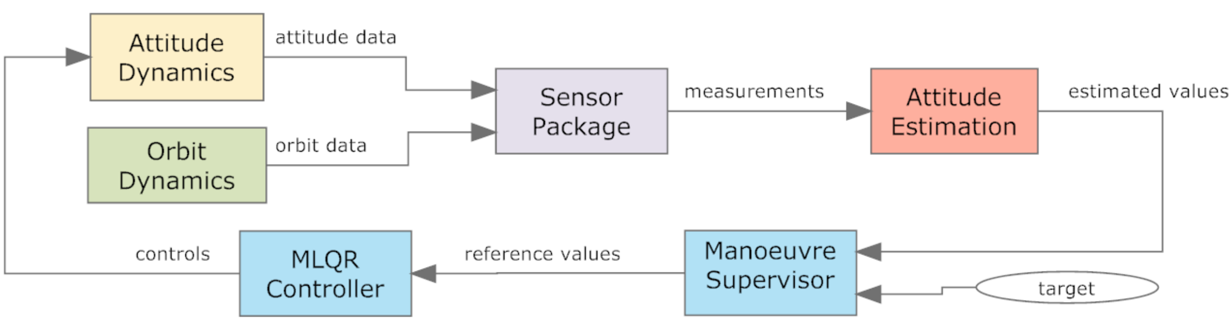

Figure 4.2 - Block Diagram for control with supervised MLQR

5. Group Attitude

So far the subject of analysis has been the stand alone SV system. An estimation algorithm and a control strategy were developed using information provided by its own on-board sensors. We now turn our attention to the problem of a group of satellites.

Section 5.1 is dedicated to a deterministic method in order to obtain relative attitude data between the group. Section 5.2 focuses on simple strategies to attain attitude alignment in the group.

5.1. Relative Attitude Determination

One technique for relative attitude determination between multiple vehicles employs the use of Line of Sight (LOS) vectors obtained through projection of beacon beams in the Focal Plane Detector (FPD). This way each SV possesses a source (beacon) and a FPD. The beacon targets the FPD of other vehicles while simultaneously its own FPD is illuminated by the other SV beams. The FPD translates relative position between two SV in the frame of the vehicle where it is installed.

In this section a deterministic solution is employed. This requires a minimum of three SV, resulting in a three pair of LOS vectors present in the formation. If a formation is constituted by four or more SV, then all combinations of three SV can be used to provide relative attitude determination. In Figure 5.1 the three SV group is illustrated along with the aforementioned LOS vectors. One of the SVs is considered the group chief whereas the other are called deputies.

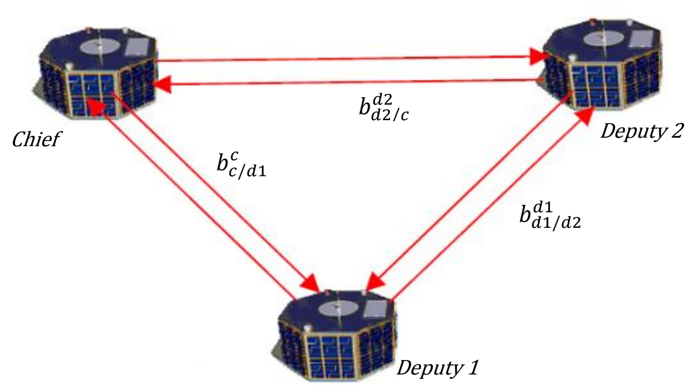

Figure 5.1 - Three vehicle configuration and respective LOS

Because different reference frames are used to represent the various LOS vectors, a structured notation is required here. A subscript will describe the vehicle for which the LOS is taken both from and to, while a superscript will denote in which reference frame the LOS is both represented and measured. For example, $\boldsymbol{b}^{x}_{x/y} = -\boldsymbol{b}^{x}_{y/x}$.

The frame work for relative attitude herein is not the quaternion as done in previous sections, but the attitude matrix with notation A_x^y instead, mapping coordinates expressed in the χ-frame into coordinates in the y-frame.

The beams between vehicles are assumed to be parallel, so that common vectors are given between SVs but in different coordinates. This means that a feedback mechanism must exist that monitors and corrects any misalignments. This is usually achieved electronically, assuring that the transmitted beam is formed on the focal point of the plane detector. The formulation presented next follows [15].

A. The Sensor Model

The direct measures for all LOS observations are the image space projections (α, β). Denoting the measurement image vector $\boldsymbol{m} = [\alpha, \beta]^T$. The measurement model follows

$$\widetilde{\boldsymbol{m}} = \boldsymbol{m} + \boldsymbol{n}_m \tag{5.1.1}$$

A typical noise model used to describe the uncertainty in the focal plane coordinate observations is given as:

$$R_{FOCAL} = \frac{\sigma_m^2}{1 + d(\alpha^2 + \beta^2)} \begin{bmatrix} (1 + d\alpha^2)^2 & (d\alpha\beta)^2 \\ (d\alpha\beta)^2 & (1 + d\alpha^2)^2 \end{bmatrix} \tag{5.1.2}$$

Where σ_m^2 is the variance of the measurement errors associated with α and β, and d is a coefficient typically with an order of magnitude of 1. This model accounts for an increased measurement standard deviation as distance from the FPD boresight increases.

The focal plane observations must be converted to unit space LOS observations. Assuming a focal length of unity the true LOS vector is given by

$$\boldsymbol{b} = \frac{1}{\sqrt{1 + \alpha^2 + \beta^2}} \begin{bmatrix} \alpha \\ \beta \\ 1 \end{bmatrix} \tag{5.1.3}$$

The unity measurement vector becomes

$$\widetilde{\boldsymbol{b}} = \boldsymbol{b} + \boldsymbol{n}_b \tag{5.1.4}$$

where $\boldsymbol{n}_b \sim N(0, \Omega)$ assuming that a normally distributed image-space vector renders an approximately Gaussian distribution over the unit space LOS vector. Because the LOS measurement is a unit vector, it must lie on a sphere, leading to a rank deficient matrix in $\mathcal{R}^3$.

The formulation presented here follows a first-order Taylor series approximation about the focal-plane axes. The partial derivative operator is used to linearly expand the focal-plane covariance in Eq. (5.1.2), yielding

$$H = \frac{\partial \boldsymbol{b}}{\partial \boldsymbol{m}} = \frac{1}{\sqrt{1 + \alpha^2 + \beta^2}} \begin{bmatrix} 1 & 0 \\ 0 & 1 \\ 0 & 0 \end{bmatrix} - \frac{1}{\sqrt{1 + \alpha^2 + \beta^2}} \boldsymbol{b}\boldsymbol{m}^T \tag{5.1.5}$$

Applying this operator to the uncertainty in the image space LOS vector gives the WFOV covariance model:

$$\Omega = H\, R^{FOCAL} H^T \tag{5.1.6}$$

Notice that Ω depends directly on the measurement values (α, β), meaning that two distinct body-frame vectors, $\boldsymbol{b}$, in general result in different covariance matrices.

B. Determination Algorithm

As mentioned this algorithm computes a set of relative attitudes matrix between at least three vehicles. The LOS equations for each vehicle pair are given by

$$\boldsymbol{b}^{c}_{c/d1} = A^{c}_{d1}\boldsymbol{b}^{d1}_{c/d1} \tag{5.1.7}$$

$$\boldsymbol{b}^{c}_{c/d2} = A^{c}_{d2}\boldsymbol{b}^{d2}_{c/d2} \tag{5.1.8}$$

$$\boldsymbol{b}^{d2}_{d2/d1} = A^{d2}_{c}A^{c}_{d1}\boldsymbol{b}^{d1}_{d2/d1} = A^{d2}_{d1}\boldsymbol{b}^{d1}_{d2/d1} \tag{5.1.9}$$

The model in Equations (5.1.7)-(5.1.9) is purely deterministic and the LOS vector considered are the true LOS vectors. These are substituted by their corresponding measured LOS vectors in realistic operation, which gives rise to errors in the computed attitude matrices. The effect of such errors is shown in the results section. Performing the inner product between both members of (5.1.7) and (5.1.8) yields:

$$\boldsymbol{b}^{c^T}_{c/d2}\boldsymbol{b}^{c}_{c/d1} = \boldsymbol{b}^{d2^T}_{c/d2}A^{d2}_{d1}\boldsymbol{b}^{d1}_{c/d1} \tag{5.1.10}$$

Eqs. (5.1.9) and (5.1.10) represent a direction and an arc-length respectively. The algorithm to determine A^{d2}_{d1} provided such information is given in [18] and is briefly reviewed here. Its objective is to compute the first relative attitude matrix of the group. As we shall see later this only needs to be done once.

In more general terms, matrix A satisfies the following relations:

$$\boldsymbol{w}_1 = A\boldsymbol{v}_1 \tag{5.1.11}$$

$$d = \boldsymbol{s}^T A\boldsymbol{v}_2 \tag{5.1.12}$$

With the arc-length d and all vectors in Eq. (5.1.11) and (5.1.13) being given. All vectors have unit length. The solution is given by

$$A = R(\widehat{\boldsymbol{w}}_1, \theta)A_0 \tag{5.1.13}$$

where A_0 is any rotation matrix satisfying $\boldsymbol{w}_1 = A_0\boldsymbol{v}_1$, and $R(\widehat{\boldsymbol{w}}_1, \theta)$ is matrix representing rotation about the $\boldsymbol{w}_1$ axis through an angle θ $(0 \le \theta < 2\pi)$ which must be also determined. By Euler's formula a rotation $R(\boldsymbol{n}, \theta)$ is given by

$$R(\widehat{\boldsymbol{w}}_1, \theta) = \cos(\theta)\, I_{3\times 3} + (1 - \cos\theta)\boldsymbol{n}\boldsymbol{n}^T + \sin\theta\, [\boldsymbol{n}\, \times] \tag{5.1.14}$$

The strategy is such that first we find a candidate matrix A_o which satisfies (5.1.11) and then determine the values of θ for which (5.1.12) is also satisfied. Let us look for A_o of the form Or the case that $\boldsymbol{w}_1 = -\boldsymbol{v}_1$ choose n_0 to be any direction perpendicular to $\boldsymbol{v}_1$ and $\theta_0 = \pi$. In all other cases one might choose

$$n_0 = \frac{\boldsymbol{w}_1 \times \boldsymbol{v}_1}{|\boldsymbol{w}_1 \times \boldsymbol{v}_1|} \tag{5.1.15}$$

Thus, in every case, $\boldsymbol{n}_0$ satisfies

$$\boldsymbol{n}_0.\boldsymbol{v}_1 = \boldsymbol{n}_0.\boldsymbol{w}_1 = 0 \tag{5.1.16}$$

When $\boldsymbol{w}_1 \neq \pm\boldsymbol{v}_1$, i.e. $\boldsymbol{w}_1$ and $\boldsymbol{v}_1$ are linearly independent, a unique solution exists for θ_0

$$\theta_0 = \arctan_2(|\boldsymbol{w}_1 \times \boldsymbol{v}_1|, (\boldsymbol{w}_1.\boldsymbol{v}_1)) \tag{5.1.17}$$

Yielding for the matrix A_0 the equivalent formula

$$A_0 = \ I_{3\times 3} + [(\boldsymbol{w}_1 \times \boldsymbol{v}_1)\times] + \frac{1}{1 + \boldsymbol{w}_1.\boldsymbol{v}_1}[(\boldsymbol{w}_1 \times \boldsymbol{v}_1)\times]^2 \tag{5.1.18}$$

Now to compute θ define

$$\boldsymbol{w}_3 = A_0\boldsymbol{v}_2 \tag{5.1.19}$$

Then θ must obey the following equation equivalent to Eq. (5.1.12)

$$\boldsymbol{s}^T R(\boldsymbol{w}_1, \theta)\boldsymbol{w}_3 \; = d_2 \tag{5.1.20}$$

Substituting Euler's formula and rearranging terms leads to

$$Bcos(\theta - \beta) = (\boldsymbol{s}.\boldsymbol{w}_1)(\boldsymbol{w}_1.\boldsymbol{w}_3) - d_2 \tag{5.1.21}$$

with

$$B = |\boldsymbol{s} \times \boldsymbol{w}_1||\boldsymbol{w}_1 \times \boldsymbol{w}_3| \tag{5.1.22}$$

$$\beta = arctan_2\left(\boldsymbol{s}(\boldsymbol{w}_1 \times \boldsymbol{w}_3), \boldsymbol{s}.\left(\boldsymbol{w}_1 \times (\boldsymbol{w}_1 \times \boldsymbol{w}_3)\right)\right) \tag{5.1.23}$$

For a solution in θ, Eq. (5.1.21) poses the following necessary condition

$$|(\boldsymbol{s}.\boldsymbol{w}_1)(\boldsymbol{w}_1.\boldsymbol{w}_3) - d_2| \leq |\boldsymbol{s} \times \boldsymbol{w}_1||\boldsymbol{w}_1 \times \boldsymbol{w}_3| \tag{5.1.24}$$

If this condition holds, then

$$\theta = \beta + \arccos\left[\frac{(\boldsymbol{s}.\boldsymbol{w}_1)(\boldsymbol{w}_1.\boldsymbol{w}_3) - d_2}{|\boldsymbol{s} \times \boldsymbol{w}_1||\boldsymbol{w}_1 \times \boldsymbol{w}_3|}\right] \tag{5.1.25}$$

Because the $arccos$ function is two valued over the interval $[0, 2\pi[$ two solutions for θ are obtained. Some criteria must be used in order to separate the correct solution. The adopted criterion is an assessment of the solution which better fits the given LOS data. This means we shall choose θ such:

$$\theta = \arg\min_{\theta}\{|d - s^T A v_2|\} \tag{5.1.26}$$

The condition imposed by inequality (5.1.24) implies that not always this determination method is solvable. If a set of vectors cannot satisfy the inequality then another set from the formation must be used, which will naturally determine a different relative attitude. Table 5. shows the combination of LOS vectors needed to compute three of the six possible relative attitude matrices of the triad formation.

Table 5.1 – Combinations of LOS measurements

Attitude Matrix	d	w_1	v_1	s	v_2
A_{d1}^{d2}	$b_{c/d2}^{c^T} b_{c/d1}^{c}$	$b_{d2/d1}^{d2}$	$b_{d2/d1}^{d1}$	$b_{c/d2}^{d2}$	$b_{c/d1}^{d1}$
A_{c}^{d1}	$b_{d2/d1}^{d2^T} b_{d2/c}^{d2}$	$b_{d1/c}^{d1}$	$b_{d1/c}^{c}$	$b_{d2/d1}^{d1}$	$b_{d2/c}^{c}$
A_{d2}^{c}	$b_{d1/c}^{d1^T} b_{d1/d2}^{d1}$	$b_{c/d2}^{c}$	$b_{c/d2}^{d2}$	$b_{d1/c}^{c}$	$b_{d1/d2}^{d2}$

The relative attitude determination method just employed is named First Attitude Matrix Determination (FAMD) for the sake of abbreviation.

The same procedure can be used to determine the remaining attitudes. However, once the first relative attitude is obtained the well-known TRIAD algorithm can be applied instead. This constitutes a computationally efficient approach. The solution of the TRIAD algorithm is given here. For a complete derivation and explanation see [18].

$$A = M_c M_d^T \tag{5.1.27}$$

$$M_c = \left[c_1 \quad \frac{c_1 \times c_2}{\|c_1 \times c_2\|} \quad \frac{c_1 \times (c_1 \times c_2)}{\|c_1 \times (c_1 \times c_2)\|}\right] \tag{5.1.28}$$

$$M_d = \left[d_1 \quad \frac{d_1 \times d_2}{\|d_1 \times d_2\|} \quad \frac{d_1 \times (d_1 \times d_2)}{\|d_1 \times (d_1 \times d_2)\|} \right] \tag{5.1.29}$$

For instance, after finding A_{d1}^{d2}, one gets A_c^{d1} by substituting $c_1 = \boldsymbol{b}_{c/d1}^{c}$, $c_2 = \boldsymbol{b}_{c/d2}^{c}$, $d_1 = \boldsymbol{b}_{c/d1}^{d1}$ and $d_2 = A_{d1}^{d2^T} \boldsymbol{b}_{c/d2}^{d2} = \boldsymbol{b}_{c/d2}^{d1}$. Once A_c^{d1} is found, we get A_{d2}^{c} and complete the overall determination procedure using

$$A_{d2}^{c} = A_{d1}^{c} A_{d2}^{d1} \tag{5.1.30}$$

The other combinations of vectors for the TRIAD algorithm are resumed in Table 5.2

Table 5.2 – Combinations of vectors for the TRIAD algorithm

Attitude Matrix	c_1	c_2	d_1	d_2
A_{d1}^{d2}	$b_{d2/d1}^{d2}$	$b_{d2/c}^{d2}$	$b_{d2/d1}^{d1}$	$b_{d2/c}^{d1} = A_c^{d1} b_{d2/c}^{c}$
A_c^{d1}	$b_{d1/c}^{d1}$	$b_{d1/d2}^{d1}$	$b_{d1/c}^{c}$	$b_{d1/d2}^{c} = A_{d2}^{c} b_{d1/d2}^{d2}$
A_{d2}^{c}	$b_{c/d2}^{c}$	$b_{c/d1}^{c}$	$b_{c/d2}^{d2}$	$b_{c/d1}^{d2} = A_{d1}^{d2} b_{c/d1}^{d1}$

The implementation of the overall algorithm must be robust. Failure in finding the first attitude matrix would imply failure of the whole determination. In order to circumvent this we introduce logic that enables to switch the attitude matrix that is first computed. Also note that the TRIAD algorithm is only subjected to flaw when $c_1 = \pm c_2$, which is a much less likely situation than the one set in the FAMD resolution. A portion of the pseudo code follows.

$[A_{21}, A_{1c}, A_{c2},] = relative\_attitude(b_{12}, b_{21}, b_{1c}, b_{c1}, b_{2c}, b_{c2})$	
$d = b_{c2}^T . b_{c1};\ w_1 = b_{21};\ v_1 = -b_{12};\ s = -b_{2c};\ v_2 = -b_{1c};$	Setting vectors for FAD
$A_{21} = FADM(d, w_1, v_1, s, v_2);$	1st attitude matrix
$if\ A21\ found: \{$	
$c_1 = b_{c1};\ c_2 = b_{c2};\ d_1 = -b_{1c};\ d_2 = A_{21}^T(-b_{2c});$	Setting vectors for TRIAD
$if\ c1 \neq \pm d1\ and\ c2 \neq \pm d2\ \{$	Check TRIAD
$A_{c1} = TRIAD(c_1, c_2, d_1, d_2);$	Compute 2nd matrix
$A_{c2} = A_{c1} A_{21}^T;\ A_{1c} = A_{c1}^T;\ return;$	Compute 3rd matrix
$else: \{$	If TRIAD failed
$c_1 = b_{c2};\ c_2 = b_{c1};\ d_1 = -b_{2c};$ $d_2 = A_{21}(-b_{1c});$ $if\ c1 \neq \pm d1\ and\ c2 \neq \pm d2: \{$	Try to compute another 2nd matrix
$A_{c2} = TRIAD(c_1, c_2, d_1, d_2);$	
$A_{1c} = A_{21}^T A_{c2}^T;\ return; \} \} \} \}$	
$d = b_{1c}^T . b_{12};\ w_1 = b_{c2};\ v_1 = -b_{2c};\ s = -b_{c1};\ v_2 = -b_{21};$	Try another 1st matrix
$A_{c2} = FADM(d, w_1, v_1, s, v_2);$	

$if\ A_{c2}\ found$: (continue)	

It is expected that such implementation allows for determination of at least one first attitude matrix in every possible situation. Also, if the TRIAD algorithm fails in one case – which is extremely unlikely – the TRIAD is called again to find another second matrix.

The main complexity of this relative attitude determination strategy lies on the attainment of the first attitude matrix, where one condition must be satisfied and one disambiguation must be performed. The small computational burden make it very adequate for a real-time system application.

5.2. Group Control

The relative determination attitude can be used to compute a redundant estimate for each SV. Also it becomes particular interesting for heterogeneous constellations where only one SV possesses the sensor package that allows determination of its absolute attitude whereas the remaining satellites of the group are only provided with relative attitude data. Communication of one absolute estimate between SV allows an estimate of the other SV absolute attitude; for instance for SV2 and SV3 we get:

$$\bar{q}_2 = \bar{q}_{21} \otimes \bar{q}_1$$
$$\bar{q}_3 = \bar{q}_{31} \otimes \bar{q}_1$$

where $\bar{q}_1$ computed via the SV1 sensor package on board and $\bar{q}_{21}$, $\bar{q}_{31}$ given by the LOS relative attitude algorithm. In this circumstances SV1 is designated the chief of the group whilst SV2 and SV3 are the deputies. In terms of sensors the latter only need the FPD with laser emitter incorporated, and a communication package to connect to the chief where all computations and other sensor readings are performed.

A prompt solution for group control is to have the deputy tracking the chief. The target attitude is calculated or passed to the chief via an uplink and it manoeuvres to the target while the deputies follow by nulling their relative attitudes.

A different strategy is to let the chief reorient to the target while the deputies remain stationary. When the chief SV stabilizes around the target, the deputies are allowed to align their attitude with the chief leading the entire group to the desired final configuration.

A celestial sphere coverage solution arises with relative attitude data. One can operate the deputies at an offset attitude from the chief. For instance three SV might be separated with 4/5 degrees from each other to hold a triangular pointing configuration.

The chief-deputies group operation works in the following way:

- The LOS vector readings in the deputies are passed to the chief where the relative determination algorithm runs
- The relative attitude matrices obtained are converted to quaternions and sent to the respective deputies
- The chief's target attitude is given by an external source, whereas for the deputies the target can be either the chief's inertial attitude or their relative attitude to the chief given.

A group of equally equipped SV can be manoeuvred without determining relative attitude. However appropriate combinations of relative attitude quaternions with absolute attitude quaternions render a redundant estimate for each satellite. For example for SV1 $\bar{q}_1 = \bar{q}_{12} \otimes \bar{q}_2$ and also $\bar{q}_1 = \bar{q}_{13} \otimes \bar{q}_3$. These additional estimates can serve several purposes:

- Validation of the inertial estimates,
- Improvement of estimate accuracy through data fusion
- Estimation of sensor misalignments in the group.

A Group Coordinator (GC) is implemented to address the problem of coordinating operations in the group. Physically the GC is installed on-board of one vehicle though its function is to monitor the group and to take the following measures:

1. establishing the target attitude or different targets for each vehicle
2. receiving information from the local SV manoeuvre supervisor
3. coordinating the manoeuvre through feedback
4. Scheduling operations such as nulling of reaction wheels speed
5. forcing a change of the estimation algorithm

The SV constellation architecture with GC constitutes a modular approach that provides flexibility to the end user. Hence the complexity of group coordination is passed to the GP leaving the low level tracking operations to each vehicle individually.

With the GC an additional category of consensus manoeuvre arises that does not drive the constellation to a specified target, but instead it only attains alignment. In this manoeuvre each SV tracks a varying target attitude, from now on called the converse attitude. For instance for SV1 its converse attitude is the middle attitude between SV2 attitude and SV3 attitude, i.e.

$$\bar{q}_{con_1} = f(\bar{q}_2, \bar{q}_3)$$

where f performs the following operations:

$$\bar{q}_{32} = \bar{q}_3 \otimes \bar{q}_2^{-1}$$
$$\theta_{half_{32}} = arccos(q_{32})$$
$$\boldsymbol{e}_{32} = \boldsymbol{q}_{32} / sin(\theta_{32})$$
$$\bar{q}_{half_{32}} = \left[\boldsymbol{e}_{32}\, sin\left(\frac{\theta_{32}}{2}\right) \quad cos\left(\frac{\theta_{32}}{2}\right)\right]$$
$$\bar{q}_{con_1} = \bar{q}_{half_{32}} \otimes \bar{q}_2$$

Hence with this strategy the SVs approach each other towards a common point that can be seen conceptually as the centre of attitude of the constellation. An illustrative analogy is to imagine a triangular whose vertexes approach each other by moving towards the barycentre. The barycentre is not fixed because of the vertexes displacement though and so it is calculated in every control cycle.

When the group reaches a certain amount of consensus, i.e. the angular distances within the three attitude set are smaller than a threshold value, then an average common attitude is imposed to the group according to:

$$\boldsymbol{Q}_w = \frac{\bar{q}_1 + \bar{q}_2 + \bar{q}_3}{3}$$

which is normalized to $\bar{q}_w = \boldsymbol{Q}_w / \|\boldsymbol{Q}_w\|$. The threshold is set to 1° between any combination of two vehicles.

6. Results

The results were obtained through simulation in the *Simulink/Matlab* environment

6.1. Attitude Estimation

The estimation results are presented here to assess and validate the estimation algorithms performance. Sensors noise characteristics that were given previously in Chapter 2 are implemented in the simulation environment. Nevertheless we resume them here whenever necessary as well as other relevant parameters of the dynamics, estimation and control.

The Star Tracker noise covariance is given through the three-vector covariance:

$$R_a = 0{,}2388 \times 10^{-6} I_{3\times 3}\ (rad/s)^2$$

meaning that the equivalent RMS error of the Star Tracker observations is approximately:

$$\sigma_{ST} = 0{,}0485°$$

The Sun sensor RMS error introduced in each axis is:

$$\sigma_{SS} = 0{,}1°$$

The Horizon sensor RMS errors introduced in each axis are:

$$\sigma_{HS,1} = 0{,}2°$$

$$\sigma_{HS,2} = 0{,}5°/s$$

Gyro noise is set by the two RMS quantities introduced in Section 2.1:

$$\sigma_v = 0{,}6957\ arcsec/s$$

$$\sigma_u = 2{,}5743 \times 10^{-4}\ arcsec/s^2$$

A. Deterministic Attitude Observer

The estimation results using the deterministic observer can be seen in Figure 6.1. The true quaternion is $\bar{q} = [0{,}3948 \quad 0{,}5090 \quad -0{,}4679 \quad 0{,}6051]^T$, the SV is at rest ($\boldsymbol{\omega} = 0$) and the initial position of the satellite in ECI coordinates is $r_{init} = [0 \quad 9400000 \quad 0]^T$. Furthermore we assume to be on the 21st of March, this way the Sun initial position in ECI frame is $p_{Sun} = 1UA \times [1 \quad 0 \quad 0]^T$. This last assumption will remain for the following simulations.

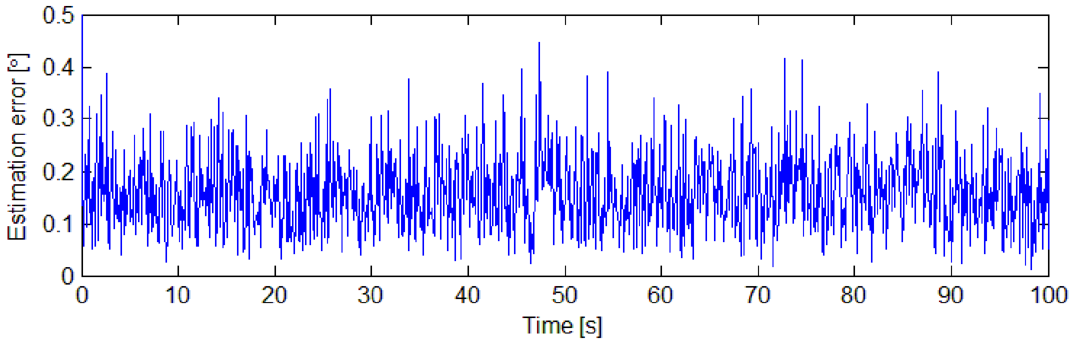

Figure 6.1 – Deterministic Observer error

The corresponding RMS error is $\sigma_{obs} = 0.2025°$. This value is somewhat dependent on the configuration of the Sun and Earth line of sight vectors. If the SV is placed in the vernal equinox line, for instance $r_{init} = [7800000\ 0\ 0]^T$ the information provided by the Sun and Earth vector is not complementary – in fact for the initial position the true Sun and Earth vectors are exactly parallel. Figure 6.2 shows the results in such a poor Sun-Earth configuration lines.

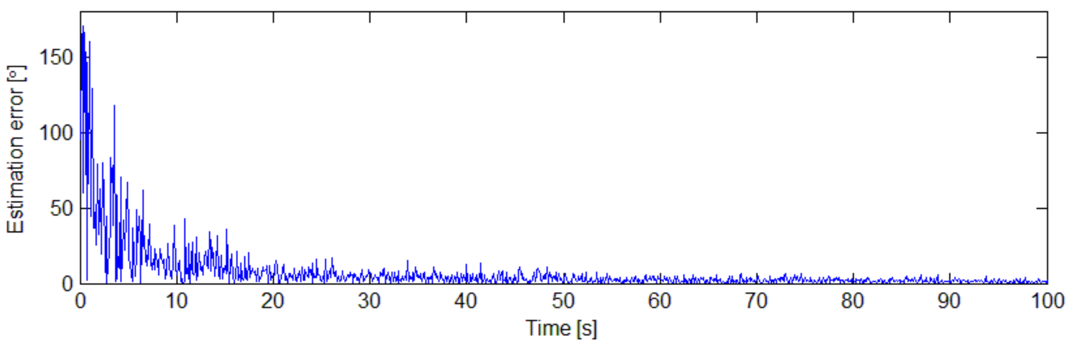

Figure 6.2 – Deterministic observer error for poor Sun-Earth configuration

Indeed the accuracy degrades considerably especially during the initial seconds when the SV remains in the vernal equinox line. As the SV continues its orbit and departs from its initial position, the Sun-Earth configuration improves rapidly and we see that after only 100 seconds the determination error decreases to less than 4°. Thus we can state that these singular conditions rarely appear during orbit.

In addition notice that the deterministic observer requires both vectors simultaneously. If umbra condition is verified at some point in the orbit, the Sun measurement will be absent and no attitude solution is provided by this algorithm.

B. Kalman Filtering

We recall here that the EKF for angular velocity is tested with the following parameters:

- Angular velocity propagation model covariance: $Q_\omega = 10^{-14} I_{3\times3}$
- Gyroscope observations covariance: $R_{gyr} = \sigma_v^2 I_{3\times3}$ with $\sigma_v = 0{,}6957\ arcsec/s$

A simulation with $\boldsymbol{\omega}_{init} = [-0{,}0336 \quad -0{,}0044 \quad -0{,}0085]\, rad/s$ ($\|\boldsymbol{\omega}_{init}\| = 2°/s$) is run. This is the order of magnitude of the angular velocities that are to be found during reorientation manoeuvres. A comparison between the filter estimate and the gyroscope output is shown in Figure 6.3.

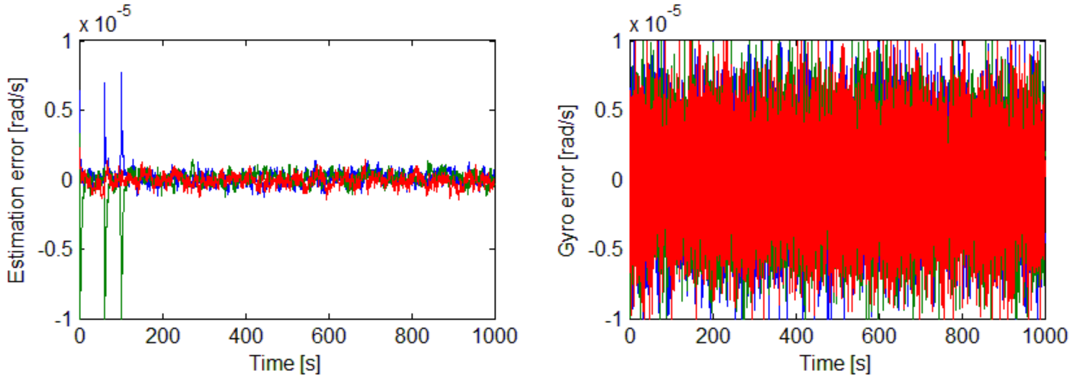

Figure 6.3 – Comparison of angular speed estimation

We observe that the noise reduction is considerable. The picky response of the filter estimate in singular initial events is the main disadvantage when compared with the raw gyroscope data. However this unsteady behaviour vanishes when the estimation covariance stabilizes.

For the MEKF that uses constant parameter tuning, the following values are used:

- Three-vector model covariance: $Q_a = \sigma_a^2 I_{3\times3} = 1{,}85 \times 10^{-11} I_{3\times3}$
- Drift model covariance: $Q_\mu = \sigma_\mu^2 I_{3\times3} = 10^{-16} I_{3\times3}$
- Constant Sun vector covariance: $R_{Sun} = 3{,}5 \times 10^{-6}$
- Constant Earth vector covariance: $R_{Earth} = 3{,}5 \times 10^{-6}$

When the MEKF uses varying parameter tuning (see Section 3.3), then:

- $Q_{a,k}$ is computed by the parameterization elaborated.
- R_{Sun} and R_{Earth} are computed using the corresponding angular measurement $\hat{m} = [\hat{\alpha} \quad \hat{\varphi}\,]$ and the appropriate covariance transformation
- R_{ST} is also computed resorting to covariance transformation that uses the observed Star Tracker quaternion

The results for the simple MEKF (i.e. without drift estimation) using solely Sun and Earth vector observations is shown in Figure 6.4. Convergence of the estimate is achieved after only $5\,s$. The true quaternion is $\bar{q} = [0{,}3948 \quad 0{,}5090 \quad -0{,}4679 \quad 0{,}6051]^T$ and the initial guess is $\bar{q} = [0 \quad 0 \quad 0 \quad 1]^T$ constituting an initial angular error of $\theta_{err}^{init} = 72.4°$. No drift is added ($\boldsymbol{\mu} = 0$) and the angular velocity is $\boldsymbol{\omega} = 0$. The filter tuning parameters are constant.

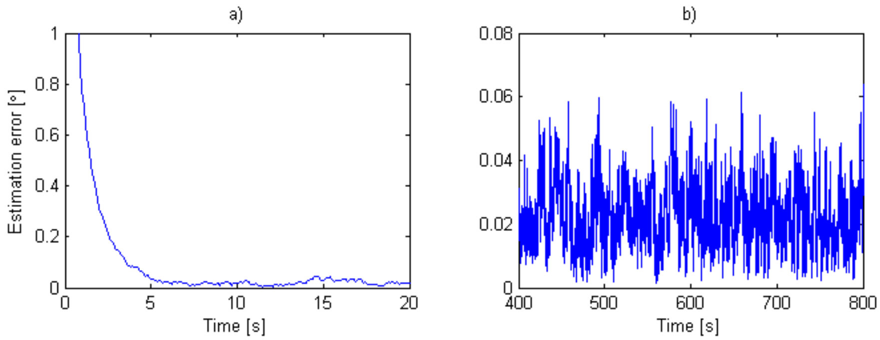

Figure 6.4 – MEKF attitude estimation using Sun and Earth vectors
a) convergence b) steady-state

The corresponding RMS error in this conditions is $\sigma_{est} = 0{,}0274°$. Compared with the deterministic observer, the accuracy of the filter is 7,4 higher. Nevertheless this value was obtained with a bad initial guess and high initial covariance. In reality if we choose a better initial guess, say with an error of $(\Delta\theta = 0.2°)$ and a much lower initial covariance $(\sigma_a^2 = 10^{-6})$ the RMS error comes down to $\sigma_{est} = 0{,}0094°$ which constitutes an accuracy 21,32 times better than the deterministic observer.

Also recall that the MEKF is able to compute estimates even in umbra conditions, therefore it is interesting to evaluate how much the accuracy will degrade in such cases. The result using only Earth vector measurement is presented in Figure 6.5. The initial estimate considered is $\Delta\theta = 0.01°$ and the initial state covariance $\sigma_a^2 = 10^{-6}$ in order to emulate convergence of the MEKF before occurrence of Sun light blockage.

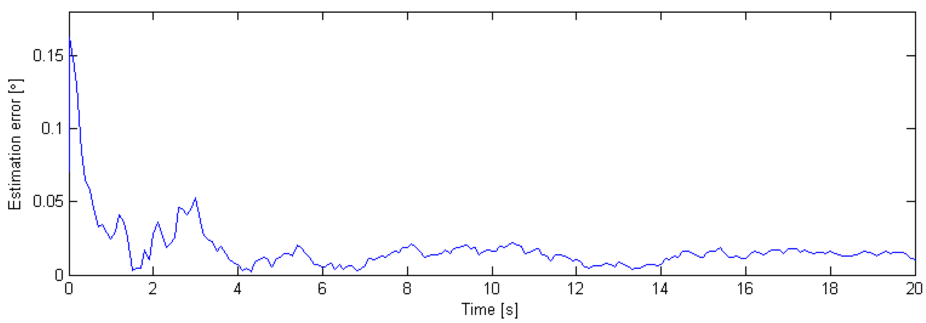

Figure 6.5 – Estimation when Sun light is blocked. Earth vector update only

The RMS error for 2000 seconds is $\sigma_{est} = 0{,}0129°$ which is slightly higher than the error with both Sun and Earth vectors. Intuitively using more observations is always beneficial in terms of accuracy gain which is according to these results. Furthermore the absence of Sun vector constitutes a fault in observability of the SV system. Nevertheless we can state that for the due period of time $(2000\ s)$ and with $\boldsymbol{\omega} = 0$ a single vector observation is enough to keep the MEKF performing under umbra conditions without significant degradation of accuracy.

The MEKF estimation results using Star Tracker data are depicted in Figure 6.6. The corresponding RMS error is $\sigma_{est} = 0{,}0024° = 8{,}7325\ arcsec$. This means that the accuracy gain of the filter is approximately 20 times the accuracy of the Star Tracker observations.

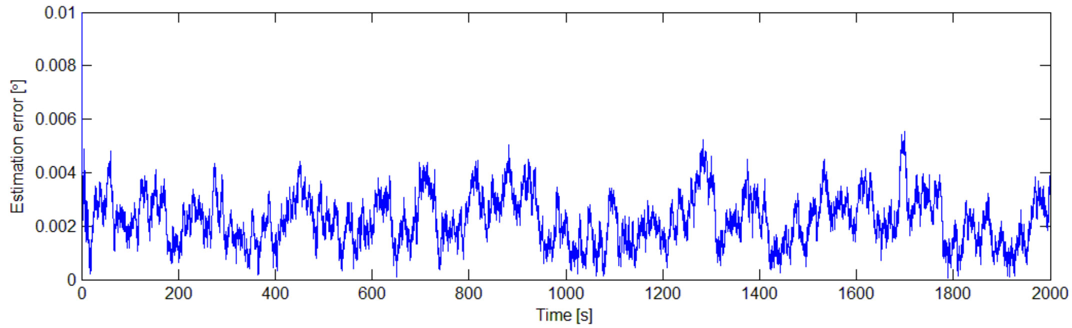

Figure 6.6 – Estimation with Star Tracker data

When the angular velocity is non-null and the same filters using constant tuning parameters are used, considerably degradation in the accuracies result. For instance consider again the two-vector update MEKF and an initial angular velocity vector of $\boldsymbol{\omega} = [-0{,}1678 \quad -0{,}0221 \quad -0{,}0427]^T\ rad/s$, $\|\boldsymbol{\omega}\| = 10°/s$. This value is quite high for a large SV and not commonly found in normal operations. A simulation in the conditions just expressed is shown in Figure 6.7.

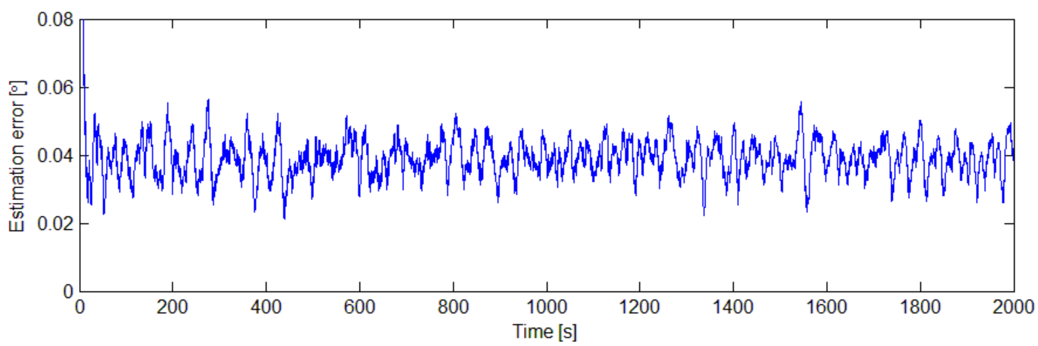

Figure 6.7 – MEKF estimation with Sun and Earth vectors update, nonzero angular velocity

The estimation error is considerably increased compared to the error in stationary state. We observe that although the estimate jitter is approximately the same, the estimates are affected by an error bias of constant magnitude. The consequence is an increase of the RMS error to $\sigma_{est} = 0.0393°$.

If the variable three vector covariance is used instead ($Q_{a,k}$) the bias lowers as shown in Figure 6.8.

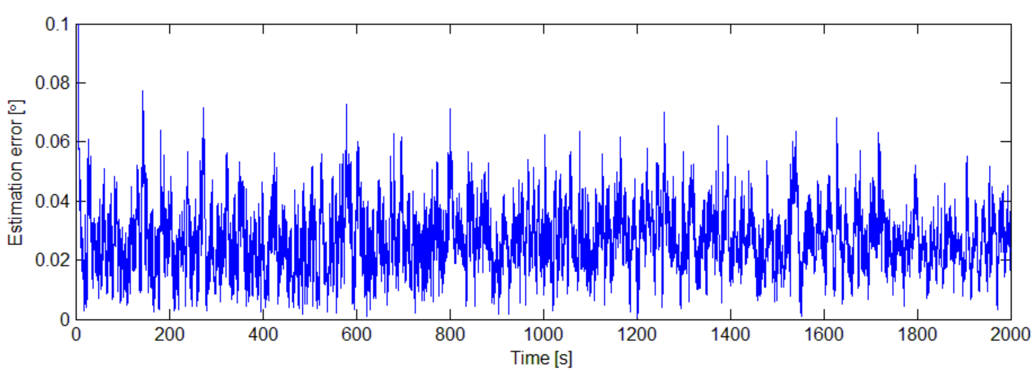

Figure 6.8 – MEKF estimation with Sun and Earth vectors, variable covariance model, nonzero angular velocity

The price to pay is an increase of the output jitter as the noisy measurements become less damped. The corresponding RMS error is $\sigma_{est} = 0{,}0289°$ which constitutes a small improvement relatively to the constant Q_a. However when higher angular velocities are applied the benefits are greater. For instance with a $30°/s$ initial angular velocity the RMS error using the fixed tuning Q_a is $\sigma_{est} = 0{,}1193°$ whereas with the variable $Q_{a,k}$ this value drops to $\sigma_{est} = 0{,}0686°$.

We now analyse the results of the MEKF including drift estimation. This filter uses constant tuning parameters. The results for attitude estimation are very similar to the ones just presented. The major difference is on the period of stabilization of the filter, which is much longer especially when ad hoc initial attitude guesses are chosen. One of the major particularities in drift estimation is that an initial accurate estimate for the drift value is inexistent, therefore we set $\hat{\boldsymbol{\mu}}_{init} = 0$. In order to test the drift estimation a constant drift is introduced in the gyro sensor $\boldsymbol{\mu}_{const} = 10^{-5}.[1 \quad -2 \quad -7]^T rad/s$. The initial angular velocity is set to $\boldsymbol{\omega} = 0$. The initial attitude guess is once more at 0,2° from the true attitude. The drift estimate results are presented in Figure 6.9.

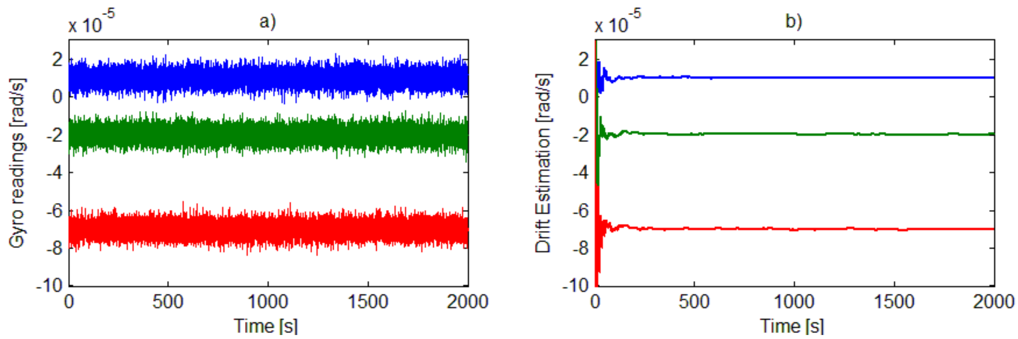

Figure 6.9 – Illustration of drift estimation.
a) Gyroscope readings, b) Drift estimate

Figure 6.9 a) shows the gyroscope measurements affected by noise and by the constant drift. In Figure 6.9 b) we observe that the drift estimate is close to the real value and exhibits good stability.

A second simulation with the exact same settings except for the initial angular velocity ($\boldsymbol{\omega} = [-0{,}3356 \quad -0{,}0442 \quad -0{,}0854]^T$, $\|\boldsymbol{\omega}\| = 20°/s$) is run. The results are depicted in Figure 6.10.

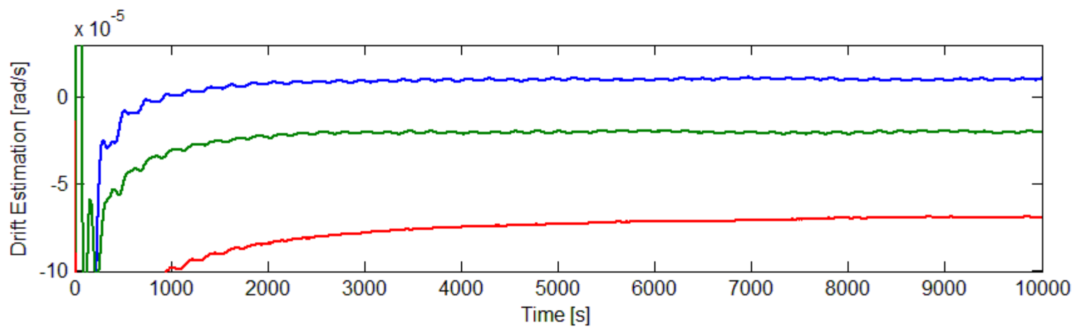

Figure 6.10 – Drift estimation for nonzero angular velocity

We observe that the estimate takes much more time to converge in this situation. In addition the graphic reveals a small oscillatory behaviour. This is due to the rotation of the SV which clearly affects the dynamics of the filter. We now compare the difference between the MEKF attitude estimate with and without drift estimation in the presence of gyro drift. The initial angular velocity in this case is set to null ($\boldsymbol{\omega} = 0$). Figure 6.11 shows clearly that the error penalty of not estimating the drift is significant.

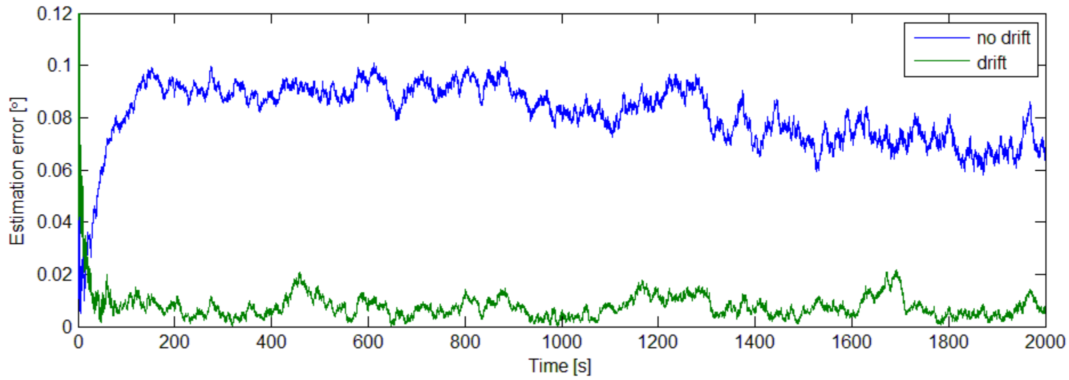

Figure 6.11 – Comparison of attitude estimate between the MEKF with and with no drift estimate

Concluding this analysis on the attitude estimate results we can state that the MEKF strategy is definitely capable of providing reliable attitude data even in less favourable conditions such as temporary loss of sensor readings and high angular velocities.

6.2. Single Vehicle Control

In this section we assess the results of attitude control of the single SV system, including steady state operation (equivalent to pointing operation mode), small and large reorientation manoeuvres. Being the MLQR an augmented version of the simple LQR only results with the MLQR controller will be presented here. In fact for a small manoeuvre ($\Delta\theta < 5°$) the MLQR performs just like the simple LQR. State information feeding the Supervisor and the MLQR comes from the Estimators block, namely ($\boldsymbol{\omega}_{est}, \bar{q}_{est}$). The wheels speed $\boldsymbol{\omega}_W$ and wheels acceleration $\dot{\boldsymbol{\omega}}_W$ are directly read from free-error sensors placed in the actuators. The Estimator used is the fixed parameter MEKF for attitude estimation only – which is equivalent to say that the drift has been estimated beforehand. All simulation settings are accordingly as those in the previous section. Additional parameters and constants used by the controllers must be defined:

The weighting matrices used to compute the feedback gains are the following:

- States weighting matrix $Q = diag([1 \quad 1 \quad 1 \quad 0{,}5 \quad 0{,}5 \quad 0{,}5]^T)$
- Wheels control weighting matrix $R_{wheel} = I_{3\times3}$
- Thrusters control weighting matrix $R_{thrust} = \frac{2}{100} I_{3\times3}$

The reaction wheels axes is set to $W^a = \begin{bmatrix} 1 & 0 & 0 \\ 0 & 1 & 0 \\ 0 & 0 & 1 \end{bmatrix}$, which means the fourth wheel is unused.

The first result presented is a small 5° angle manoeuvre. Initially the SV attitude is given by $\bar{q}_{init} = [-0{,}6480 \quad -0{,}5437 \quad -0{,}4473 \quad 0{,}2905]^T$ and the angular speed is null ($\boldsymbol{\omega}_{init} = 0$). Figure

6.12Figure shows the error evolution during transition to the target. We observe that the thrusters perform a faster manoeuvre than the wheels.

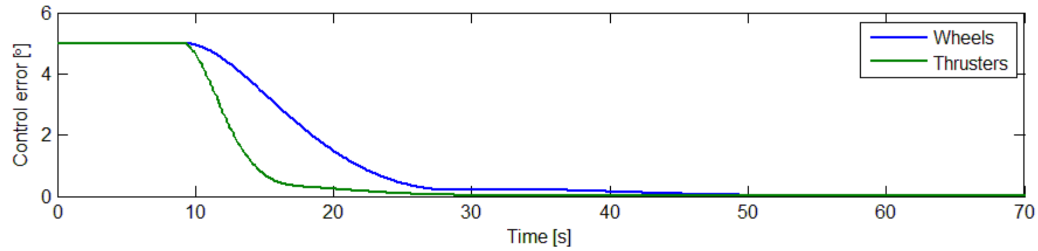

Figure 6.12 – Small manoeuvre comparison between wheels and thrusters

A large 120° manoeuvre is tested in the same initial conditions as before. The results are depicted in Figure 6.13 and again we see that manoeuvring with thrusters is faster than with the wheels.

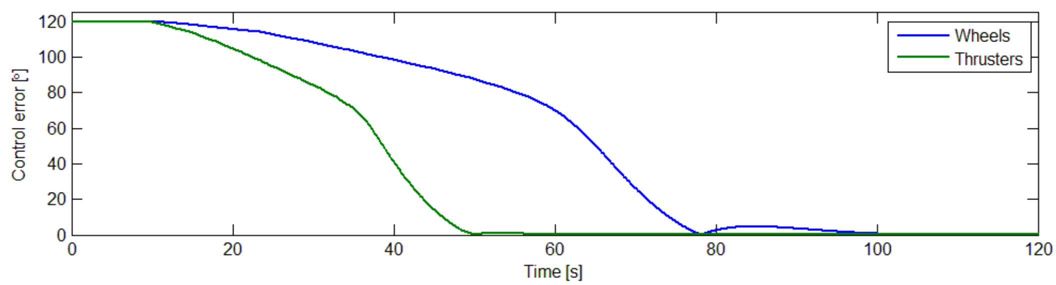

Figure 6.13 – Large manoeuvre

In order to clearly demonstrate the nonlinear nature of the SV system and its control mechanism another 120° manoeuvre is performed with a different $\bar{q}_{target}$ but again the same $\bar{q}_{init}$. One can see that the control error has a completely different evolution towards zero as depicted in Figure 6.14Figure .

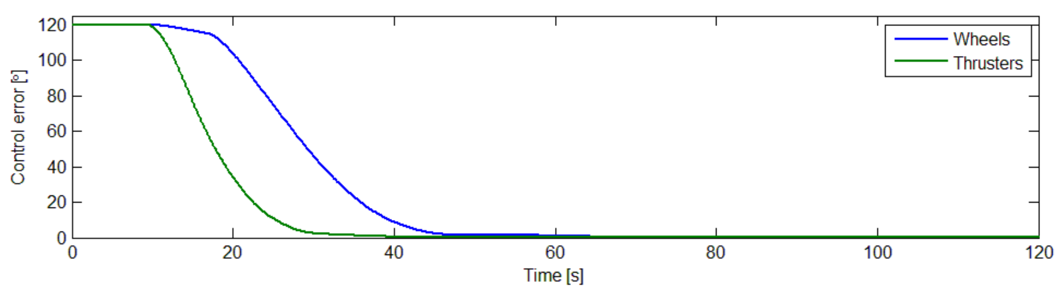

Figure 6.14 - Large manoeuvre with same initial conditions but different target attitude

So far the control mechanism has only been tested under null angular velocity. However in most realistic applications the SV might be deployed in orbit with a slight rotational movement. Hence it is required that the controller is able to stabilize the SV whilst converging to the target. Such situation is tested with:

$\boldsymbol{\omega}_{init} = [-0{,}087 \quad 0{,}0038 \quad 0{,}0048]^T \; rad/s \Leftrightarrow (\|\boldsymbol{\omega}_{init}\| = 5°/s)$,

$\bar{q}_{init} = [-0{,}5766 \quad 0{,}3462 \quad -0{,}5867 \quad 0{,}4512]^T$ and an angle displacement of 137,3° for $\bar{q}_{target} = [-0{,}8905 \quad -0{,}0610 \quad 0{,}3915 \quad 0{,}2237]^T$. The results are shown in Figure 6.15.

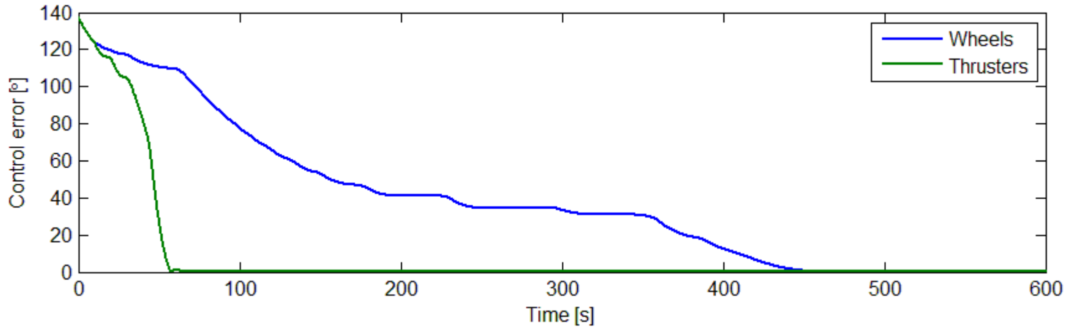

Figure 6.15 – Control under nonzero initial angular velocity

We see that with both types of actuation the SV system is able to stabilize around the target. The evident difference is time of manoeuvre: with thrusters the control error is quickly nulled, whereas with reaction wheels the SV wobbles more before getting close to the target. A nonzero initial angular velocity implies a nonzero total angular momentum of the SV that must be absorbed by the control actuators. While the thrusters perform this by altering the total angular momentum, the reaction wheels exchange momentum with the SV body leading to considerable increase in wheels speed and consequently to greater gyroscopic effects.

Another factor that affects the dynamic behaviour of the SV is a nonzero internal momentum previously installed in the reaction wheels at the beginning of a manoeuvre. In fact if this internal momentum is large enough, even low SV angular velocities can produce large gyroscopic effects. Therefore a simulation with initial internal momentum of the wheels equal to $W^I \boldsymbol{\omega}_w$ is set up where the initial and target attitude are the same as before. The initial angular speed of the wheels is $\boldsymbol{\omega}_w = [190{,}99 \quad -286{,}47 \quad -171{,}89]^T$ rpm. Figure 6.16 depicts the control results in the situation just described.

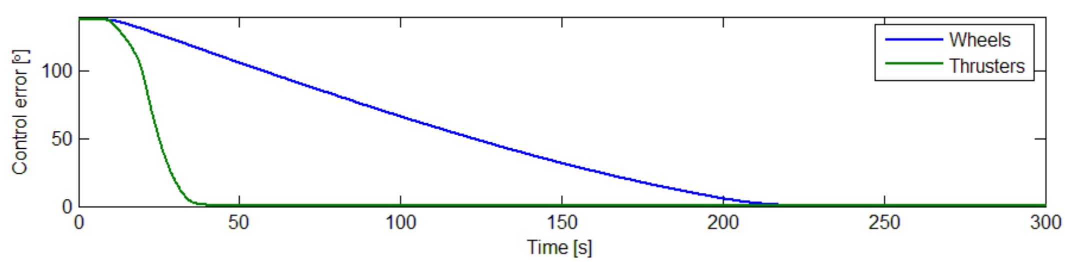

Figure 6.16 – Manoeuvre under initial nonzero internal momentum

The results presented until now concern a perfect actuated SV. The following simulations will address the effects of the non-ideal reaction wheels and thrusters. As mentioned before we consider the dynamics of the reaction wheels as per Section 2.1 and introduce the also previously considered dead zone of $X_{dc} = 0{,}0001$. Concerning the thrusters we emulate their commanded pulse mechanism through the coarse discretization of the thrusters as also described in Section 2.1.

The initial attitude for this manoeuvre is $\bar{q}_{init} = [0{,}3948 \quad 0{,}5090 \quad -0{,}4679 \quad 0{,}6051]^T$. The final attitude is $\bar{q}_{target} = [0{,}4707 \quad 0{,}5019 \quad -0{,}4314 \quad 0{,}5835]^T$. This setting corresponds to an initial angle displacement of 10°. Figure 6.17 shows the manoeuvre resulting with non-ideal actuators.

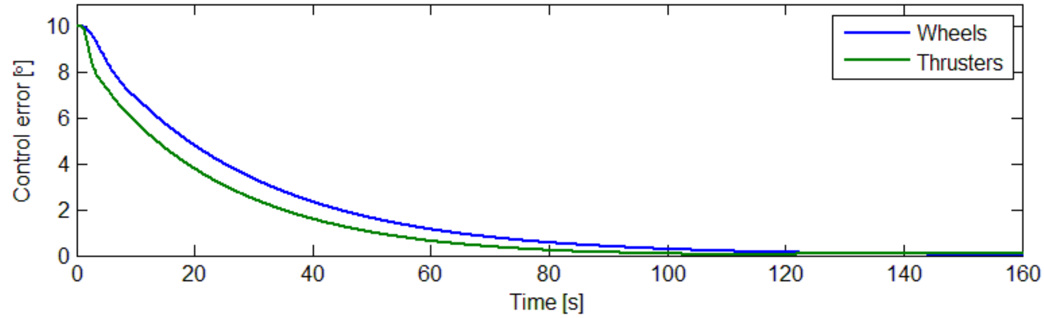

Figure 6.17 – Manoeuvre with non-ideal actuators

Additionally a zoom on the steady state behaviour around the target attitude is presented in Figure 6.18Figure 6..

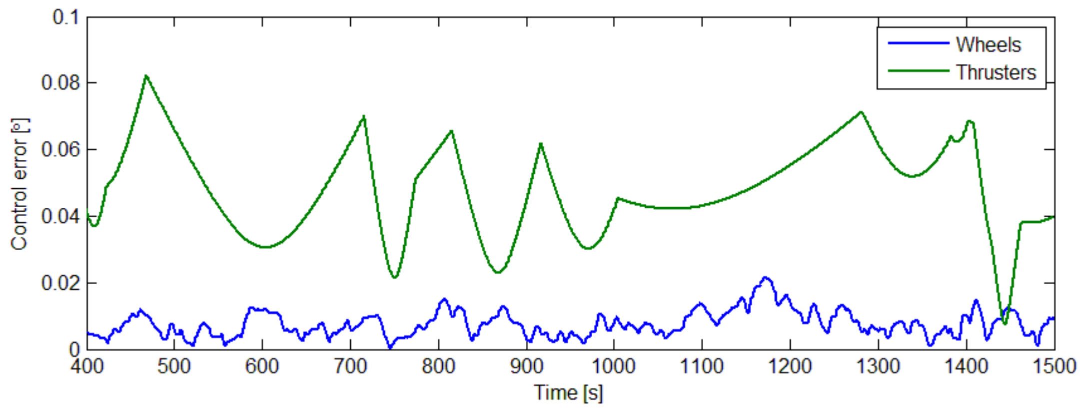

Figure 6.18 – Steady State with non-ideal actuators

One clearly identifies the type of impulsive-like control by the thrusters whereas reaction wheels render an evident finer control.

The results discussed demonstrate that the control mechanism developed provide effective means to reorient the SV in diverse situations, with either thrusters actuation or reaction wheels actuation. We now present the pointing accuracies (σ_{point}) with ideal wheels and thrusters using the two different sets of sensor observations used previously in the MEKF: two-vector observation of Sun and Earth vectors, or Star Tracker quaternion solely. Table 6.2 resumes the accuracy of the four combinations of actuation and sensor observations.

Table 6.1 – Pointing RMS errors for four combinations of sensing and actuation

	Reaction Wheels	Thrusters
Sun and Earth vectors	0,0087°	0,0091°
Star Tracker quaternion	0,0024°	0,0025°

We see that the RMS errors are practically independent on the actuation used but directly dependent on the quality of the estimation. Indeed Star Tracker observations render almost 3,7 times more pointing accuracy than two-vector observations. In fact notice that the pointing accuracy with Star Tracker observations equals the corresponding estimation accuracy previously mentioned of $\sigma_{est} = 0{,}0024°$. Pointing accuracy using two-vector observations is slightly better than the estimation accuracy itself, meaning that there is a small damping factor from the estimation output to the SV systems output when the feedback loop is closed (from $\sigma_{est} = 0{,}0129°$ to $\sigma_{point} = 0{,}0087°$ using wheels).

A similar evaluation is done for non-ideal actuators. Table 6.2 shows the steady state pointing errors corresponding to one simulation run.

Table 6.2 – Pointing RMS errors with non-ideal thrusters

	Reaction Wheels	Thrusters
Sun and Earth vectors	0,0079°	0,0696°
Star Tracker quaternion	0,0024°	0,0779°

The results show that pointing accuracy with non-ideal wheels is actually larger than with ideal wheels when Sun and Earth vectors are used. Concerning the thrusters we see that for this particular simulation the error using the Start Tracker measurement is higher than with two-vector measurements at least. This suggests that pointing performance with such non-ideal thrusters is somewhat independent on the accuracy of the estimate. In this particular case it turned out to be better with two-vector measurements for the given initial and target attitudes pair.

The simplicity of the non-ideal actuators model considered carries a significant drawback. The results given present large sensitivity to parameters selection of the non-ideal dynamics, mainly the dead zone width for the wheels and the quantization division for the thrusters. For instance, if instead of a 0,001 dead zone width, a value of 0,005 was chosen, the SV would not be able to reach the target in reasonable amount of time due to lack of actuation.

To conclude the results of the single SV control, the reaction wheels resetting operation is tested. Typically in such a scenario the SV angular velocity is zero $\boldsymbol{\omega}_{init} = \mathbf{0}$.

The initial true attitude is set close to the target: $\bar{q}_{init} = [0{,}3948 \quad 0{,}5090 \quad -0{,}4679 \quad 0{,}6051]^T$ and $\bar{q}_{target} = [-0{,}3944 \quad 0{,}5088 \quad -0{,}4675 \quad 0{,}6058]^T$, a 0,1° angular separation, meaning that the SV is assumed to be in the vicinity of the target when the wheel resetting operation is triggered. The initial reaction wheels speed is $\boldsymbol{\omega}_{\mathrm{w}} = [1500 \quad 1500 \quad 1500]^T$ rpm, corresponding to the highest internal angular momentum attainable.

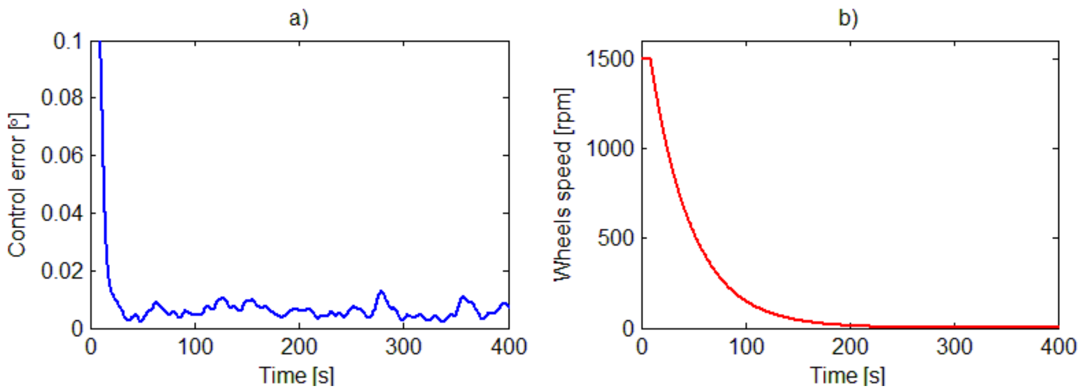

Figure 6.19 – Reaction wheels resetting operation.

Figure 6.19 shows the efficiency of the resetting manoeuvre. We observe in 6.19 b) the smooth evolution of the wheel speed. Also because the thrusters balance the wheels torque, the SV is able to approach the target attitude.

6.3. Group

A. Relative Attitude Determination

Relative attitude determination results using the FPD observations strategy as explained in chapter 5 are now presented. Noise in the LOS vector measurements is introduced via focal plane additive white Noise with covariance given by Eq. (5.1.2). The corresponding variance of the measurement angles in the FPD is set to $\sigma_m^2 = 1{,}7 \times 10^{-5}$. The three true quaternions are:

$$\bar{q}_1 = [0{,}3948 \quad 0{,}5090 \quad -0{,}4679 \quad 0{,}6051]^T$$
$$\bar{q}_2 = [0{,}6923 \quad 0{,}2217 \quad -0{,}6740 \quad 0{,}1320]^T$$
$$\bar{q}_3 = [-0{,}3145 \quad 0{,}0666 \quad 0{,}6496 \quad 0{,}6890]^T$$

and the angular velocities are all equal to zero: $\boldsymbol{\omega}_1 = \boldsymbol{\omega}_2 = \boldsymbol{\omega}_3 = \mathbf{0}$. Also relative attitude estimation is dependent on relative position of the SV's. In order to stand out this influence we place them along the same line, more concretely in the Earth vector line:

$$pos_1^{init} = [0 \quad 9400000 \quad 0]^T$$
$$pos_2^{init} = [0 \quad 9500000 \quad 0]^T$$
$$pos_3^{init} = [0 \quad 9600000 \quad 0]^T$$

though different directions are set to their orbital velocities:

$$vel_1^{init} = [4000 \quad 0 \quad 5000]^T$$
$$vel_2^{init} = [-4000 \quad 0 \quad 5000]^T$$
$$vel_3^{init} = [4000 \quad 0 \quad -5000]^T$$

This manner the SV's will quickly form a triad configuration which is desired for proper relative attitude determination. The relative attitude errors for a 100 second run (equivalent to 1000 trials) is presented in Figure 6.20

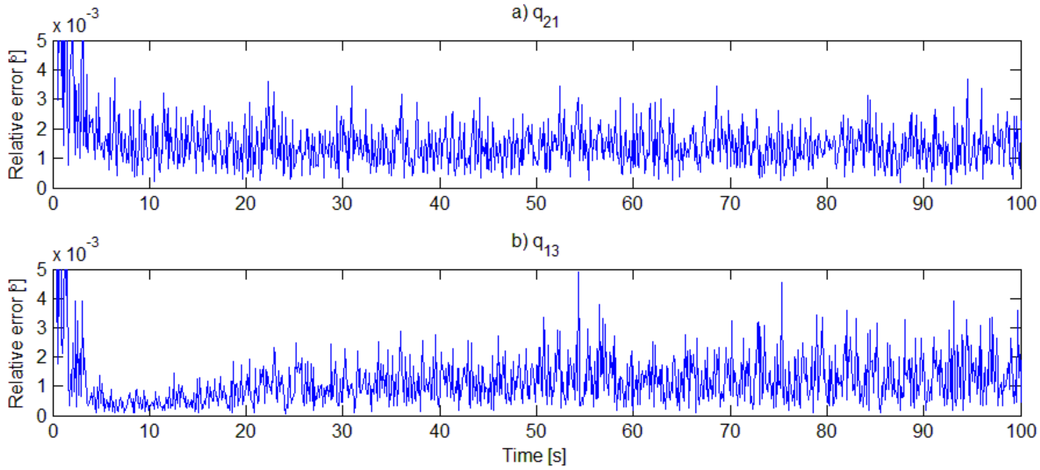

Figure 6.20 –Relative Attitude Error

It is evident in the three graphics that initially the errors are well above the nominal errors. The stationary RMS errors for the same simulation were $\sigma_{21} = 0{,}0015°$, $\sigma_{13} = 0{,}0015°$, $\sigma_{32} = 0{,}0014°$. These values are low compared to the estimation errors of the inertial attitudes of the single SV previously obtained. They prove the usefulness of this relative attitude estimation technique in providing accurate information for computing redundant inertial attitude.

B. Group Control

The first and most simple group strategy is to use three equally equipped SVs, where the target attitude is broadcast through the constellation. Each SV then manoeuvres independently, aiming to null its own attitude error to the target $\bar{q}_{target} = [0{,}7298 \quad 0{,}4742 \quad -0{,}4440 \quad 0{,}2128]^T$. Figure 6.21Figure shows the evolution of the angles between vehicles while the three independent manoeuvres take place.

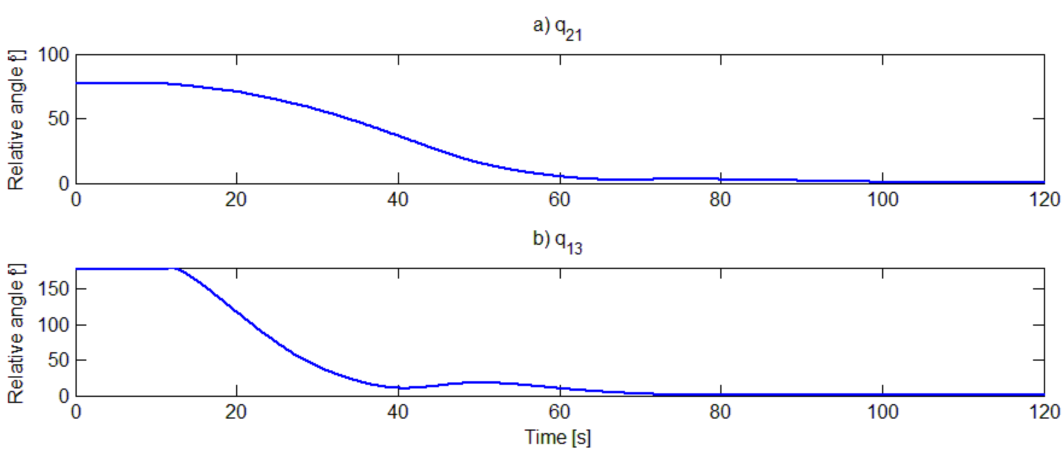

Figure 6.21 – Independently manoeuvred group

We observe in this case that while SV1 and SV3 quickly reach an angle separation of less than 10° after only 40 seconds since manoeuvre start, whereas SV2 takes longer to join them. This is only a consequence of the initial group attitude set and the target attitude, as each SV chooses the shortest path to the target not taking into account the other SVs trajectories.

In the leader following strategy SV1 is assigned as the chief of the group, while SV2 and SV3 are the deputy vehicles which do not possess the inertial sensory package. A solution with this approach broadcasts the inertial attitude of SV1. The results for the same group attitude given as before are depicted in Figure 6.22.

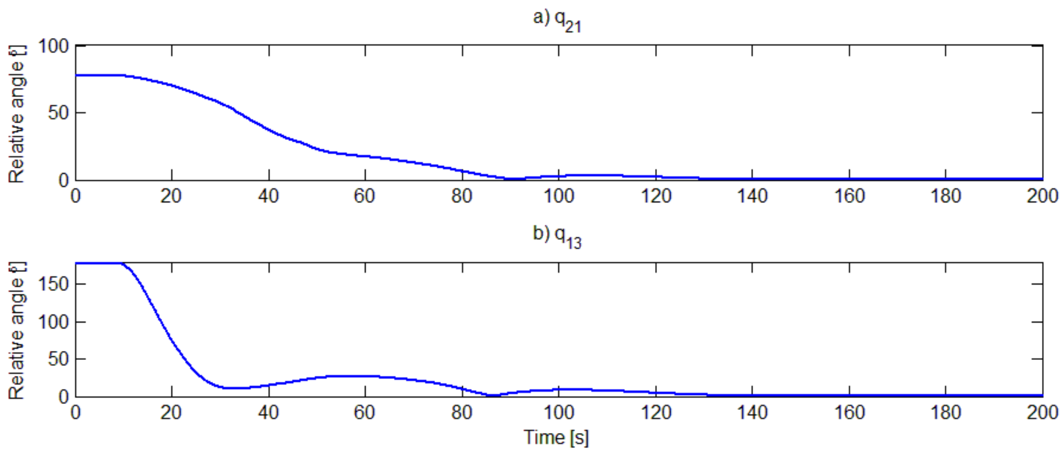

Figure 6.22 – Leader following strategy

The differences are notorious as we that SV2 and SV3 take more time to stabilize around the SV1 attitude. Because SV1 is manoeuvring its attitude changes over-time and consequently the target for SV2 and SV3 is unsteady.

In the second leader following strategy only relative attitude information is available to the deputies. This way the supervisor employed in SV2 and SV3 suffers small modifications previously discussed. A simulation is run with the same initial group attitude configuration as well as the same target attitude used for the previous results. Actuation is again provided by the reaction wheels for comparison. Figure 6.23 presents the results of evolution of relative angles between chief and deputy vehicles in such conditions.

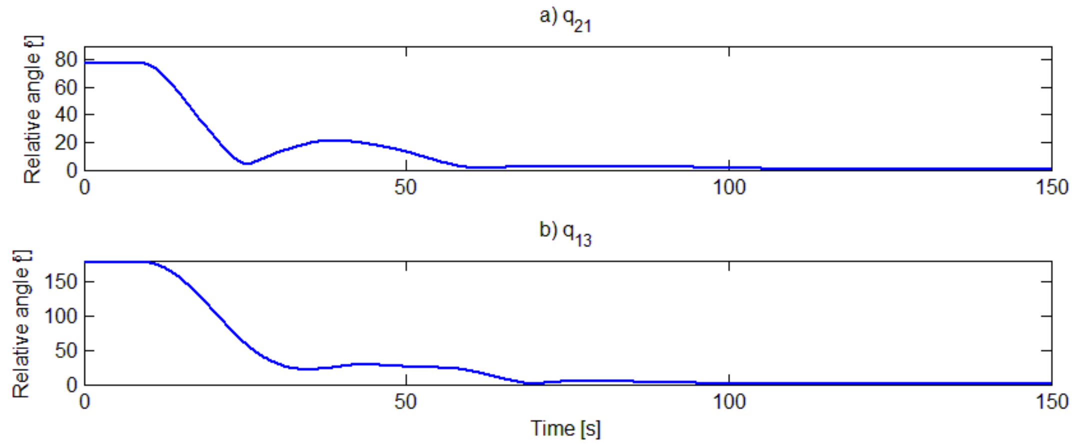

Figure 6.23 – Leader following strategy provided only relative attitude information

It is evident that for manoeuvring purposes there is virtual no advantage of using absolute attitude over relative attitude.

The fourth coordination strategy uses the coordinator to monitor the manoeuvre while assigning the aforementioned converse target attitude for each SV. Figure 6.24 shows a considerably faster convergence of the group towards a common attitude, which proves the utility of the strategy.

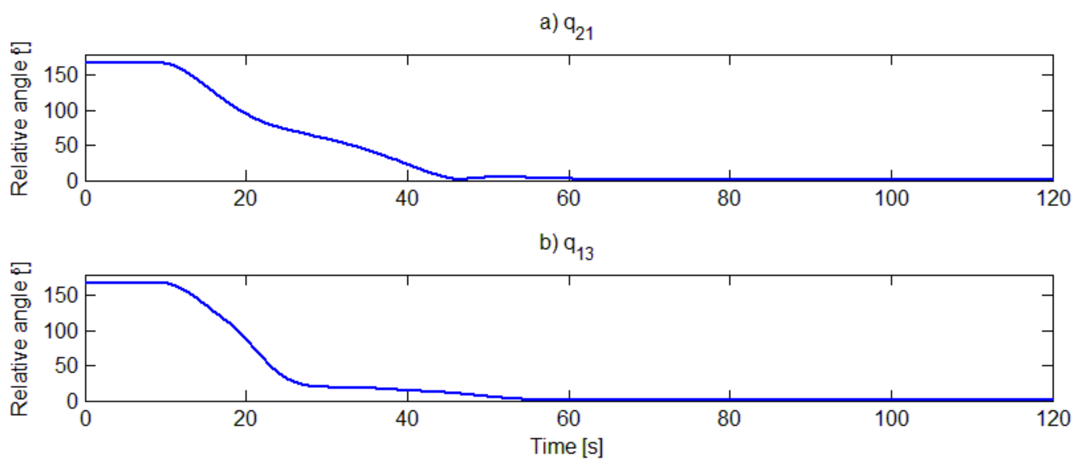

Figure 6.24 – Group control for inexistent target attitude

This concludes the analysis of formation control results.

7. Conclusion and Future Work

The state estimators used are based on Kalman Filtering techniques which do not guarantee convergence. Despite this, in all tested situations convergence was rapidly achieved. The estimation errors were considerably lower when compared with the precision of on-board sensors, as evidenced by the deterministic observer that only rely on the accuracy of the Sun and Horizon sensors. Similarly the accuracy gain of the estimate relatively to the Star Tracker observation is notable.

The single vehicle control strategy developed was able to drive the SV to the desired attitude yet in a segmented manoeuvre. During each segment the control can be regarded as quasi-optimal according to the LQR objective. The manoeuvre supervisor commanding the MLQR is crucial to ensure a smooth transition between manoeuvre stages. Due to its reference setting function the supervisor needs to be cautiously designed in order to account for a wide range of situations during manoeuvre. Small changes in the supervisor often lead to radical changes in the overall behaviour of the system. The designed method is not easily prone to generalization and it is highly dependent on the experience and intuition of the designer. Therefore thorough testing in order to detect pitfalls should be conducted. Although more systematic methods are available for nonlinear control such as the family of Lyapunov based methods, this control strategy highlights that linear-based approaches manage to provide an adequate response for SV attitude control in certain circumstances. On regard of the single SV control future work should step into low frequency disturbance rejection with an augmented state system. Additional features may include moving target tracking or angular velocity tracking.

The group formation control is an extrapolation of the single SV control. The results suggest that the group control strategy here developed is effective and drives the formation to the desired attitude in several scenarios. Also control provisions were made in order to cope with less favourable conditions such as nonzero initial angular velocities and large internal momentum stored in by the wheels. Nevertheless the formation dynamics are not regarded as an integrated system, instead each vehicle tries to track an assigned target attitude corresponding in some cases to an inertial attitude or in others to a relative attitude. Further work using the developed strategy would add additional features to the group coordinator for optimal group manoeuvre planning dependent on the initial configuration of the group.

On the other hand a cooperative approach would describe the formation as a set of differential equations on vehicles states $(\bar{q}_1, \boldsymbol{\omega}_1, \bar{q}_2, \boldsymbol{\omega}_2, \bar{q}_3, \boldsymbol{\omega}_3)$ combinations. The amount of control required for each SV would no longer depend solely on its own state but on the overall formation state or a subset of it.

Another interesting feature to explore given a fully equipped group of vehicles is the fact that accurate relative attitude information provide redundant inertial attitude estimates which can be used to mitigate sensor misalignment errors.

8. Appendix

A. Mathematical Notation and Symbols

It is often convenient to express the cross product operator in matrix form:

$$\boldsymbol{v} \times \boldsymbol{u} = [\boldsymbol{v} \times]\, \boldsymbol{u} \tag{A.1}$$

where

$$[\boldsymbol{v} \times] = \begin{bmatrix} 0 & -v_3 & v_2 \\ v_3 & 0 & -v_1 \\ -v_2 & v_1 & 0 \end{bmatrix} \tag{A.2}$$

Attitude parameterization, the quaternion

Quaternions generalize complex numbers and can be used to represent rotations in much the same way as complex numbers on the unit circle can be used to represent planar rotations. Unlike Euler angles, quaternions give a global parameterization of $SO(3)$, at the cost of using four numbers instead of three to represent a rotation.

Formally a quaternion is a vector quantity (q_1, q_2, q_3, q_4)

$$\bar{q} \equiv iq_1 + jq_2 + kq_3 + q_4 = \boldsymbol{q} + q_4 \tag{A.3}$$

where q_4 is the scalar component of $\bar{q}$ and $\boldsymbol{q} = (q_1, q_2, q_3)$ is the vector component. A convenient shorthand notation is $\bar{q} = (\boldsymbol{q}, q_4)$. The conjugate of a quaternion is given by $\bar{q}^* = (-\boldsymbol{q}, q_4)$ and the magnitude of a quaternion satisfies

$$\|\bar{q}\|^2 = q_1^2 + q_2^2 + q_3^2 + q_4^2 \tag{A.4}$$

The inverse of a quaternion is $\bar{q}^{-1} = \bar{q}^*/\|\bar{q}\|^2$ and $\bar{q} = (0,1)$ is the identity element quaternion multiplication. The product between two quaternions has a simple form in terms of the inner and cross products in $\mathbb{R}^3$. I can be shown algebraically that the product of two quaternions satisfies:

$$\bar{p}.\bar{q} = \bar{p} \otimes \bar{q} = (p_4\boldsymbol{q} + q_4\boldsymbol{p} - \boldsymbol{p} \times \boldsymbol{q},\ p_4 q_4 - \boldsymbol{p}.\boldsymbol{q}) \tag{A.5}$$

We shall consider only *unit quaternions*. They are the subset of all $\bar{q}$ such that $\|\bar{q}\| = 1$ and have a direct relation with rotations. Given a rotation matrix $R = \exp([\hat{\boldsymbol{\omega}} \times]\theta)$, we define the associated unit quaternion as $\bar{q} = \left(\hat{\boldsymbol{\omega}} \sin(\theta/2) \cos(\theta/2)\right)$, where $\hat{\boldsymbol{\omega}} \in \mathbb{R}^3$ represents the unit axis of rotation and $\theta \in \mathbb{R}$ represents the angle of rotation. A detailed calculation shows that if $\bar{q}_{ab}$ represents a rotation from frame A to frame B, and $\bar{q}_{bc}$ represents a rotation from frame B to frame C, then the rotation from A to C is given by the quaternion $\bar{q}_{ac} = \bar{q}_{ab}.\bar{q}_{bc}$. The quaternion multiplication convention defined earlier has the advantage that the order of quaternion multiplication is the same as the order of matrix multiplication.

Thus, the group operation $\otimes$ on unit quaternion directly corresponds to the group operation for rotations. Given a unit quaternion $\bar{q}$ one extracts the corresponding rotation by setting

$$\theta = 2\cos^{-1} q_4 \qquad \hat{\boldsymbol{\omega}} = \begin{cases} \dfrac{\boldsymbol{q}}{\sin(\theta/2)} & \text{if } \theta \neq 0 \\ 0 & \text{otherwise,} \end{cases} \tag{A.6}$$

and $R = \exp([\hat{\boldsymbol{\omega}} \times]\theta)$.

The transformation of a vector v, corresponding to multiplication by matrix A is

$$v' = Av$$

In quaternion algebra it is expressed by the operation

$$v' = \bar{q}^* v \bar{q} \tag{A.7}$$

The direction cosine matrix A can be expressed in terms of the quaternion $\bar{q}$ as

$$A(Q) = (q_4^2 - \boldsymbol{q}^2) I_{3\times3} + 2\boldsymbol{q}\boldsymbol{q}^T - 2q_4[\boldsymbol{q}\,\times] \tag{A.8}$$

The quaternion quantity provides an efficient representation for rotations which do not suffer from singularities but it is a two-fold representation, i.e. given any rotation A represented by $\bar{q}$ than $-\bar{q}$ also represents the same rotation A. This is intuitive taking into account the relation between $\bar{q}$ and $R = \exp([\widehat{\boldsymbol{\omega}}\,\times]\theta)$ given before; notice that rotating θ radians through the axis $\boldsymbol{\omega}$ is the same as rotating $2\pi - \theta$ radians in the opposite axis direction $-\widehat{\boldsymbol{\omega}}$. It is easy to verifyd that

$$\bar{q}(-\widehat{\boldsymbol{\omega}}, 2\pi - \theta) = \left(-\widehat{\boldsymbol{\omega}}\sin\left(\frac{\theta}{2}\right), -\cos(\theta/2)\right) = -\bar{q}(\widehat{\boldsymbol{\omega}}, \theta).$$

Quaternion kinematics

The quaternion kinematics can be proven to yield the following differential equation:

$$\dot{\bar{q}} = \frac{1}{2}\Omega(\boldsymbol{\omega})\bar{q} \tag{A.9}$$

with $\Omega(\boldsymbol{\omega}) = \begin{bmatrix} -[\boldsymbol{\omega}\,\times] & \boldsymbol{\omega} \\ -\boldsymbol{\omega}^T & 0 \end{bmatrix}$, or alternatively:

$$\dot{\bar{q}} = \frac{1}{2}\Xi(\bar{q})\boldsymbol{\omega} \tag{A.10}$$

with $\Xi(\bar{q}) = \begin{bmatrix} q_4 I_{3\times3} + [\boldsymbol{q}\,\times] \\ -\boldsymbol{q}^T \end{bmatrix}$

B. The Extended Kalman Filter

The EKF is an extension of the Kalman Filter (KF) in order to address estimation of systems with nonlinear dynamics and/or observations. For more detailed information the reader may consult reference [6].

The idea behind the EKF is to linearize the dynamics around points which are expected to lie within a close range to the true state. The discrete EKF problem may be formulated along the following lines:

$$x_{k+1} = f(x_k, u_k, n_k) \quad \text{B.1}$$
$$x_{k+1} = h(x_k, v_k) \quad \text{B.2}$$

where:

- K parameterizes the time instant $t_k = t.h$, where h is the sampling period
- x_k represents the system state vector,
- $f()$ is the nonlinear function that defines the system dynamics
- u_k is the control vector
- n_k is the vector that conveys the error dynamics representation
- y_k is the observation vector
- $h()$ is the nonlinear function that defines the observation model
- v_k is the vector of measurement noise

When functions $f()$ and $h()$ are both linear and the disturbances are characterized by zero mean white Gaussian noises, then the EKF degenerates to the KF problem. The filter objective is to get an optimal estimate of the system state x_k in the sense that it minimizes the covariance of the estimation. Assuming the error probability density functions (PDF) are given by Gaussians the KF operates over the space of Gaussian functions, with the estimate being a Gaussian as well. This is so because of the linearity of the system. When nonlinear functions arise in the description of the system the Gaussian function no longer characterizes the PDF of the state, instead it becomes deformed throughout the estimation. However if the linearization is good enough the EKF approach is keen to propagate a close Gaussian approximation of PDF characterizing the main features of the real PDF.

Briefly the EKF estimation comprises two steps: the prediction step and the update or filtering step.

In the prediction step the filter uses knowledge of the dynamics to propagate the state, so an intermediate estimate called the predicted estimate is computed.

In the filtering step the measurement model is used in order to correct the predicted estimate based on observations.

Predict Step

Let F_k be the Jacobian matrix of f_k, $P_{k|k}$ be the covariance matrix of the state, Q_k the covariance of the model error modelled by matrix G_k at time k. Then

$$F_k = \nabla f_k | \hat{x}_{k|k} \quad \text{B.3}$$
$$\hat{x}_{k+1|k} = f_k(\hat{x}_{k|k}, u_k) \quad \text{B.4}$$
$$P_{k+1|k} = F_k P_{k|k} F_k^T + G_k Q_k G_k^T \quad \text{B.5}$$

Update Step

Let H_k be the Jacobian matrix of h_k, K_k the Kalman gain, and R_k the covariance of the measurement at time k. Then

$$H_k = \nabla h_k | \hat{x}_{k|k} \quad \text{B.6}$$
$$K_{k+1} = P_{k+1|k} H_k^T \left[H_k P_{k+1|k} H_k^T + R_k \right]^{-1} \quad \text{B.7}$$
$$P_{k+1|k+1} = [I - K_{k+1} H_{k+1}] P_{k+1|k} \quad \text{B.8}$$
$$\hat{x}_{k+1|k+1} = \hat{x}_{k+1|k} + K_{k+1}\left(y_{k+1} - h_k(\hat{x}_{k+1|k})\right) \quad \text{B.9}$$

Additional Considerations

The two EKF steps follow each other consecutively. Often the error covariance matrices are assumed to be constant though some types of sensors have accuracies that depend on the state.

One of the advantages of Kalman filtering estimation - where the EKF is included - is that more than one measurement source can be included in the estimation process. All one needs is to compute equations A.6-A.9 corresponding to the new observation and using the last estimate obtained. The propagation step though only occurs once in the beginning of the cycle. Therefore integrating several measurements comes down to repeat these systematic steps and using the most updated values of the estimate and covariance.

9. References

[1] Wertz, James R. *Spacecraft Attitude Determination and Control*, Dordrecht, Kluwer Academic Publishers, 1978

[2] Yonatan Winetraub, San Bitan & Uval dd & Anna B. Heller. *Attitude Determination – Advanced Sun Sensors for Pico-satellites*, Handasaim School, Tel-Aviv University, Israel

[3] Rycroft, Michael J. Stengel, Robert F. *Spacecraft Dynamics and Control,* Cambridge University Press 1997

[4] William E. Wiesel, *Spaceflight Dynamics*, Irwin McGraw-Hill, 2nd Edition

[5] Malcolm D. Shuster, *Deterministic Three-Axis Attitude Determination*, The Journal of the Astronautical Sciences, Vol. 52, No. 3, July-September 2004, pp. 405-419

[6] Maria Isabel Ribeiro, *Kalman and Extended Kalman Filters: Concept, Derivation and Properties*, Institute for Systems and Robotics, Instituto Superior Técnico, February 2004

[7] Balbach, Oliver & Eissfeller, Bernd & Gunter W. Hein. *Tracking GPS above GPS Satellite Altitude: First Results of the GPS experiment on the HEO Mission Equator-S*

[8] F. Landis, Markley, *Multiplicative vs. Additive Filtering for Spacecraft Attitude Determination,* NASA's Goddard Space Flight Center

[9] F. Landis, Markley, *Attitude Estimation or Quaternion Estimation?*, NASA's Goddard Space Flight Center

[10] Richard M. Murray, Zexiang Li, S. Shankar Sastry, *A Mathematical Introduction to Robotic Manupulation*, chapter 2. CRC Press, 1994

[11] Grace Wahba, *A Least Squares Estimate of Satellite Attitude*. SIAM Review, Vol. 8, No. 3, (Jul., 1966), 384-286

[12] F. Landis Markley, "*Fast Quaternion Attitude Estimation from Two Vector Measurements"* Guidance, Navigation and Control Systems Engineering Branch, code 571. NASA's Goddard Space Flight Center, Greenbelt, MD20771

[13] J. Miranda Lemos, "*Introdução ao Controlo Óptimo*", Class notes. IST 2012

[14] HE BAi, Murat Arcak, John Wen," *Cooperative Control Design: A Systematic, Passivity-Based Approach*". Springer

[15] Michael S. Andrle, Baro Hyun, John L. Crassidis, Richard Linares, "*Deterministic Relative Attitude Determination of Formation Flying Spacecraft*". University of Buffalo, State University of New York, Amherst, NY, 14260-4400

[16] Rand W. Beard, Jonathan Lawton, Fred Hadaegh, "*A Coordinated Architecture for Spacecraft Formation Control*". IEEE Transactions on Control systems Technology, Vol. 9, No. 6, 2001

[17] Robert Strengel, "Spacecraft Sensors and Actuators", Space System Design, MAE 342, Princeton University

[18] Malcolm D. Shuster, "Deterministic Three-Axis Attitude Determination", The Journal of the Astronautical Sciences, Vol. 52, pp. 405–419